AD-A140 160 A PARAMETRIC STUDY OF SURFACE TRANSFORMATION HARDENING WITH HIGH-POWER LA..(U) WESTINGHOUSE RESEARCH AND DEVELOPMENT CENTER PITTSBURGH PA G E GROTKE ET AL. 1/2

UNCLASSIFIED 02 FEB 84 84-9D4-SURFC-R1 N00014-82-C-2339 F/G 20/5 NL

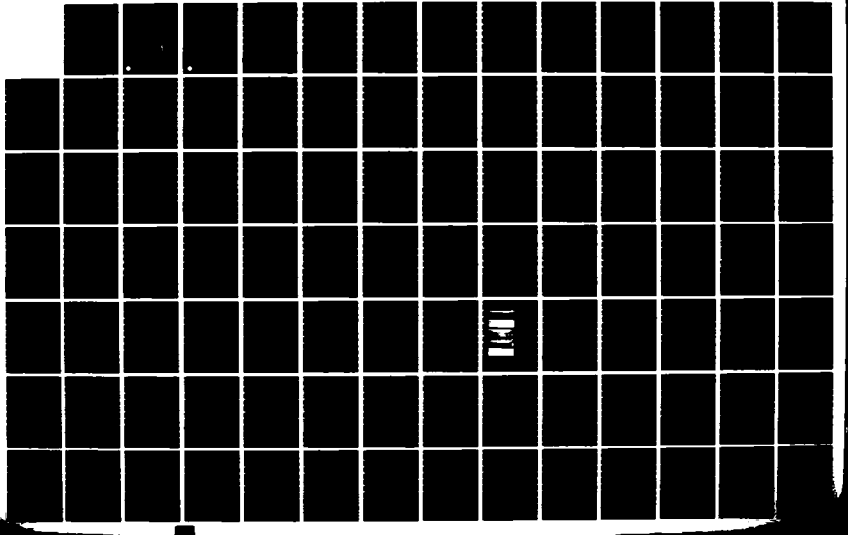

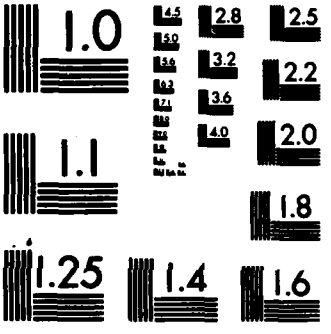

MICROCOPY RESOLUTION TEST CHART
NATIONAL BUREAU OF STANDARDS-1963-A

(12)

A PARAMETRIC STUDY OF SURFACE TRANSFORMATION HARDENING WITH HIGH-POWER LASERS

G. E. Grotke, G. J. Bruck,
J. E. Smith and J. I. Nurminen

February 2, 1984

Prepared for:

United States Department of the Navy
Contract No. N00014-82-C-2339

AD A140160

DTIC FILE COPY

DTIC
ELECTE
APR 16 1984
S D
A

This document has been approved for public release and sale; its distribution is unlimited.

Westinghouse R&D Center
1310 Beulah Road
Pittsburgh, Pennsylvania 15235

84 03 15 002

A PARAMETRIC STUDY OF SURFACE TRANSFORMATION HARDENING WITH HIGH-POWER LASERS

G. E. Grotke, G. J. Bruck,
J. E. Smith and J. I. Nurminen

February 2, 1984

Prepared for:

United States Department of the Navy
Contract No. N00014-82-C-2339

Accession For
NTIS GRA&I
DTIC TAB
Unannounced
Justification
Distribution/
Availability Codes
Dist | Avail and/or Special
A-1

DTIC COPY INSPECTED

Westinghouse R&D Center
1310 Beulah Road
Pittsburgh, Pennsylvania 15235

NOTICE

This report was prepared as an account of work sponsored by an agency of the United States Government. Neither the United States Government nor any agency thereof, nor any of their employees, makes any warranty, expressed or implied, or assumes any legal liability or responsibility for any third party's use or the results of such use of any information, apparatus, product or process disclosed in this report or represents that its use by such third party would not infringe privately owned rights.

TABLE OF CONTENTS

A-1

Preface

This report was prepared in performance of United States Department of the Navy Contract No. N00014-82-C-2339. The contracting officer is Mr. S. C. Toleman. Administration is provided by the technical representative, Dr. E. A. Metzbower (Code 6320), Naval Research Laboratory. The Westinghouse Electric Company program manager is Dr. J. I. Nurminen, Research and Development Center.

LIST OF TABLES

LIST OF FIGURES

R&D Report 84-9D4-SURFC-R1 February 2, 1984

A PARAMETRIC STUDY OF SURFACE TRANSFORMATION HARDENING WITH HIGH-POWER LASERS

G. E. Grotke, G. J. Bruck, J. E. Smith and J. I. Nurminen
Westinghouse R&D Center
Pittsburgh, Pennsylvania 15235

ABSTRACT

High-power, continuous-wave CO_2 lasers were employed in a parametric study of penetration, cross-sectional area, and hardness in nine steels that provided a wide range in composition, carbon content, hardenability, and response to heat treatment (1018, 4140, 4340, 2-1/4 Cr-1 Mo, HY-100, HY-80, H-11, Type 422 and 17-4 PH). The test conditions included laser output powers from 5.0 to 12.5 KW and travel speeds in the range 20 to 100 ipm which, with the beam sizes used, resulted in energy densities from 0.52 to 7.01 KJ/cm^2.

Laser transformation hardening treatment resulted in appreciable hardness in all the steels that had adequate carbon content and good hardenability (4140, 4340, 2-1/4 Cr-1 Mo, HY-100, HY-80 and H-11). The maximum and average hardness produced in these steels corresponds to martensite contents of 90 to 100 per cent.

INTRODUCTION

Laser transformation hardening is a fast, controllable and reproducible method for producing a hardened surface with minimal distortion that requires little or no finish machining. Quenching liquids are generally not needed, the procedure is environmentally clean, special fixturing is not required, any surface that can be exposed to the beam may be hardened, and the process is readily adapted to computer numerical control.

For several years, the Westinghouse R&D Center has been involved in demonstrating the technical feasibility of the laser hardening process and in developing the process parameters for hardening marine gears of varying pitch and tooth configurations. Parametric studies have evaluated the effect of laser optics configuration, surface coatings for enhancing beam-coupling efficiency, laser power density, and the interaction time for hardening the flanks of gear-teeth to obtain a uniform case thickness. Pinion gears with both spur and helical tooth configurations have been successfully hardened with excellent dimensional uniformity. Parameters have been established, using a modified 4340 steel, that will provide a uniform martensitic case from 0.040 to 0.10 inch in depth, that is free from cracks or spalls. The results of the gear hardening program have been extremely encouraging. The process is being readied for manufacturing implementation.

The present work extends the parametric investigations to determine the influence of laser power density and travel speed on the onset of hardening and melting, the depth of case penetration, and the hardness that may be obtained in several different steels.

MATERIALS AND EXPERIMENTAL PROCEDURE

Laser hardening studies were conducted with nine steels that provided a wide range in composition, carbon content, hardenability and response to heat treatment. The identification of the materials, their initial hardnesses, and other pertinent information is presented in Table I. The majority of the steels, 1018, 4140, 4340, 2-1/4Cr-1Mo, HY-100 and HY-80, are in common use and their characteristics are familiar. Type 422 is a hardenable, 12Cr, corrosion-resistant steel similar to Type 403 stainless; H-11 is a high-carbon, 5Cr-1.5Mo, hot-work die steel; and 17-4 PH is a 17Cr-4Ni-4Cu martensitic stainless, hardenable only by precipitation. The specified or nominal composition of each material together with the results of a check analysis for carbon made at the R&D Center are shown in Table II.

As indicated in Table I, the laser-hardening treatments were conducted at two locations. The earliest tests were made by R&D Center personnel at AVCO Everett Metalworking Lasers, Boston, MA, using a 20 KW AVCO-HPL continuous-wave CO_2 laser work station leased for proprietary laser metalworking activities. Later studies were conducted by the same personnel using a similar AVCO-HPL laser, capable of 25 KW of power output, subsequently installed at the Westinghouse Laser Center located at the Marine Division, Sunnyvale, CA.

The test specimens were 12-inches long and 3-inches wide, allowing two laser passes to be made on each surface (four passes per specimen) if the thickness of the material was adequate. In studies of this sort, when relatively high energy densities are to be employed, a minimum thickness of 1/2 inch is desirable, though the minimum thickness that is actually acceptable has not been determined. In three instances, when heavier stock could not be located, thicknesses under 1/2 inch were used. Tests of Type 422 stainless were conducted with 3/8 inch thick

specimens. Specimens of HY-100 steel were 5/16 inch thick. Tests conducted with HY-80 steel involved two specimen thicknesses, 5/8 and 1/4 inch.

Scale was removed from the surfaces of the specimens, usually by milling or coarse grinding operations noted by "rough machined" in Table I. Two steels, 4140 and 4340, were tested using both smooth, surface-ground specimens and rough-machined specimens to determine whether this difference would influence the beam coupling and hardening characteristics. All specimens received a spray coat of flat-black paint (KRYLON 1602) to enhance the beam-coupling efficiency. Measurements of the area of the heat-affected region (including fused metal if surface melting occurred), the maximum penetration of the heat-affected region, and the penetration of any fused metal were obtained from 5X macrographs of the individual sections. Figure 1 shows typical macrographs obtained from 4340 steel specimens heat treated with 10.0 KW of laser power in the range 20 to 100 ipm (0.84 to 4.2 cm/sec). No evidence of cracks or spalls was observed in any of the sections.

Tests of Type 422 stainless were conducted with pairs of specimens, one of which was flooded with nitrogen to determine whether the hardness could be enhanced by formation of nitrides. The procedure did not produce a detectable change in the hardness or any other characteristic. Data for these pairs of specimens have simply been treated as duplicate runs.

TEST PARAMETERS AND RESULTS

The laser hardening parameters and the results of penetration, area, and hardness measurements are summarized in Tables III through XIII. Each table shows a laser power level (either 5.0, 7.5, 10.0, or 12.5 KW) for laser output and a lower value indicating the power at the specimen surface after transmission losses. Throughout this report the higher value (aero window power) is used to identify each power level employed even though the calculated power densities and energy densities are based on power at the specimen surface.

Tests at AVCO used output powers in the range 7.5 to 12.5 KW and travel speeds from 20 to 60 ipm (0.84 to 2.52 cm/sec). At the Westinghouse Laser Center, the power outputs ranged from 5.0 to 12.5 KW; speeds from 20 to 100 ipm (0.84 to 4.2 cm/sec). A summary of the test parameters and the number of specimens of each steel that were employed is presented in Table XIV. Inspection of this table reveals that tests at the Westinghouse Laser Center, with the exception of tests of 17-4 PH, involved a wider range of energy densities* which, as will be discussed, spanned from densities that were insufficient to cause hardening to those that resulted in significant surface melting. In tests at AVCO, the high-side energy densities were sufficient to cause melting, but, at the low end, did not permit determination of the minimum energy density necessary to initiate hardening. The energy density range was sufficient, however, to yield useful information.

---

*$\overline{E}$, Energy density = $\frac{\text{power to work}}{\text{beam area}}$ x interaction time

where: The interaction time is a measure of the dwell time of beam impingement on a given region.

This work employed an integrated-beam optics system which produces a beam of square configuration, on the work surface, that can be optically adjusted to the required size. The incoming laser beam to the work station is reflected from a multi-faceted concave mirror and broken up into a multiplicity of mini-beams that are then reimaged by a spherical, concave mirror and superimposed (integrated) upon each other to produce the square configuration, with essentially uniform power density, on the work surface. The sections shown in Fig. 1 illustrate the uniform penetration obtained with a 1.91 cm square integrated beam at travel speeds as slow as 40 ipm (1.68 cm/sec).

The dimensions of the integrated beam used at the two locations was slightly different. The integrated beam size used at the Westinghouse Laser Center was 1.91 cm (0.752 in.) square. In tests conducted at AVCO the beam was slightly smaller, 1.78 cm (0.701 in.) square, resulting in roughly a 7 per cent increase in energy density under otherwise identical conditions. The difference in beam sizes is also responsible for the different interaction times, for identical travel speeds, shown in Table XIV.

EXAMPLES OF ENERGY DENSITY CALCULATIONS

Tests at AVCO Everett

The integrated beam used at AVCO was 1.78 cm (0.701 in) square and the beam transmission system employed four copper mirrors, each introducing a power loss of 2 per cent, resulting in a transfer efficiency of 84 per cent.*

Conditions:		
	Laser power output	7.5KW
	Transfer Efficiency	84%
	Beam Size	1.78 cm (0.701 in) square
	Travel Speed	0.84 cm/sec (20 ipm)

Power to Work = Laser output x Transfer Efficiency
= 7.5 KW x 0.84
= 6.3 KW

$$\text{Power Density} = \frac{\text{Power to Work}}{\text{Beam Area}} = \frac{6.3 \text{ KW}}{(1.78)^2 \text{ cm}^2} = 1.99 \text{ KW/cm}^2$$

$$\text{Interaction Time} = \frac{\text{Length of Integrated Beam}}{\text{Travel Speed}} = \frac{1.78 \text{ cm}}{0.84 \text{ cm/sec}} = 2.12 \text{ sec}$$

$\bar{E}$, Energy Density = Power Density x Interaction Time
= 1.99 KW/cm^2 x 2.12 sec
= 4.22 KJ/cm^2

Tests at Westinghouse Laser Center

Conditions as given above except for a 1.91 cm (0.751 in) square beam. The power delivered to the work remains unchanged at 6.3 KW

$$\text{Power Density} = \frac{6.3 \text{ KW}}{(1.91)^2 \text{ cm}^2} = 1.73 \text{ KW/cm}^2$$

$$\text{Interaction Time} = \frac{1.91 \text{ cm}}{0.84 \text{ cm/sec}} = 2.27 \text{ sec}$$

$\bar{E}$, Energy Density, = 1.73 KW/cm^2 x 2.27 sec
= 3.93 KJ/cm^2

*Subsequent test at the WLC using a water-cooled calorimeter confirmed the 84% figure.

PENETRATION

Effect of Surface Condition

In all instances, the steels involved in this study were tested with specimens having rough-machined surfaces. Tests of 4140 and 4340 steels were also conducted, at laser powers of 7.5 and 10.0KW, with surface-ground specimens to determine if the beam coupling would be affected and the hardening characteristics would be altered. Figures 2 and 3 for 4140 and 4340 steels, respectively, show the total penetration obtained in these steels as a function of $\bar{E}$, the energy density. Solid points indicate data obtained with ground specimens; open points the data for rough specimens. The comparisons employed specimens that were identical in both width and thickness.

It is apparent in both figures that the data show little scatter and conform to best-fit lines with closely matching slopes and intercepts, indicating that the penetration is insensitive to the surface conditions used. Consequently, the data for rough-machined and surface-ground specimens (4140 Codes BX and BY; 4340 Codes CX and CY) have been combined in the data presented later.

General Influence of Energy Density on Penetration

Curves showing the total penetration of the heat-affected region and the penetration of the fused region, if melting occurred, are presented in Figs. 4 through 12. Each figure provides the equation for the penetration and a critical value for the energy density above which there is the risk of encountering surface melting. The penetration of the heat-affected zone corresponding to the critical energy density is also shown. The pertinent data from Figs. 4 through 12 are summarized in Table XV.

Though curves of the type shown in Figs. 4 through 12 provide sufficient information to permit selection of operating parameters (particularly when the data are limited), there are some restrictions on their use which should be recognized. The energy density is the product of a power density and an interaction time determined by the speed of travel. Two conditions that will result in the same energy density, one obtained by using a low power density operating for a very long time, the other obtained by using a high power density and a brief interaction time, will not result in similar penetrations. The results for 1018, 4140 and 4340 steels provide examples. In these three cases, as is shown in Table XIV, a large number of specimens were tested, four levels of power density were employed, and the travel speed range was wide, 20 to 100 ipm (0.84 to 4.2 cm/sec). The data for these three steels have been replotted in Figs. 13, 14 and 15 with some changes:

- o The penetrations for specimens that showed surface melting have not been included.
- o Best-fit lines for the various laser powers employed (different power densities) are shown separately.
- o Some zero-penetration data points have been included. These points, for the highest energy density conditions

that did not result in formation of a heat-affected region, were not used in the linear-regression calculations.

All three figures show similar shift in slope and decrease in intercept with reduced laser power, illustrating that at low energy densities deeper penetration is obtained with high power/short interaction time conditions. The various power densities and travel speeds employed in tests of these steels permits a comparison of the penetration at essentially constant energy density (about 1.3 KJ/cm^2) at all four levels of laser power, see Table XVI. At this energy density, the average penetrations for the 5.0, 7.5, 10.0 and 12.5KW power levels are, respectively, 0, 13, 32 and 36 mils (0, 0.33, 0.81 and 0.91 mm). This behavior could introduce complications if an operator, knowing only the penetration/energy density relationship for a single power level, should change to another power level (at constant energy density) that is much different from the first. As the data show, the difference in penetration between operation at 12.5 KW and at 10.0 KW is negligible. However, a change from operation at 12.5 KW to 7.5 KW (with compensating speed reduction to hold the same energy density) would reduce the depth of penetration to about one third. Use of a 5.0 KW beam would not result in a hardened region.

Figures 13, 14 and 15 reveal another feature of the penetration/energy density relationship. The onset of surface melting is also influenced by the power density employed. At higher energy densities, deeper, melt-free penetration can be obtained by using low power-density conditions. Figure 13, for 1018 steel, indicates the critical energy density (obtained from Fig. 4) of 2.6 KJ/cm^2 for the initiation of melting. This figure also shows that the lowest energy density to actually cause melting in 1018 steel specimens was 3.27 KJ/cm^2 with 12.5 KW conditions, and 3.49 KJ/cm^2 under 10.0 KW conditions. Melting would be expected to occur in these specimens since the critical energy density was exceeded. However, surface melting would also be anticipated for the 7.5 KW specimen run at an energy density of 3.93 KJ/cm^2; about 1.4 KJ/cm^2 higher than the critical energy density. Instead, this particular specimen was melt-free and exhibited the greatest penetration of any in the 1018 steel series. It is interesting to note that the

lowest energy density that resulted in melting in a 12.5KW specimen was 3.27 KJ/cm^2. The lowest energy density producing melting in a 10.0KW specimen was higher, 3.49 KJ/cm^2. The lowest energy density that will produce melting under 7.5KW conditions is unknown but higher still; exceeding 3.93 KJ/cm^2.

The observation for 1018 steel, that melting is initiated at lower energy densities under high power conditions, is also evident in Fig. 14, which presents data for 4140 steel. In this instance, however, melting did occur in a duplicate 7.5KW specimen tested at an energy density of 3.93 KJ/cm^2. The lowest energy density values to produce melting for the 12.5, 10.0 and 7.5KW conditions are 3.27, 3.49 and 3.93 KJ/cm^2, respectively.

Figure 15, data for 4340 steel, supports the same trend, but only partially. Melting did not occur in either 7.5KW, 4340 steel specimen tested at an energy density of 3.93 KJ/cm^2; well above the critical energy density indicated by Fig. 6. Melting in a 10.0KW specimen occurred, as would be expected, at a lower energy density, 3.49 KJ/cm^2. In this instance, however, melting was not detected in the 12.5KW specimen tested at 3.27 KJ/cm^2, but occurred at the next higher test level, 4.36 KJ/cm^2; off-scale in Fig. 15. It is evident, then, that the penetration/energy density relationships for materials tested over a wide range of energy densities appears somewhat as shown schematically in Fig. 16, which illustrates how the use of high power conditions shift both the initiation of penetration and the initiation of melting to lower energy densities.

The plotted data for 1018, 4140, and 4340 does not include points for melted specimens. A similar treatment cannot be used for the other materials that were less extensively investigated. Therefore, solid, melted-specimen points have been shown in Figs. 17 through 22. These figures illustrate the influence of laser power on the penetration/energy density relationship for 2-1/4 Cr-1 Mo, HY-100, HY-80, H-11, Type 422 and 17-4PH steel. If we ignore, for the present, the data for

HY-100 and HY-80 steel that includes some tests with thin specimens and Fig. 21 for Type 422 that was examined at a single power level, the balance show the same trend observed previously. With some exceptions, a decrease in laser power leads to an increase in slope and a decrease in intercept.

The penetration equations for all the materials are summarized in Table XVII which presents the equations for 1018, 4140 and 4340 steel in two forms; with and without consideration of specimens that exhibited melting. It can be seen by comparing the data for higher laser powers that omitting the melted-specimen points resulted in a slight increase in slope (an indication of greater penetrations than when melted-specimen data are considered).

Effect of Specimen Thickness

Tests of both HY-100 steel and HY-80 steel were conducted, either totally or in part, with specimens that were thinner than desired. The possibility that these specimens might not provide adequate heat transmission was recognized.

All of the HY-100 specimens were 5/16 inch (7.9 mm) thick. All of the HY-80 steel specimens tested at 10.0 KW and three of those tested at 7.5 KW (at the lowest travel speeds) were only 1/4-inch (6.4 mm) thick. The remainder of the HY-80 specimens; five tested at 12.5 KW and two tested at the highest speeds at 7.5 KW, were 5/8-inch (15.9 mm) thick.

Inspection of Table XVII reveals that the slopes of the penetration equations for thin-section HY-100 and HY-80 steel are high, indicating deeper penetration in these steels with increasing energy density than in the other ferritic materials. In fact, the slopes for 5/16-inch-thick HY-100 steel at 12.5 and 10.0 KW appear to match best with the slopes for martensitic 17-4 PH steel which, as a consequence of its high alloy content, has a thermal conductivity of the same order as austenitic Type 304 stainless steel and would be expected to exhibit deeper penetration under any given conditions.

Since the thermal properties of low-alloy ferritic steels are similar, the data in Table XVII have been used to compare the depth of penetration in the HY steels with the penetration predicted in 1018, 4140, 4340 and 2-1/4 Cr-1 Mo steel, see Table XVIII. The calculations are based on energy densities of 1.0 and 6.0 KJ/cm^2 at power levels of 7.5, 10.0 and 12.5 KW. For consistency, the equations used are those that included melted-specimen data. Boxed values in Table XVIII direct attention to the unusually deep penetration

predicted for HY-100 and HY-80 steel in the instances where thin specimens were employed. The difference is most noticeable at the higher energy density and at the lower energy density at power levels of 7.5 and 10.0 KW. Under 12.5 KW conditions, the calculated penetration for HY-100 steel is negative and the value for HY-80 is also low. These values are a result of the displacement of the penetration curves which include erroneously high values at higher energy densities.

Figures 23, 24, and 25, for tests at 7.5, 10.0 and 12.5 KW, respectively, show the general scatterband for the low-alloy ferritic steels and the individual curves for HY-100 and HY-80. Excessive penetration in 5/16-inch-thick HY-100 steel shows that these data are not representative of the thicker sections. The data for HY-80 steel at 12.5 KW using 5/8-inch-thick specimens is in acceptable agreement with the general scatterband. However, the balance of the HY-80 results, obtained totally or partially with 1/4-inch-thick specimens are also not representative of thick-section behavior.

Type 422 stainless was investigated with 3/8-inch-thick specimens at one laser power, 10.0 KW. The thermal conductivity of Type 422 (13 Cr-1 Mo) is unknown but it should not differ significantly from the thermal conductivity of 12 Cr, Type 410 stainless which is about 200 BTU/ft^2/hr/in/°F; in turn, similar to the thermal conductivity of H-11 die steel. If the data obtained with Type 422 specimens were not influenced by their thickness, the penetration should be similar to the penetration observed in H-11 steel and less than the penetration observed in low-conductivity 17-4 PH specimens. The table below compares the penetration in 10.0 KW tests for the three materials at energy densities of 1.0 and 6.0 KJ/cm^2.

Steel	Laser Power, KW	Thickness, in.	Approximate Thermal Conductivity, BTU/ft^2/hr/in/°F	Penetration (mm) at the Energy Density Shown	
				1.0 KJ/cm^2	6.0 KJ/cm^2
17-4 PH	10.0	1/2	160	1.11	7.06
Type 422	10.0	3/8	200	0.49	3.19
H-11	10.0	7/8	200	0.44	3.79

It appears that the data obtained with 3/8-inch-thick Type 422 stainless, at a laser power of 10.0 KW, is representative of the penetration in thicker sections.

HEAT-AFFECTED AREA

Area and Energy Density

The area*/energy density relationships for the various materials, showing the individual effect of different levels of laser power, are presented in Figs. 26 through 34. An analysis of the data obtained with both rough-machined and surface-ground specimens of 4140 steel (Codes BX and BY) and 4340 steel (Codes CX and CY) has shown that the areas (like penetrations) are not influenced by these surface conditions. Therefore, Fig. 26 for 4140 steel, and Fig. 27 for 4340 steel, include data points for both types of specimens.

Inspection of these figures (excluding those for HY-100 and HY-80 that involve thin specimens) shows that the area data also conforms to the general pattern for the penetration data shown schematically in Fig. 16. Significant differences in area are observed, at constant energy density, at least at the low end of the energy density range. The area equations for the various steels, at each level of laser power, are summarized in Table XIX.

Effect of Specimen Thickness

The equations in Table XIX provide another opportunity to check the validity of the data obtained with thin specimens of HY-100 and HY-80 steel. The slopes of the equations for conditions involving

*Heat-affected area includes fused metal in those instances where surface melting occurred.

thin sections (boxed values) may again be seen to be appreciably higher than the slopes for the other conventional steels indicating that the heat-affected areas at higher energy densities are unusually large. Table XX provides a comparison of the areas for the conventional steels and the HY steels at three levels of laser power, calculated as before at energy densities of 1.0 and 6.0 KJ/cm^2. Boxed values illustrate the significantly increased penetrations indicated for the thin-specimen tests. Scatterband comparisons for the conventional steels and the individual lines for HY-100 and HY-80 steel at power levels of 7.5, 10.0 and 12.5 KW are provided in Figs. 35, 36 and 37, respectively. Inspection shows that only the data for HY-80 obtained with 5/8-inch thick specimens at 12.5 KW can be considered to be typical of thick-section behavior.

The calculated penetrations, under 10.0 KW conditions, at energy densities of 1.0 and 6.0 KJ/cm^2 for 3/8-inch thick Type 422 stainless and thicker-section H-11 and 17-4 PH steel are compared below:

Steel	Laser Power, KW	Thickness, in.	Approximate Thermal Conductivity BTU/ft^2/hr/in/°F	Area (mm^2) at the Energy Density Shown 1.0 KJ/cm^2	6.0 KJ/cm^2
17-4 PH	10.0	1/2	160	16.8	90.3
Type 422	10.0	3/8	200	9.2	54.7
H-11	10.0	7/8	200	18.2	80.3

The heat-affected area developed in Type 422 is, as it should be, smaller than the area predicted for the lower conductivity material, 17-4 PH; indicating that the 3/8-inch specimens were adequate. In contrast to the penetration data, the areas predicted for similar-conductivity H-11 and Type 422 do not agree. However, their relationship confirms an assumption that the data obtained with 3/8-inch thick Type 422 is valid for thicker sections.

HARDNESS

Hardening requires that the material immediately below the surface of the specimen be heated to a temperature where it will transform to austenite and then cool at a rate fast enough to result in complete, or at least substantial, transformation to martensite. The potential for formation of martensite under any given cooling condition is determined by the hardenability of the steel. The hardness obtainable in martensite is primarily determined by the carbon content.

If specimens having adequate carbon and alloy content are traversed by a laser beam over a range of decreasing travel speeds, so that the heat input is continually increased, the hardness/energy density relationship will be similar to that shown schematically in Fig. 38. There are four characteristic regions:

Region A: Fast travel speeds result in brief thermal excursions with low heat input. The peak temperatures attained are insufficient for transformation. Hardening cannot occur. Depending on the prior thermal/mechanical history of the steel, however, some reduction in hardness may occur when the peak temperatures approach A_{C1}.

Region B: In this region the heat inputs will result in peak temperatures between A_{C1} and A_{C3}. The microstructure will be partially reaustenitized. A significant increase in hardness cannot occur until the peak temperatures are high enough to cause nearly complete transformation to austenite.

Region C: In region C the steel will experience thermal excursions with peak temperatures above the A_{C3}, and will be fully austenitic. Higher heat inputs will lead to high peak temperatures causing grain growth and solution of the less refractory carbides, thereby increasing the local hardenability. Over most of the range of peak temperatures the cooling rates will be fast. The steel will quench to form martensite. At the highest energy densities (longest interaction times) some reduction in hardness may be observed. The reduction could result from:

1. A slower rate of cooling and formation of transformation products other than martensite.
2. Increased decarburization.
3. Both

Region D: Heat inputs sufficient to cause melting.

Maximum and Average Hardness in Ferritic Steels

The surface hardness/energy density relationships for the ferritic steels (4140, 4340, 1018, 2-1/4 Cr-1 Mo, HY-100 and HY-80) are presented in Figs. 39 through 45. Inspection will show that, under the proper conditions, appreciable hardening was obtained. Table XXI summarizes the data for all the steels, showing the maximum hardness, the carbon content, the hardness anticipated at each carbon level in specimens quenched to form various amounts of martensite between 100 and 50%, and the calculated hardenability (Ideal Diameter)* of each composition based on bainitic factors given by Hollomon and Jaffe.[1]

*The Ideal Diameters are approximate. The carbon content of the various steels was determined by analysis. The balance of the calculations were based on nominal compositions and an assumed grain size of ASTM #7. The values given will suffice for comparison. Those for 1018, 4140 and 4340 steel are in good agreement with other values given in the literature.

Comparison of the predicted hardness values and the maximum hardness measured in any specimen reveals that, with the exception of the plain-carbon 1018 steel, the maximum hardnesses correspond to martensite contents of 90% or more. Actually, the 90% martensite value may be somewhat low, since it pertains to the HY-80 steel tested at a thickness of 1/4 inch. This material had a higher carbon content than the 5/8-inch thick HY-80 steel. Under equivalent conditions, somewhat greater hardness would be anticipated in the thin-section material. Instead it was lower. It is probable, therefore, that the quench rate for the thin specimens was somewhat slow. The average hardnesses obtainable by laser treatment are presented in Table XXII. The values were obtained by inspecting Figs. 39 through 45 and isolating the points that appear to correspond to region"C" in the schematic, Fig. 38; energy densities sufficient to fully reaustenitize, but not sufficient to melt. Again, (with the exception of the low-hardenability 1018 steel) the hardnesses are high, with indicated martensite levels of 90% or more, if we dismiss the suspiciously low value for the thin-section HY-80 steel.

Effect of Specimen Thickness

It is apparent from the data in Tables XXI and XXII that the cooling rate in the 1/4 inch thick HY-80 steel specimens was somewhat slow and the hardness obtained is not representative of the hardness expected in thick sections. Despite a higher carbon content (0.17% for 1/4"; 0.15% for 5/8") the maximum hardness in thin-section HY-80 was $2R_C$ lower than the maximum hardness in the thicker specimens. Similarly, the average hardness for the 1/4-inch specimens was $4R_C$ lower. Figure 44 showing the HY-80 data provides confirmation. The figure includes check marks indicating the hardness values for 5/8-inch thick specimens. In all instances, these points are on the high side of the scatter band.

The case for data obtained with 5/16-inch thick HY-100 steel specimens is not so clear. The HY-100 steel and the 5/8-inch thick HY-80 steel have identical carbon contents and developed the same maximum hardness. This is as it should be under the same cooling conditions. The average hardness for the HY-100 steel, however, is lower than the average hardness exhibited by the thicker HY-80 specimens. The difference, $2R_C$, may not be significant considering the small number of specimens involved and the usual scatter in hardness measurements. It appears that the data for HY-100 steel is probably acceptable. If there is a hardness decrease resulting from slower cooling in 5/16-inch thick specimens the effect is certainly a minor one.

Hardness/Energy Density Relationships

Of the various hardness/energy density curves for the ferritic steels, shown in Figs. 39 through 44, only those for 4140 steel and 4340 steel (Figs. 39 and 40, respectively) show reasonable similarity to the schematic, Fig. 38. Development of a curve showing all the characteristic of the schematic requires a steel with reasonably high carbon and alloy content and tests over a wide range of conditions. The plain-carbon steel, 1018, can develop significant hardness (about 43 R_C) but only in very small specimens subjected to an extremely fast quench. The hardenability is low. All of the other ferritic steels have adequate carbon and good hardenability and did show a significant hardness increase. However, the lower energy densities needed to show the inception of hardening were not always investigated.

The hardness/energy density plots are useful in showing the hardness that can be obtained with a given steel by judicious selection of energy densities. They are, however, a composite of individual curves for each power level employed, and the range of applicability is somewhat restricted. The data for 4140 steel, Fig. 39, can be used for illustration. Examination of Fig. 39 shows that at a constant energy density a wide variation in hardness is possible. At about 1.3 KJ/cm^2, for example, the hardness can range from 32 R_{30N} (indicating some softening of the material) to over 70 R_{30N}. At the lowest laser power, 5.0 KW, the material was softened. The next higher power, 7.5 KW, resulted in moderate hardening. Significant hardness was obtained only when the laser powers were high, 10.0 and 12.5 KW. The data for 4340 steel, Fig. 40, shows an identical trend at an energy density of 1.3 KJ/cm^2.

It is possible, using the data for either 4140 or 4340 steel, to select a range of energy densities over which consistent hardening and freedom from melting would be anticipated. The range from 1.5 to 3.0 KJ/cm^2 would appear to be suitable, if consideration was restricted to the three highest laser powers investigated. At the 5.0 KW level the data are sparse. At 5.0 KW of laser power, an energy density of 1.3 KJ/cm^2 did not result in hardening in any material. Appreciable hardening occurred at an energy density of 2.6 KJ/cm^2. However, the energy density that initiates hardening was not established.

The data for both 4140 and 4340 steel shows that somewhat above 3.0 KJ/cm^2 melting may be encountered, appearing first as the energy density increases, in specimens exposed to the higher power beams, 10.0 and 12.5 KW. Figures 39 and 40 both include points at energy densities of about 4.0 KJ/cm^2 for specimens treated at 7.5 KW that did not exhibit melting. Melting did occur at lower energy densities, however, when the laser power was higher. Melting was observed in a 12.5 KW specimens at 3.25 KJ/cm^2, and in three 10.0 KW specimens at an energy density of 3.5 KJ/cm^2. The same pattern may be seen in other hardness/energy density plots. These plots are a composite of individual curves applicable to the specific power levels investigated, each having its unique hardening-initiation and melt-initiation points as illustrated schematically in Fig. 46.

Development of a family of curves of the type shown in Fig. 46 requires many tests conducted over a wide range of energy densities.

Ideally, higher power conditions should be investigated over a lower range of energy densities (faster travel speeds to obtain shorter interaction times) while the lower power conditions should be more fully explored at higher energy densities (slower travel to increase interaction times). In the present investigation, only 4140 and 4340 steel were tested over a wide travel speed range (20 to 100 ipm) at all four power levels, and also developed significant hardness. Even then, we now know that the interaction time at 100 ipm (0.45 sec) was still too long to permit determination of the start of hardening when the power levels were 10.0 and 12.5 KW. Also, when the lowest power level, 5.0 KW, was employed, the interaction time (2.27 sec) at the slowest travel, 20 ipm, was still insufficient to cause melting. In all the other instances, the steels either did not harden significantly or travel speeds above 60 ipm were not investigated, limiting the data for the shorter interaction times.

The influence of travel speed on the hardness of the ferritic steels, at each laser power investigated, is shown in Figs. 47 through 53. Figures 47 and 48 for 4140 and 4340 steel (combined data for both rough-machined and surface-ground specimens in both instances) show the start of hardening at the lower powers, 5.0 and 7.5 KW, but do not indicate where melting would begin under these conditions. At 10.0 and 12.5 KW the travel speeds that introduced the risk of melting are defined, but the initiation of hardening was not determined. It is apparent, however, that when the higher powers are used, travel speeds faster than 4.2 cm/sec (100 ipm) can probably be used for hardening these high-hardenability steels. The other steels were all tested over a more restricted range of travel speeds. The onset of hardening is not apparent in these instances.

However, Figs. 50, 51, and 52 for 2-1/4 Cr-1 Mo, HY-100, and HY-80 steel, permit selection of conditions that will insure acceptable hardness and freedom from melting. In all cases, investigation of travel speeds faster than 2.52 cm/sec (60 ipm) is justified at power levels of 10.0 and 12.5 KW. The data for H-11 steel, see Fig. 53, was obtained over a very small speed range, 1.68 to 2.52 cm/sec (40 to 60 ipm), using a large number of specimens, and shows appreciable scatter. Additional tests would be required to establish conditions that would provide good, and consistent hardening. Specifically, tests at 12.5 KW would be needed at shorter interaction times to avoid surface melting. Melting was encountered at all travel speeds slower than 2.52 cm/sec (60 ipm) at the 12.5 KW level.

Hardening of Type 422 Stainless

Hardness data for Type 422 martensitic stainless steel is provided in Figs. 54 and 55. This hardenable, 12% chromium steel was treated only at 10.0 KW using travel speeds in the range 0.84 to 2.52 cm/sec (20 to 60 ipm). The corresponding energy densities

ranged from 5.6 to 1.9 KJ/cm^2. Melting occurred at energy densities of 3.2 KJ/cm^2 or more. The hardness values are summarized below:

Base Hardness		Laser-Treated Hardness			
		Range		Average	
R_{30N}	R_c	R_{30N}	R_c	R_{30N}	R_c
52	32	63/71	44/53	67	48

Type 422 stainess is reported to harden to between 70 and 73R_{30N} (51 and 55 R_c) when it is oil quenched.[2] The lower value refers to austenitization at 1750°F, the higher value to austenitization between 1900 and 2050°F; hold time one hour in either instance. Hardnesses obtained by laser treatments were lower. The highest individual value was 70R_{30N} (51 R_c) The average was 67 R_{30N} (48 R_c). The lower hardness may be a consequence of the brief thermal excursions typical of laser treatments and the sluggish transformation of the 12% chromium composition. Also, the carbon content of the material was low. The specified carbon for Type 422 is 0.20 to 0.25%. Two analyses of the material used in these tests showed 0.20 and 0.21%.

Hardening of 17-4 PH

Hardness data for 17-4 PH are shown in Figs. 56 and 57. This precipitation-hardenable stainless steel can attain hardnesses of 59-64R_{30N} (40-45 R_c) in the aged condition. It does not respond to quenching. The base hardness, in the annealed condition, was 56R_{30N} (37 R_c). Following laser treating, the average hardness was 54R_{30N} (35 R_c).

SUMMARY AND CONCLUSIONS

1. Data are presented showing the penetration and the cross-sectional area of the heat-affected zone, and the hardness produced by laser transformation-hardening treatments of a variety of steels (1018, 4140, 4340, 2-1/4 Cr-1 Mo, HY-100, HY-80, Type 422 and 17-4 PH). In general, the test conditions include laser output powers from 5.0 to 12.5 KW and travel speeds in the range 20 to 100 ipm (0.84 to 4.2 cm/sec) which, under the beam-size conditions used, translates to an energy density range from 0.52 to 7.01 KJ/cm^2. The full range of conditions was not, however, employed in tests of all the steels.

2. The depth of penetration and the cross-sectional area data are given in the form of plots versus the energy density, refined where possible, to illustrate the influence of laser power. The relationship for both penetration and area are linear over most of the energy-density range. Predictive equations are given in tables. The applicable energy-density range for the equations (energy density to initiate penetration or to initiate surface melting) can be obtained from the individual plots. The general effect of increased laser power is to reduce the energy density needed to form a heat-affected region and the energy density at which surface melting will occur.

3. The hardness data are presented in two forms, in plots giving the combined results at various laser powers as a function of energy density, and as hardness versus travel speed to better illustrate the influence of laser power level.

4. All of the tests of HY-100 steel and the majority of tests of HY-80 steel were conducted with relatively thin specimens, respectively, 5/16 and 1/4-inch thick. A comparison, under the same conditions, of the depth of penetration and cross-sectional area in these steels with the penetration and area in similar ferritic steels shows that the data for thin HY steels is not representative of truly thick material. However, the data obtained with 5/8-inch thick HY-80 steel (tests at a laser power of 12.5 KW) is acceptable.

5. Tests of Type 422 stainless, a martensitic 12 Cr-1 Mo composition, were conducted with 3/8-inch thick material; also under the 1/2-inch size considered most desirable. The penetration and area data obtained with these specimens is probably typical of what would be anticipated in thicker sections. Lower than expected hardness values can be ascribed to other causes which are discussed below.

6. All of the ferritic steels possessing adequate carbon and good hardenability (4140, 4340, 2-1/4 Cr-1 Mo, HY-100, HY-80 and H-11 with Ideal Diameters from 4.2 to 1.0 inches) showed a significant increase in hardness. In all cases where the specimens were thick enough to provide a rapid quench the maximum hardness corresponded to martensite contents between 95 and 100 per cent. The maximum hardness attained with 1/4 inch-thick HY-80 steel specimens indicated a martensite content of 90 per cent.

7. The average hardness for the above steels, with the exception of tests conducted with 1/4-inch thick HY-80 steel, indicates martensite contents in the range 90 to 95 per cent. The martensite content predicted by the average hardness in thin-section HY-80 steel specimens was 80 per cent.

8. The rate of quenching obtained by laser treatment of 1018 steel was not sufficient to produce significant hardness in this low-hardenability material (Ideal Diameter 0.5 inch). Both the maximum and the average hardnesses indicate a martensite content appreciably less than 50 per cent.

9. The hardness developed in 5/16-inch thick HY-100 steel specimens is evidently representative of the hardness that would be anticipated in thicker sections. If the use of 5/16-inch thick specimens resulted in a reduced rate of quenching the effect is a minor one.

10. The cooling rate in 1/4-inch thick HY-80 steel specimens was insufficient for the development of maximum transformation hardening. The maximum and average hardness measured in the thin HY-80 steel specimens ranged from 2 to 4 R_C lower than the hardness of 5/8-inch thick specimens which had a slightly lower carbon content.

11. The average hardness in transformation-hardened Type 422 martensitic-stainless was 48 R_C. Greater hardness (51-55 R_C) can be obtained by conventional heat treatment using long soak times and high austenitizing temperatures. In these tests, the influence of sluggish transformation was probable compounded by a carbon content on the low side of the specified range.

12. Tests were conducted with 4140 and 4340 steel using both rough-machined (milled or coarse ground) and surface-ground specimens. The difference in surface condition had no effect on the depth of penetration, cross-sectional area, or the hardness produced by laser treatments.

13. Comparison tests employing Type 422 martensitic, stainless steel specimens undertaken to determine if a nitrogen atmosphere would enhance hardness through formation of carbides showed the method was ineffective.

14. In the course of this investigation, about 250 transformation-hardened sections were etched and examined. Cracks or spalls were not observed.

REFERENCES

1. Hollomon, J. H., and Jaffe, L. D., "Ferrous Metallurgical Design", John Wiley and Sons, Inc., New York, NY.
2. "Alloy Digest", File Code: SS-173, Engineering Alloy Digest, Inc., Upper Montclair, NJ.

TABLE I

IDENTIFICATION OF MATERIALS

Code	Steel	Surface Finish	Thickness, in.	Initial Hardness	Tested At
AX	AISI 1018	Rough Machined	1/2	88 R_B	WLC
BX	AISI 4140	Rough Machined	1/2	20 R_C	WLC
BY	AISI 4140	Surface Ground	1/2	20 R_C	WLC
CX	AISI 4340	Rough Machined	1/2	21 R_C	WLC
CY	AISI 4340	Surface Ground	1/2	21 R_C	WLC
DX	17-4 PH	Rough Machined	1/2	37 R_C	WLC
5	Type 422	Rough Machined	3/8	32 R_C	AVCO
6	H-11	Rough Machined	7/8	86 R_B	AVCO
7	2-1/4Cr-1Mo	Rough Machined	1/2	80 R_B	AVCO
8	HY-100	Rough Machined	5/16	25 R_C	AVCO
9	HY-80	Rough Machined	5/8 1/4	96 R_B 95 R_B	AVCO AVCO

WLC = Westinghouse Laser Center, Sunnyvale, CA
AVCO = AVCO Everett Metalworking Lasers, Boston, MA

TABLE II

CHEMICAL COMPOSITIONS

Code	Steel	R&D C	Specified or Nominal Composition, Weight % C	Mn	Si	S	P	Ni	Cr	Mo	V	Cu	Ti	W	Cb
AX	1018	0.18	.15 .18	.60 .90		.05 max	.04 max								
BX/BY	4140	0.42	.38 .43	.75 1.00	.20 .35	.04 max	.04 max		.80 1.10	.15 .25					
CX/CY	4340	0.43	.38 .43	.60 .80	.20 .35	.04 max	.04 max	1.65 2.00	.70 .90	.20 .30					
DX	17-4PH		.04	.40	.50			4.25	16.5			3.6			2.5
5	Type 422*	0.20/0.21	.20 .25	1.00 max	1.00 max	.03 max	.04 max	.50 1.00	12.0 14.0	.75 1.25	.20 .50			.75 1.25	
6	H-11	0.42	.35	.30	.90				5.00	1.5	.40				
7	2-1/4Cr-1Mo	0.09	.15 max	.30 .60	.50 max	.03 max	.03 max		2.00 2.50	.90 1.10					
8	HY-100	0.15	.20 max	.10 .40	.15 35	.025 max	.025 max	2.25 3.50	1.00 1.80	.20 .60					
9	HY-80	0.15** 0.17***	.18 max	.10 .40	.15 .35	.025 max	.025 max	2.00 3.25	1.00 1.80	.20 .60					

*R&D Check: Mn .63, Ni .27, Cr 11.7, Mo 1.12

**5/8" thick

***1/4" thick

Dwg. 5608C 61

TABLE III

LASER HARDENING DATA FOR AISI 1018 STEEL

1/2" Thick, Base Hardness 88 R_B. Laser Beam 1.91 cm Square

Specimen	Laser Power, KW: Aero Window	Laser Power, KW: To Work	Travel: ipm	Travel: cm/sec	Interaction Time sec	Power Density KW/cm^2	Energy Density KJ/cm^2	Penetration: Total: in	Penetration: Total: mm	Penetration: Melt: in	Penetration: Melt: mm	Heat Affected Area: in^2	Heat Affected Area: mm^2	Average Surface Hardness R30N
AX7-4	5.0	4.2	20	0.84	2.27	1.16	2.63	.058	1.48			.035	22.6	21
AX8-1	5.0	4.2	40	1.68	1.14	1.16	1.31							26
AX8-2	5.0	4.2	60	2.52	0.76	1.16	0.88							29
AX8-3	5.1	4.2	80	3.36	0.57	1.16	0.66							26
AX8-4	5.0	4.2	100	4.20	0.45	1.16	0.52							25
AX1-1A	7.5	6.3	20	0.84	2.77	1.73	3.93	.114	2.49			.036	23.2	23
AX1-3	7.5	6.3	40	1.68	1.14	1.73	1.97	.046	1.16			.022	14.2	29
AX1-4	7.5	6.3	50	2.10	0.91	1.73	1.58	.026	0.67			.017	11.0	29
AX2-1	7.5	6.3	60	2.52	0.76	1.73	1.32	.017	0.42			.006	3.9	21
AX2-3	7.5	6.3	80	3.36	0.57	1.73	0.99							24
AX2-4	7.5	6.3	90	3.78	0.51	1.73	0.87							23
AX2-2	7.5	6.3	100	4.20	0.45	1.73	0.78							22
AX2-1	7.5	6.3	100	4.20	0.45	1.73	0.78							
AX3-2	10.0	8.4	20	0.84	2.27	2.31	5.24	.117	2.98	.013	0.32	.055	35.5	30
AX3-3	10.0	8.4	30	1.26	1.52	2.31	3.49	.085	2.17	.006	0.14	.049	31.6	28
AX3-4	10.0	8.4	40	1.68	1.14	2.31	2.61	.062	1.57			.032	20.6	33
AX4-1	10.0	8.4	50	2.10	0.91	2.31	2.10	.056	1.41			.024	15.5	31
AX4-2	10.0	8.4	60	2.52	0.76	2.31	1.76	.049	1.25			.018	11.6	28
AX4-3	10.0	8.4	70	2.94	0.65	2.31	1.50	.039	1.00			.022	14.2	34
AX4-4	10.0	8.4	80	3.36	0.57	2.31	1.32	.036	0.91			.018	11.6	31
AX5-1	10.0	8.4	90	3.78	0.51	2.31	1.16	.026	0.67			.010	6.5	23
AX5-2	10.0	8.4	100	4.20	0.45	2.31	1.04	.023	0.58			.010	6.5	29
AX5-3	12.5	10.5	20	0.84	2.27	2.89	6.56	.113	2.88	.023	0.59	.077	49.7	19
AX5-4	12.5	10.5	30	1.26	1.52	2.89	4.36	.092	2.33	.009	0.22	.055	35.5	29
AX6-1	12.5	10.5	40	1.68	1.14	2.89	3.27	.069	1.75	.006	0.14	.042	27.1	39
AX6-2	12.5	10.5	50	2.10	0.91	2.89	2.63	.059	1.50			.038	24.5	37
AX6-3	12.5	10.5	60	2.52	0.76	2.89	2.20	.052	1.33			.036	23.2	41
AX6-4	12.5	10.5	70	2.94	0.65	2.89	1.88	.056	1.41			.036	23.2	41
AX7-1	12.5	10.5	80	3.36	0.57	2.89	1.65	.054	1.38			.019	12.3	34
AX7-2	12.5	10.5	90	3.78	0.51	2.89	1.45	.036	0.91			.019	12.3	35
AX7-3	12.5	10.5	100	4.20	0.45	2.89	1.30	.035	0.88			.026	16.8	37

Dwg. 4264874

TABLE IV

LASER HARDENING DATA FOR AISI 4140 STEEL

1/2" Thick, Base Hardness 20 R_C, Laser Beam 1.91 cm Square

Specimen	Laser Power, KW		Travel		Interaction Time	Power Density	Energy Density	Penetration				Heat Affected Area		Average Surface Hardness	
								Total		Melt					
	Aero Window	To Work	ipm	cm/sec	sec	KW/cm^2	KJ/cm^2	in	mm	in	mm	in^2	mm^2	R30N	Rc
BX1-1A	7.5	6.3	20	0.84	2.27	1.73	3.93	.082	2.09	.015	0.40	.042	27.1	66	47
BX1-3	7.5	6.3	40	1.68	1.14	1.73	1.97	.052	1.31			.018	11.6	73	55
BX1-4	7.5	6.3	50	2.10	0.91	1.73	1.58	.029	0.74			.014	9.0	76	59
BX2-1	7.5	6.3	60	2.52	0.76	1.73	1.32	.009	0.22			.005	3.2	57	32
BX2-2	7.5	6.3	70	2.94	0.65	1.73	1.13							44	22
BX2-3	7.5	6.3	80	3.36	0.57	1.73	0.99							39	
BX2-4	7.5	6.3	90	3.78	0.51	1.73	0.87							33	
BX3-1	7.5	6.3	100	4.20	0.45	1.73	0.78							40	
BX3-2	10.0	8.4	20	0.84	2.27	2.31	5.24	.119	3.01	.025	0.64	.070	45.2	50	30
BX3-3	10.0	8.4	40	1.68	1.14	2.31	2.61	.066	1.68			.038	24.5	72	54
BX3-4	10.0	8.4	60	2.52	0.76	2.31	1.76	.041	1.03			.022	14.2	72	54
BX4-1	10.0	8.4	70	2.94	0.65	2.31	1.50	.031	0.78			.018	11.6	71	52
BX4-2	10.0	8.4	80	3.36	0.57	2.31	1.32	.027	0.68			.012	7.7	72	54
BX4-3	10.0	8.4	90	3.78	0.51	2.31	1.16	.021	0.54			.009	5.8	69	50
BX4-4	10.0	8.4	100	4.20	0.45	2.31	1.04	.016	0.41			.009	5.8	75	57

Dwg. 5608C62

TABLE V

LASER HARDENING DATA FOR AISI 4140 STEEL - SURFACE GROUND

1/2" Thick, Base Hardness 20 R_c, Laser Beam 1.91 cm Square

Specimen	Laser Power, KW: Aero Window	Laser Power, KW: To Work	Travel: ipm	Travel: cm/sec	Interaction Time sec	Power Density KW/cm^2	Energy Density KJ/cm^2	Penetration: Total: in	Penetration: Total: mm	Penetration: Melt: in	Penetration: Melt: mm	Heat Affected Area: in^2	Heat Affected Area: mm^2	Average Surface Hardness: R30N	Average Surface Hardness: Rc
BY7-4	5.0	4.2	20	0.84	2.27	1.16	2.63	.064	1.62			.028	18.1	64	45
BY8-1	5.0	4.2	40	1.68	1.14	1.16	1.31							33	
BY8-2	5.0	4.2	60	2.52	0.76	1.16	0.88							33	
BY8-3	5.0	4.2	80	3.36	0.57	1.16	0.66							34	
BY8-4	5.0	4.2	100	4.20	0.45	1.16	0.52							33	
BY1-1A	7.5	6.3	20	0.84	2.27	1.73	3.93	.081	2.07			.042	27.1	69	51
BY1-3	7.5	6.3	40	1.68	1.14	1.73	1.97	.040	1.01			.016	10.3	69	51
BY1-4	7.5	6.3	50	2.10	0.91	1.73	1.58	.029	0.73			.014	9.0	70	52
BY2-1	7.5	6.3	60	2.52	0.76	1.73	1.32	.009	0.23			.008	5.2	53	53
BY2-3	7.5	6.3	80	3.36	0.57	1.73	0.99							33	
BY2-4	7.5	6.3	90	3.78	0.51	1.73	0.87							32	
BY2-2	7.5	6.3	100	4.20	0.45	1.73	0.78							32	
BY3-1	7.5	6.3	100	4.20	0.45	1.73	0.78							33	
BY3-2	10.0	8.4	20	0.84	2.27	2.31	5.24	.126	3.20	.027	0.68	.068	43.9	56	36
BY3-3	10.0	8.4	30	1.26	1.52	2.31	3.49	.091	2.30	.007	0.19	.050	32.3	64	45
BY3-4	10.0	8.4	40	1.68	1.14	2.31	2.61	.069	1.76			.040	25.8	64	45
BY4-1	10.0	8.4	50	2.10	0.91	2.31	2.10	.048	1.22			.024	15.5	66	47
BY4-2	10.0	8.4	60	2.52	0.76	2.31	1.76	.038	0.96			.017	11.0	68	50
BY4-3	10.0	8.4	70	2.94	0.65	2.31	1.50	.033	0.83			.017	11.0	68	50
BY4-4	10.0	8.4	80	3.36	0.57	2.31	1.32	.029	0.74			.016	10.3	66	47
BY5-1	10.0	8.4	90	3.78	0.51	2.31	1.16	.016	0.41			.012	7.7	60	41
BY5-2	10.0	8.4	100	4.20	0.45	2.31	1.04							70	52
BY5-3	12.5	10.5	20	0.84	2.27	2.89	6.56	.118	3.00	.028	0.70	.074	47.7	56	38
BY5-4	12.5	10.5	30	1.26	1.52	2.89	4.36	.104	2.63	.023	0.59	.058	37.4	66	47
BY6-1	12.5	10.5	40	1.68	1.14	2.89	3.27	.075	1.90	.002	0.05	.044	28.4	69	51
BY6-2	12.5	10.5	50	2.10	0.91	2.89	2.63	.065	1.66			.038	24.5	69	50
BY6-3	12.5	10.5	60	2.52	0.76	2.89	2.20	.065	1.64			.036	23.2	67	49
BY6-4	12.5	10.5	70	2.94	0.65	2.89	1.88	.060	1.52			.033	21.3	64	44
BY7-1	12.5	10.5	80	3.36	0.57	2.89	1.65	.058	1.47			.022	14.2	67	49
BY7-2	12.5	10.5	90	3.78	0.51	2.89	1.45	.047	1.19			.017	11.0	69	51
BY7-3	12.5	10.5	100	4.20	0.45	2.89	1.30	.035	0.89			.037	23.9	66	48

Dwg. 4264875

TABLE VI

LASER HARDENING DATA FOR AISI 4340 STEEL

1/2" Thick, Base Hardness 21 R_c, Laser Beam 1.91 cm Square

Specimen	Laser Power, KW		Travel		Interaction Time	Power Density	Energy Density	Penetration				Heat Affected Area		Average Surface Hardness	
								Total		Melt					
	Aero Window	To Work	ipm	cm/sec	sec	KW/cm^2	KJ/cm^2	In	mm	In	mm	In^2	mm^2	R30N	Rc
CX1-1A	7.5	6.3	20	0.84	2.27	1.73	3.93	.101	2.57			.054	34.8	54	33
CX1-3	7.5	6.3	40	1.68	1.14	1.73	1.97	.042	1.07			.022	14.2	75	58
CX1-4	7.5	6.3	50	2.10	0.91	1.73	1.58	.032	0.82			.016	10.3	76	59
CX2-1	7.5	6.3	60	2.52	0.76	1.73	1.32	.014	0.36			.006	3.9	68	51
CX2-2	7.5	6.3	70	2.94	0.65	1.73	1.13							57	37
CX2-3	7.5	6.3	80	3.36	0.57	1.73	0.99							58	38
CX2-4	7.5	6.3	90	3.78	0.51	1.73	0.87							49	28
CX3-1	7.5	6.3	100	4.20	0.45	1.73	0.78							44	23
CX3-2	10.0	8.4	20	0.84	2.27	2.31	5.24	.135	3.42	.024	0.61	.075	48.4	62	43
CX3-3	10.0	8.4	30	1.26	1.52	2.31	3.49	.089	2.26	.008	0.20	.050	32.3	64	45
CX3-4	10.0	8.4	40	1.68	1.14	2.31	2.61	.070	1.79			.041	26.5	71	53
CX4-1	10.0	8.4	50	2.10	0.91	2.31	2.10	.053	1.34			.028	18.1	70	52
CX4-2	10.0	8.4	60	2.52	0.76	2.31	1.76	.041	1.03			.021	13.6	72	54
CX4-3	10.0	8.4	70	2.94	0.65	2.31	1.50	.037	0.94			.022	14.2	72	54
CX4-4	10.0	8.4	80	3.36	0.57	2.31	1.32	.030	0.76			.014	9.0	77	60
CX5-1	10.0	8.4	90	3.78	0.51	2.31	1.16	.021	0.53			.012	7.7	70	51
CX5-2	10.0	8.4	100	4.20	0.45	2.31	1.04	.015	0.38			.008	5.2	76	59

TABLE VII

LASER HARDENING DATA FOR AISI 4340 STEEL - SURFACE GROUND

1/2" Thick, Base Hardness 21 R_c, Laser Beam 1.91 cm Square

Specimen	Laser Power, KW: Aero Window	Laser Power, KW: To Work	Travel: ipm	Travel: cm/sec	Interaction Time sec	Power Density KW/cm^2	Energy Density KJ/cm^2	Penetration: Total in	Penetration: Total mm	Penetration: Melt in	Penetration: Melt mm	Heat Affected Area: in^2	Heat Affected Area: mm^2	Average Surface Hardness: R30N	Average Surface Hardness: Rc
CY7-4	5.0	4.2	20	0.84	2.27	1.16	2.63	.064	1.65			.027	17.4	70	52
CY8-1	5.0	4.2	40	1.68	1.14	1.16	1.31							37	
CY8-2	5.0	4.2	60	2.52	0.76	1.16	0.88							33	
CY8-3	5.0	4.2	80	3.36	0.57	1.16	0.66							37	
CY8-4	5.0	4.2	100	4.20	0.45	1.16	0.52							40	
CY1-1A	7.5	6.3	20	0.84	2.27	1.73	3.93	.098	2.48			.052	33.5	64	45
CY1-3	7.5	6.3	40	1.68	1.14	1.73	1.97	.041	1.05			.025	16.1	74	58
CY1-4	7.5	6.3	50	2.10	0.91	1.73	1.58	.037	0.93			.018	11.6	73	55
CY2-1	7.5	6.3	60	2.52	0.76	1.73	1.32	.015	0.39			.006	3.9	66	47
CY2-3	7.5	6.3	80	3.36	0.57	1.73	0.99							35	
CY2-4	7.5	6.3	90	3.78	0.51	1.73	0.87							39	
CY2-2	7.5	6.3	100	4.20	0.45	1.73	0.78							34	
CY2-1	7.5	6.3	100	4.20	0.45	1.73	0.78							37	
CY3-2	10.0	8.4	20	0.84	2.27	2.31	5.24	.131	3.33	.022	0.55	.074	47.7	50	30
CY3-3	10.0	8.4	30	1.26	1.52	2.31	3.49	.094	2.38	.006	0.16	.054	34.8	62	42
CY3-4	10.0	8.4	40	1.68	1.14	2.31	2.61	.070	1.79			.042	27.1	65	46
CY4-1	10.0	8.4	50	2.10	0.91	2.31	2.10	.056	1.42			.030	19.4	70	51
CY4-2	10.0	8.4	60	2.52	0.76	2.31	1.76	.041	1.05			.025	16.1	70	51
CY4-3	10.0	8.4	70	2.94	0.65	2.31	1.50	.034	0.87			.020	12.9	73	56
CY4-4	10.0	8.4	80	3.36	0.57	2.31	1.32	.030	0.76			.019	12.3	75	57
CY5-1	10.0	8.4	90	3.78	0.51	2.31	1.16	.024	0.62			.012	7.7	62	43
CY5-2	10.0	8.4	100	4.20	0.45	2.31	1.04	.020	0.50			.013	8.4	71	53
CY5-3	12.5	10.5	20	0.84	2.27	2.89	6.56	.144	3.65	.030	0.76	.094	60.6	63	44
CY5-4	12.5	10.5	30	1.26	1.52	2.89	4.36	.119	3.01	.024	0.61	.072	46.5	62	43
CY6-1	12.5	10.5	40	1.68	1.14	2.89	3.27	.083	2.10			.050	32.3	70	51
CY6-2	12.5	10.5	50	2.10	0.91	2.89	2.63	.071	1.80			.040	25.8	69	51
CY6-3	12.5	10.5	60	2.52	0.76	2.89	2.20	.059	1.51			.038	24.5	69	50
CY6-4	12.5	10.5	70	2.94	0.65	2.89	1.88	.059	1.51			.036	23.2	67	49
CY7-1	12.5	10.5	80	3.36	0.57	2.89	1.65	.043	1.08			.024	15.5	66	47
CY7-2	12.5	10.5	90	3.78	0.51	2.89	1.45	.043	1.10			.021	13.5	70	52
CY7-3	12.5	10.5	100	4.20	0.45	2.89	1.30	.037	0.95			.038	24.5	68	50

Dwg. 4264876

TABLE VIII

LASER HARDENING DATA FOR 17-4 PH STEEL

1/2" Thick, Base Hardness 37 R_c, Laser Beam 1.91 cm Square

Specimen	Laser Power, KW: Aero Window	Laser Power, KW: To Work	Travel: ipm	Travel: cm/sec	Interaction Time sec	Power Density KW/cm^2	Energy Density KJ/cm^2	Penetration: Total: In	Penetration: Total: mm	Penetration: Melt: In	Penetration: Melt: mm	Heat Affected Area: in^2	Heat Affected Area: mm^2	Average Surface Hardness: R30N	Average Surface Hardness: Rc
DX3-1	5.0	4.2	40	1.68	1.14	1.16	1.31	.049	1.25			.026	16.8	51	31
DX3-2	5.0	4.2	60	2.52	0.76	1.16	0.88	.026	0.67			.013	8.4	59	40
DX3-3	5.0	4.2	80	3.36	0.57	1.16	0.66							61	42
DX3-4	5.0	4.2	100	4.20	0.45	1.16	0.52							54	34
DX1-1	7.5	6.3	40	1.68	1.14	1.73	1.97	.062	1.58			.031	20.0	57	37
DX1-2	7.5	6.3	60	2.52	0.76	1.73	1.32	.043	1.08			.020	12.9	47	26
DX1-3	7.5	6.3	80	3.36	0.57	1.73	0.99	.026	0.67			.014	9.0	56	37
DX1-4	7.5	6.3	100	4.20	0.45	1.73	0.78							53	33
DX2-1	10.0	8.4	40	1.68	1.14	2.31	2.61	.118	2.99	.030	0.75	.064	41.3	59	40
DX2-2	10.0	8.4	60	2.52	0.76	2.31	1.76	.085	2.16			.041	26.5	54	34
DX2-3	10.0	8.4	80	3.36	0.57	2.31	1.32	.056	1.41			.034	21.9	53	33
DX2-4	10.0	8.4	100	4.20	0.45	2.31	1.04	.046	1.16			.028	18.1	54	34

Dwg. 4264849

TABLE IX

LASER HARDENING DATA FOR TYPE 422

3/8" Thick, Base Hardness 32 R_c, Laser Beam 1.78 cm Square

Specimen	Laser Power, KW		Travel		Interaction Time	Power Density	Energy Density	Shield	Penetration				Heat Affected Area		Average Surface Hardness	
	Aero Window	To Work	ipm	cm/sec	sec	KW/cm^2	KJ/cm^2		Total		Melt		in^2	mm^2	R30N*	Rc
									in	mm	in	mm				
5-1-1	10.0	8.4	20	0.84	2.12	2.65	5.62	Nitrogen	0.117	2.97			0.078	50.3	59	39
5-1-2	10.0	8.4	20	0.84	2.12	2.65	5.62		0.113	2.87	0.015	0.40	0.081	52.3	64	45
5-2-1	10.0	8.4	25	1.05	1.70	2.65	4.51	Nitrogen	0.100	2.54			0.060	38.7	61	42
5-2-2	10.0	8.4	25	1.05	1.70	2.65	4.51		0.097	2.46	0.011	0.29	0.063	40.6	69	51
5-3-1	10.0	8.4	30	1.26	1.41	2.65	3.74	Nitrogen	0.078	1.98			0.057	36.8	60	41
5-3-2	10.0	8.4	30	1.26	1.41	2.65	3.74		0.081	2.06	0.009	0.22	0.054	34.8	68	49
5-4-1	10.0	8.4	35	1.47	1.21	2.65	3.21	Nitrogen	0.062	1.57			0.041	26.5	66	48
5-4-2	10.0	8.4	35	1.47	1.21	2.65	3.21		0.074	1.88	0.005	0.13	0.054	34.8	68	50
5-5-1	10.0	8.4	40	1.68	1.06	2.65	2.81	Nitrogen	0.043	1.09			0.030	19.4	69	51
5-5-2	10.0	8.4	40	1.68	1.06	2.65	2.81		0.061	1.55			0.043	27.7	71	53
5-6-1	10.0	8.4	45	1.89	0.94	2.65	2.49	Nitrogen	0.048	1.22			0.029	18.7	63	44
5-6-2	10.0	8.4	45	1.89	0.94	2.65	2.49		0.055	1.40			0.038	24.5	65	47
5-7-1	10.0	8.4	50	2.10	0.85	2.65	2.25	Nitrogen	0.034	0.86			0.026	16.8	68	50
5-7-2	10.0	8.4	50	2.10	0.85	2.65	2.25		0.050	1.27			0.035	22.6	63	44
5-8-1	10.0	8.4	55	2.31	0.77	2.65	2.04	Nitrogen	0.043	1.09			0.029	18.7	68	50
5-8-2	10.0	8.4	55	2.31	0.77	2.65	2.04		0.043	1.09			0.033	21.3	68	49
5-9-1	10.0	8.4	60	2.52	0.71	2.65	1.88	Nitrogen	0.043	1.09			0.028	18.1	65	47
5-9-2	10.0	8.4	60	2.52	0.71	2.65	1.88		0.040	1.02			0.026	16.8	65	47

*Converted From Rc

Dwg. 5608C56

TABLE X

LASER HARDENING DATA FOR H-11 STEEL

7/8" Thick. Base Hardness 86 R_B. Laser Beam 1.78 cm Square

Specimen	Laser Power, KW Aero Window	Laser Power, KW To Work	Travel ipm	Travel cm/sec	Interaction Time sec	Power Density KW/cm^2	Energy Density KJ/cm^2	Penetration Total in	Penetration Total mm	Penetration Melt in	Penetration Melt mm	Heat Affected Area in^2	Heat Affected Area mm^2	Average Surface Hardness R30N*	Average Surface Hardness Rc
6-1-2	7.5	6.3	40	1.68	1.06	1.99	2.11	0.048	1.22			0.031	20.0	74	56
6-6-1	7.5	6.3	40	1.68	1.06	1.99	2.11	0.036	0.91			0.024	15.5	68	50
6-2-2	7.5	6.3	45	1.89	0.94	1.99	1.87	0.041	1.04			0.022	14.2	67	48
6-7-1	7.5	6.3	45	1.89	0.94	1.99	1.87	0.032	0.81			0.020	12.9	63	44
6-3-2	7.5	6.3	50	2.10	0.85	1.99	1.69	0.030	0.76			0.020	12.9	76	59
6-6-2	7.5	6.3	50	2.10	0.85	1.99	1.69	0.020	0.51			0.012	7.7	57	33
6-4-2	7.5	6.3	55	2.31	0.77	1.99	1.53	0.023	0.58			0.013	8.4	65	47
6-5-2	7.5	6.3	60	2.52	0.71	1.99	1.41	0.022	0.59			0.015	9.7	65	46
6-7-2	7.5	6.3	60	2.52	0.71	1.99	1.41	0.015	0.38			0.008	5.2	61	42
6-1-1	10.0	8.4	40	1.68	1.06	2.65	2.81	0.070	1.78			0.048	31.0	73	55
6-6-3	10.0	8.4	40	1.68	1.06	2.65	2.81	0.062	1.57	0.011	0.27	0.045	29.0	76	60
6-7-4	10.0	8.4	42.5	1.79	0.99	2.65	2.62	0.060	1.52	0.009	0.22	0.040	25.8	76	60
6-2-1	10.0	8.4	45	1.89	0.94	2.65	2.49	0.062	1.57			0.040	25.8	65	46
6-7-3	10.0	8.4	45	1.89	0.94	2.65	2.49	0.054	1.37			0.036	23.2	76	59
6-3-1	10.0	8.4	50	2.10	0.85	2.65	2.25	0.052	1.32			0.034	21.9	76	59
6-6-4	10.0	8.4	50	2.10	0.85	2.65	2.25	0.047	1.19	0.003	0.07	0.032	20.6	75	58
6-4-1	10.0	8.4	55	2.31	0.77	2.65	2.04	0.048	1.22			0.032	20.6	65	46
6-5-1	10.0	8.4	60	2.52	0.71	2.65	1.88	0.040	1.02			0.028	18.1	65	46
6-1-3	12.5	10.5	40	1.68	1.06	3.31	3.51	0.071	1.80	0.012	0.28	0.056	36.1	74	56
6-2-3	12.5	10.5	42.5	1.79	0.99	3.31	3.28	0.077	1.96			0.052	33.5	73	55
6-8-3	12.5	10.5	42.5	1.79	0.99	3.31	3.28	0.070	1.78	0.016	0.39	0.049	31.6	79	62
6-3-3	12.5	10.5	45	1.89	0.94	3.31	3.11	0.069	1.75			0.051	32.9	68	49
6-8-1	12.5	10.5	45	1.89	0.94	3.31	3.11	0.064	1.63	0.012	0.31	0.043	27.7	79	62
6-4-3	12.5	10.5	47.5	2.00	0.89	3.31	2.95	0.066	1.68			0.047	30.3	72	54
6-9-3	12.5	10.5	47.5	2.00	0.89	3.31	2.95	0.065	1.65	0.014	0.35	0.043	27.7	78	61
6-5-3	12.5	10.5	50	2.10	0.85	3.31	2.81	0.062	1.57			0.044	28.4	76	60
6-9-1	12.5	10.5	50	2.10	0.85	3.31	2.81	0.063	1.60	0.011	0.28	0.042	27.1	78	61
6-1-4	12.5	10.5	52.5	2.21	0.81	3.31	2.68	0.063	1.60			0.043	27.7	73	55
6-8-4	12.5	10.5	52.5	2.21	0.81	3.31	2.68	0.059	1.58	0.014	0.36	0.040	25.8	79	62
6-2-4	12.5	10.5	55	2.31	0.77	3.31	2.55	0.066	1.68			0.048	31.0	76	59
6-8-2	12.5	10.5	55	2.31	0.77	3.31	2.55	0.057	1.45	0.011	0.27	0.040	25.8	79	62
6-3-4	12.5	10.5	57.5	2.42	0.74	3.31	2.45	0.059	1.50			0.042	27.1	69	51
6-9-4	12.5	10.5	57.5	2.42	0.74	3.31	2.45	0.056	1.42	0.009	0.23	0.036	23.2	79	62
6-4-4	12.5	10.5	60	2.52	0.71	3.31	2.35	0.057	1.45			0.040	25.8	69	52
6-9-2	12.5	10.5	60	2.52	0.71	3.31	2.35	0.053	1.35			0.035	22.6	79	62

*Converted From Rc

Dwg. 4264847

TABLE XI

LASER HARDENING DATA FOR 2 1/4 Cr – 1 Mo STEEL

1/2" Thick, Base Hardness 80 R_B, Laser Beam 1.78 cm Square

Specimen	Laser Power, KW		Travel		Interaction Time	Power Density	Energy Density	Penetration				Heat Affected Area		Average Surface Hardness	
								Total		Melt					
	Aero Window	To Work	ipm	cm/sec	sec	KW/cm^2	KJ/cm^2	in	mm	in	mm	in^2	mm^2	R30N	Rc
7-1-1	7.5	6.3	20	0.84	2.12	1.99	4.22	0.082	2.08			0.049	31.6	50	29
7-1-2	7.5	6.3	25	1.05	1.70	1.99	3.38	0.070	1.78			0.042	27.1	52	31
7-1-3	7.5	6.3	30	1.26	1.41	1.99	2.81	0.056	1.42			0.032	20.6	52	31
7-2-1	7.5	6.3	35	1.47	1.21	1.99	2.41	0.048	1.22			0.027	17.4	56	36
7-2-2	7.5	6.3	40	1.68	1.06	1.99	2.11	0.047	1.19			0.024	15.5	54	34
7-2-3	7.5	6.3	45	1.89	0.94	1.99	1.87	0.043	1.09			0.022	14.2	56	36
7-3-1	7.5	6.3	50	2.10	0.85	1.99	1.69	0.036	0.91			0.017	11.0	53	33
7-3-2	7.5	6.3	55	2.31	0.77	1.99	1.53	0.033	0.84			0.017	11.0	47	26
7-3-3	7.5	6.3	60	2.52	0.71	1.99	1.41	0.030	0.76			0.020	12.9	45	24
7-4-1	10.0	8.4	20	0.84	2.12	2.65	5.62	0.129	3.28			0.075	48.4	45	24
7-4-2	10.0	8.4	25	1.05	1.70	2.65	4.51	0.118	3.00			0.070	45.2	46	25
7-4-3	10.0	8.4	30	1.26	1.41	2.65	3.74	0.098	2.49	0.020	0.50	0.054	34.8	54	34
7-5-1	10.0	8.4	35	1.47	1.21	2.65	3.21	0.086	2.18			0.048	31.0	53	33
7-5-2	10.0	8.4	40	1.68	1.06	2.65	2.81	0.070	1.78			0.039	25.2	53	32
7-5-3	10.0	8.4	45	1.89	0.94	2.65	2.49	0.059	1.50			0.036	23.2	54	34
7-6-1	10.0	8.4	50	2.10	0.85	2.65	2.25	0.049	1.24			0.032	20.6	57	37
7-6-2	10.0	8.4	55	2.31	0.77	2.65	2.04	0.051	1.30			0.033	21.3	56	36
7-6-3	10.0	8.4	60	2.52	0.71	2.65	1.88	0.046	1.16			0.025	16.1	53	33
7-7-1	12.5	10.5	20	0.84	2.12	3.31	7.01	0.160	4.06	0.053	1.35	0.094	60.6	41	19
7-7-2	12.5	10.5	25	1.05	1.70	3.31	5.63	0.144	3.66	0.047	1.20	0.085	54.8	44	23
7-7-3	12.5	10.5	30	1.26	1.41	3.31	4.67	0.120	3.05	0.033	0.85	0.067	43.2	49	28
7-8-1	12.5	10.5	35	1.47	1.21	3.31	4.01	0.095	2.65	0.025	0.63	0.054	34.8	52	31
7-8-2	12.5	10.5	40	1.68	1.06	3.31	3.51	0.088	2.23	0.018	0.45	0.054	34.8	50	29
7-8-3	12.5	10.5	45	1.89	0.94	3.31	3.11	0.076	1.93	0.013	0.33	0.044	28.4	52	31
7-2-4	12.5	10.5	50	2.10	0.85	3.31	2.81	0.073	1.65	0.006	0.15	0.045	29.0	57	37
7-2-5	12.5	10.5	55	2.31	0.77	3.31	2.55	0.072	1.83			0.043	27.7	56	36
7-2-6	12.5	10.5	60	2.52	0.71	3.31	2.35	0.052	1.32			0.034	21.9	57	37

Dwg. 4264848

TABLE XII

LASER HARDENING DATA FOR HY-100 STEEL

5/16" Thick, Base Hardness 25 R_c, Laser Beam 1.78 cm Square

Specimen	Laser Power, KW		Travel		Interaction Time	Power Density	Energy Density	Penetration				Heat Affected Area		Average Surface Hardness	
	Aero Window	To Work						Total		Melt					
			ipm	cm/sec	sec	KW/cm^2	KJ/cm^2	in	mm	in	mm	in^2	mm^2	R30N	Rc
8-7-1	7.5	6.3	20	0.84	2.12	1.99	4.22	0.131	3.33			0.075	48.4	48	27
8-7-2	7.5	6.3	30	1.26	1.41	1.99	2.81	0.082	2.08			0.046	29.7	53	32
8-8-1	7.5	6.3	40	1.68	1.06	1.99	2.11	0.066	1.68			0.039	25.2	58	38
8-8-2	7.5	6.3	50	2.10	0.85	1.99	1.69	0.058	1.47			0.033	21.3	58	38
8-4-1	10.0	8.4	20	0.84	2.12	2.65	5.62	0.211	5.36	0.011	0.27	0.113	72.9	41	19
8-4-2	10.0	8.4	30	1.26	1.41	2.65	3.74	0.116	2.95	0.006	0.15	0.069	44.5	50	29
8-5-1	10.0	8.4	35	1.47	1.21	2.65	3.21	0.102	2.59	0.005	0.12	0.060	38.7	55	35
8-5-2	10.0	8.4	40	1.68	1.06	2.65	2.81	0.097	2.21			0.052	33.5	56	36
8-6-1	10.0	8.4	50	2.10	0.85	2.65	2.25	0.056	1.42			0.036	23.2	55	35
8-6-2	10.0	8.4	60	2.52	0.71	2.65	1.88	0.056	1.42			0.033	21.3	59	39
8-1-1	12.5	10.5	20	0.84	2.12	3.31	7.01	0.315*	8.00*			0.165	106.5	44	22
8-1-2	12.5	10.5	30	1.26	1.41	3.31	4.67	0.148	3.76	0.011	0.29	0.085	54.8	48	27
8-2-1	12.5	10.5	40	1.68	1.06	3.31	3.51	0.111	2.82	0.009	0.22	0.069	44.5	52	31
8-2-2	12.5	10.5	50	2.10	0.85	3.31	2.81	0.083	2.11	0.004	0.11	0.049	31.6	54	34
8-3-1	12.5	10.5	60	2.52	0.71	3.31	2.35	0.073	1.85			0.046	29.7	56	36

*Full Thickness of Specimen.

Dwg. 4264845

TABLE XIII

LASER HARDENING DATA FOR HY-80 STEEL

1/4" and 5/8" Thick, Base Hardness 95 R_B, Laser Beam 1.78 cm Square

Specimen	Laser Power, KW		Travel		Interaction Time	Power Density	Energy Density	Penetration				Heat Affected Area		Average Surface Hardness	
								Total		Melt					
	Aero Window	To Work	ipm	cm/sec	sec	KW/cm^2	KJ/cm^2	in	mm	in	mm	in^2	mm^2	R30N	Rc
9-6-2	7.5	6.3	20	0.84	2.12	1.99	4.22	0.135	3.43			0.074	47.7	47	26
9-7-1	7.5	6.3	30	1.26	1.41	1.99	2.81	0.080	2.03			0.043	27.7	52	31
9-7-2	7.5	6.3	40	1.68	1.21	1.99	2.11	0.063	1.60			0.036	23.2	55	35
9-3-3*	7.5	6.3	50	2.10	0.85	1.99	1.69	0.054	1.37			0.032	20.6	59	39
9-3-4*	7.5	6.3	60	2.52	0.71	1.99	1.41	0.040	1.02			0.022	14.2	57	37
9-3-2	10.0	8.4	20	0.84	2.12	2.65	5.62	0.172	4.37	0.017	0.42	0.105	67.7	51	30
9-4-1	10.0	8.4	30	1.26	1.41	2.65	3.74	0.125	3.18	0.017	0.44	0.071	45.8	52	31
9-4-2	10.0	8.4	35	1.47	1.21	2.65	3.21	0.107	2.72	0.007	0.19	0.064	41.3	53	33
9-5-1	10.0	8.4	40	1.68	1.06	2.65	2.81	0.074	1.88			0.042	27.1	53	33
9-5-2	10.0	8.4	50	2.10	0.85	2.65	2.25	0.063	1.60			0.035	22.6	54	34
9-6-1	10.0	8.4	60	2.52	0.71	2.65	1.88	0.048	1.22			0.027	17.4	57	37
9-1-1*	12.5	10.5	20	0.84	2.12	3.31	7.01	0.182	4.62	0.017	0.44	0.109	70.3	53	32
9-1-2*	12.5	10.5	30	1.26	1.41	3.31	4.67	0.096	2.44	0.017	0.44	0.057	36.8	57	37
9-2-1*	12.5	10.5	40	1.68	1.06	3.31	3.51	0.091	2.31	0.007	0.18	0.051	32.9	56	36
9-2-2*	12.5	10.5	50	2.10	0.85	3.31	2.81	0.073	1.85			0.042	27.1	57	37
9-3-1*	12.5	10.5	60	2.52	0.71	3.31	2.35	0.048	1.22			0.028	18.1	59	39

*5/8" Thick Specimens

TABLE XIV

Summary of Test Parameters and Specimens

Code	Steel	Tested At	Number of Specimens Tested at the Specified Laser Power, KW				Travel Speed Range		Interaction Time Range, sec	Energy Density Range, KJ/cm^2
			5.0	7.5	10.0	12.5	ipm	cm/sec		
AX	1018	WLC	5	8	9	9	20/100	0.84/4.20	2.27/0.45	0.52/6.56
BX & BY*	4140	WLC	5	16	16	9	20/100	0.84/4.20	2.27/0.45	0.52/6.56
CX & CY*	4340	WLC	5	16	16	9	20/100	0.84/4.20	2.27/0.45	0.52/6.56
DX	17-4PH	WLC	4	4	4		40/100	1.68/4.20	1.13/0.45	0.52/2.61
5	Type 422	AVCO			18		20/60	0.84/2.52	2.11/0.71	1.88/5.62
6	H-11	AVCO		9	9	17	40/60	1.68/2.52	1.06/0.71	1.41/3.51
7	2-1/4 Cr-1 Mo	AVCO		9	9	9	20/60	0.84/2.52	2.11/0.71	1.41/7.01
8	HY-100	AVCO		4	6	5	20/60	0.84/2.52	2.11/0.71	1.41/7.01
9	HY-80	AVCO		5	6	5	20/60	0.84/2.52	2.11/0.71	1.41/7.01

*Combined number of specimens in both the rough machined and surface ground conditions.

TABLE XV

SUMMARY OF DATA FROM THE GENERAL PENETRATION/ENERGY DENSITY CURVES

Steel	Critical Energy Density KJ/cm^2	Heat Affected Zone Penetration at the Critical Energy Density mm	in	Total Penetration Equation, mm
4140	3.0	1.7	0.067	$0.55\bar{E} + 0.05$
4340	2.9	1.8	0.071	$0.65\bar{E} - 0.01$
1018	2.6	1.5	0.059	$0.49\bar{E} + 0.23$
2-1/4Cr-1Mo	2.3	1.25	0.049	$0.61\bar{E} - 0.14$
HY-100	2.2	1.65	0.065	$0.82\bar{E} - 0.13$
HY-80	2.0	1.4	0.055	$0.72\bar{E} - 0.03$
H-11	1.8	0.65	0.025	$2.9 - \frac{4.1}{E}$
Type 422	1.8	0.90	0.035	$0.54\bar{E} - 0.05$
17-4 PH	2.0	2.3	0.091	$0.86\bar{E}^{-1.28}$

TABLE XVI

COMPARISON OF PENETRATION AT ESSENTIALLY CONSTANT ENERGY DENSITY

Steel	Laser Power KW	Travel ipm	Travel cm/sec	Interaction Time, sec	Power Density, KW/cm^2	Energy Density KJ/cm^2	HAZ Penetration mm	HAZ Penetration in
1018	5.0	40	1.68	1.14	1.16	1.31	-	-
	7.5	60	2.52	0.76	1.73	1.32	0.42	0.016
	10.0	80	3.36	0.57	2.31	1.32	0.91	0.036
	12.5	100	4.20	0.45	2.89	1.30	0.88	0.035
4140	5.0G	40	1.68	1.14	1.16	1.31	-	-
	7.5G	60	2.52	0.76	1.73	1.32	0.23	0.009
	7.5R	60	2.52	0.76	1.73	1.32	0.22	0.009
	10.0G	80	3.36	0.57	2.31	1.32	0.74	0.029
	10.0R	80	3.36	0.57	2.31	1.32	0.68	0.027
	12.5G	100	4.20	0.45	2.89	1.30	0.89	0.035
4340	5.0G	40	1.68	1.14	1.16	1.31	-	-
	7.5G	60	2.52	0.76	1.73	1.32	0.39	0.015
	7.5R	60	2.52	0.76	1.73	1.32	0.36	0.014
	10.0G	80	3.36	0.57	2.31	1.32	0.76	0.030
	10.0R	80	3.36	0.57	2.31	1.32	0.76	0.030
	12.5G	100	4.20	0.45	2.89	1.30	0.95	0.037

G = Ground specimen data (Code BY for 4140; Code CX for 4340)
R = Rough-machined specimen data (Code BX for 4140; Code CX for 4340)

TABLE XVII

SUMMARY OF PENETRATION DATA FOR SELECTED LASER POWERS

Steel	Laser Power, KW	Thickness in	Penetration Equation (mm) Including Melt Data	Excluding Melt Data
1018	12.5	1/2	$0.37\bar{E} + 0.56$	$0.44\bar{E} + 0.42$
	10.0	1/2	$0.52\bar{E} + 0.18$	$0.64\bar{E} + 0.00$
	7.5	1/2	$0.77\bar{E} - 0.52$	$0.77\bar{E} - 0.52$
4140	12.5	1/2	$0.38\bar{E} + 0.71$	$0.53\bar{E} + 0.41$
	10.0	1/2	$0.65\bar{E} - 0.15$	$0.82\bar{E} - 0.43$
	7.5	1/2	$0.70\bar{E} - 0.41$	$0.66\bar{E} - 0.39$
4340	12.5	1/2	$0.53\bar{E} + 0.36$	$0.58\bar{E} + 0.24$
	10.0	1/2	$0.70\bar{E} - 0.16$	$0.84\bar{E} - 0.39$
	7.5	1/2	$0.77\bar{E} - 0.49$	$0.77\bar{E} - 0.44$
2-1/4Cr-1Mo	12.5	1/2	$0.57\bar{E} + 0.21$	
	10.0	1/2	$0.62\bar{E} + 0.03$	
	7.5	1/2	$0.47\bar{E} + 0.14$	
HY-100	12.5	5/16	$1.32\bar{E} - 1.68$	
	10.0	5/16	$1.08\bar{E} - 0.87$	
	7.5	5/16	$0.75\bar{E} + 0.12$	
HY-80	12.5	5/8	$0.67\bar{E} - 0.25$	
	10.0	1/4	$0.86\bar{E} - 0.30$	
	7.5	*	$0.83\bar{E} - 0.14$	
H-11	12.5	7/8	$0.39\bar{E} + 0.53$	
	10.0	7/8	$0.67\bar{E} - 0.23$	
	7.5	7/8	$0.87\bar{E} - 0.76$	
Type 422	10.0	3/8	$0.54\bar{E} - 0.05$	
17-4 PH	10.0	1/2	$1.19\bar{E} - 0.08$	
	7.5	1/2	$0.91\bar{E} - 0.18$	
	5.0	1/2	$1.35\bar{E} - 0.52$	

*In 7.5KW tests of HY-80 steel, two specimens tested at the lowest energy densities were 5/8" thick. Four specimens tested at higher energy densities were 1/4" thick.

TABLE XVIII

PENETRATION COMPARISONS FOR CONVENTIONAL STEELS

Steel	Laser Power, KW	Thickness, in	Penetration (mm) at Energy Density Shown	
			1.0KJ/cm^2	6.0KJ/cm^2
1018	7.5	1/2	0.25	4.10
4140	7.5	1/2	0.29	3.79
4340	7.5	1/2	0.28	4.13
2-1/4Cr-1Mo	7.5	1/2	0.61	2.96
HY-100	7.5	5/16	0.87	4.62
HY-80	7.5	*	0.69	4.84
1018	10.0	1/2	0.70	3.30
4140	10.0	1/2	0.50	3.75
4340	10.0	1/2	0.54	4.04
2-1/4Cr-1Mo	10.0	1/2	0.65	3.75
HY-100	10.0	5/16	0.21	5.61
HY-80	10.0	1/4	0.56	4.86
1018	12.5	1/2	0.93	2.78
4140	12.5	1/2	1.09	2.99
4340	12.5	1/2	0.89	3.54
2-1/4Cr-1Mo	12.5	1/2	0.78	3.63
HY-100	12.5	5/16	-0.36	6.24
HY-80	12.5	5/8	0.42	3.77

*In 7.5KW tests of HY-80 steel, two specimens tested at the lowest energy densities were 5/8" thick. Four specimens tested at higher energy densities were 1/4" thick.

TABLE XIX

SUMMARY OF AREA DATA FOR SELECTED LASER POWERS

Steel	Laser Power, KW	Thickness, in.	Area Equation (mm^2)
1018	12.5	1/2	6.7 $\overline{E}$ + 6.1
	10.0	1/2	6.8 $\overline{E}$ + 1.1
	7.5	1/2	6.3 $\overline{E}$ - 0.9
4140	12.5	1/2	6.8 $\overline{E}$ + 5.7
	10.0	1/2	9.4 $\overline{E}$ - 3.1
	7.5	1/2	8.4 $\overline{E}$ - 5.5
4340	12.5	1/2	9.1 $\overline{E}$ + 2.8
	10.0	1/2	10.0 $\overline{E}$ - 2.3
	7.5	1/2	10.8 $\overline{E}$ - 7.7
2-1/4 Cr-1 Mo	12.5	1/2	8.3 $\overline{E}$ + 4.4
	10.0	1/2	8.9 $\overline{E}$ + 1.4
	7.5	1/2	7.6 $\overline{E}$ - 0.2
HY-100	12.5	5/16	16.6 $\overline{E}$ - 14.1
	10.0	5/16	14.1 $\overline{E}$ - 6.7
	7.5	5/16	10.7 $\overline{E}$ + 2.2
HY-80	12.5	5/8	10.5 $\overline{E}$ - 5.5
	10.0	1/4	13.7 $\overline{E}$ - 7.6
	7.5	*	11.2 $\overline{E}$ - 0.7
H-11	12.5	7/8	8.6 $\overline{E}$ + 4.2
	10.0	7/8	12.4 $\overline{E}$ + 5.9
	7.5	7/8	14.2 $\overline{E}$ - 15.0
Type 422	10.0	3/8	9.1 $\overline{E}$ + 0.1
17-4 PH	10.0	1/2	14.7 $\overline{E}$ + 2.1
	7.5	1/2	11.2 $\overline{E}$ - 2.0

*In 7.5 KW tests of HY-80 steel, two specimens tested at the lowest energy densities were 5/8" thick. Four specimens tested at higher energy densities were 1/4" thick.

TABLE XX

AREA COMPARISONS FOR CONVENTIONAL STEELS

Steel	Power, KW	Thickness, in.	Area (mm^2) at Energy Density Shown	
			1.0 KJ/cm^2	6.0 KJ/cm^2
1018	7.5	1/2	5.4	36.9
4140	7.5	1/2	2.9	44.9
4340	7.5	1/2	3.1	57.1
2-1/4 Cr-1 Mo	7.5	1/2	7.4	45.4
HY-100	7.5	5/16	12.9	66.4
HY-80	7.5	*	10.5	66.5
1018	10.0	1/2	7.9	41.9
4140	10.0	1/2	6.3	53.3
4340	10.0	1/2	7.7	57.7
2-1/4 Cr-1 Mo	10.0	1/2	10.3	54.8
HY-100	10.0	5/16	7.4	77.9
HY-80	10.0	1/4	6.1	74.6
1018	12.5	1/2	12.8	46.3
4140	12.5	1/2	12.5	46.5
4340	12.5	1/2	11.9	57.4
2-1/4 Cr-1 Mo	12.5	1/2	12.7	54.2
HY-100	12.5	5/16	2.5	85.5
HY-80	12.5	5/8	5.0	57.5

*In 7.5 KW tests of HY-80 steel, two specimens tested at the lowest energy density were 5/8" thick. Four specimens tested at higher energy densities were 1/4" thick.

TABLE XXI

MAXIMUM HARDNESS AND ESTIMATED MARTENSITE CONTENT

Steel	Carbon Content, %	Maximum Hardness, Rc	Predicted Hardness, Rc, at Indicated Martensite %					Estimated Martensite, %	Ideal Diameter, in.
			99.9	95	90	80	50		
1018	0.18	20*	43	39	38	35	31	<50	0.5
4140	0.42	59	56	53	50	47	43	100	2.0
4340	0.43	60	57	54	51	48	44	100	3.1
2-1/4Cr-1 Mo	0.09	37	38	33	32	30	27	100	1.0
HY-100	0.15	39	41	37	36	33	29	95/100	1.6
HY-80	0.15**	39	41	37	36	33	29	95/100	1.5
	0.17***	37	43	39	38	35	31	90	1.6
H-11	0.42	62	56	53	50	47	43	100	4.2

*Converted from Rockwell 30N

**5/8" thick specimens

***1/4" thick specimens

TABLE XXII

AVERAGE HARDNESS AND ESTIMATED MARTENSITE CONTENT

Steel	Carbon Content, %	Hardness, Rc		Predicted Hardness, Rc, at Indicated Martensite, %					Estimated Martensite, %	Ideal Diameter, in.
		Range	Avg.	99.9	95	90	80	50		
1018	0.18	(6)/20	(12)	43	39	38	35	31	<50	0.5
4140	0.42	45/59	51	56	53	50	47	43	90	2.0
4340	0.43	46/60	52	57	54	51	48	44	90	3.1
2-1/4Cr-1Mo	0.09	32/37	34	38	33	32	30	27	95	1.0
HY-100	0.15	33/39	36	41	37	36	33	29	90	1.6
HY-80	0.15*	37/39	38	41	37	36	33	29	95	1.5
	0.17**	32/36	34	43	39	38	35	31	80	1.6
H-11	0.42	46/62	53	56	53	50	47	43	95	4.2

( ) Indicates values below the normal Rc Range

* 5/8" thick specimens
** 1/4" thick specimens

Travel: 100 ipm
Energy Density: 1.04 KJ/cm^2
Penetration: 0.020 in.
Area: 0.013 in^2

Travel: 80 ipm
Energy Density: 1.32 KJ/cm^2
Penetration: 0.030 in.
Area: 0.019 in^2

Travel: 60 ipm
Energy Density: 1.76 KJ/cm^2
Penetration: 0.041 in.
Area: 0.025 in^2

Travel: 40 ipm
Energy Density: 2.61 KJ/cm^2
Penetration: 0.070 in.
Area: 0.042 in^2

Travel: 20 ipm
Energy Density: 5.24 KJ/cm^2
Penetration: 0.131 in.
Area: 0.074 in^2
(Melt Depth: 0.022 in)

Figure 1 - Typical Sections from 4340 Steel Specimens (Series CY) at 10.0 KW Laser Power (5X).

Curve 746052-A

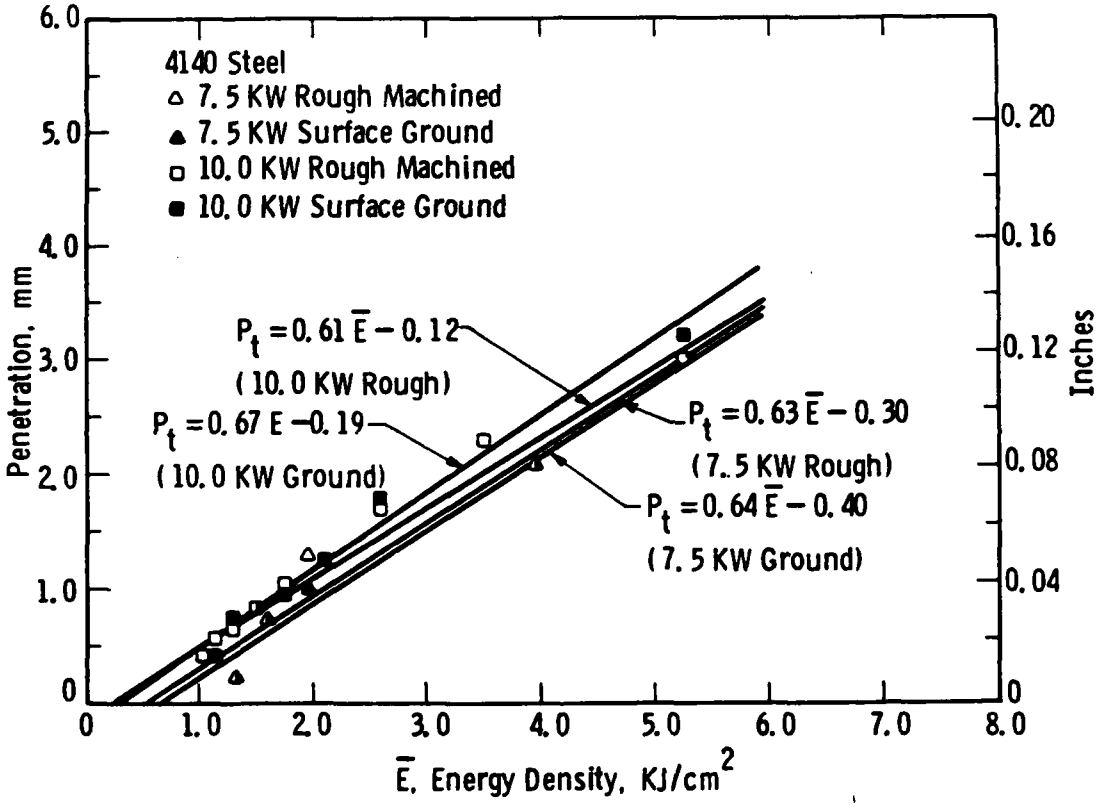

Figure 2--Comparison of Penetration in 4140 Steel with Rough Machined or Surface Ground Specimens.

Curve 746053-A

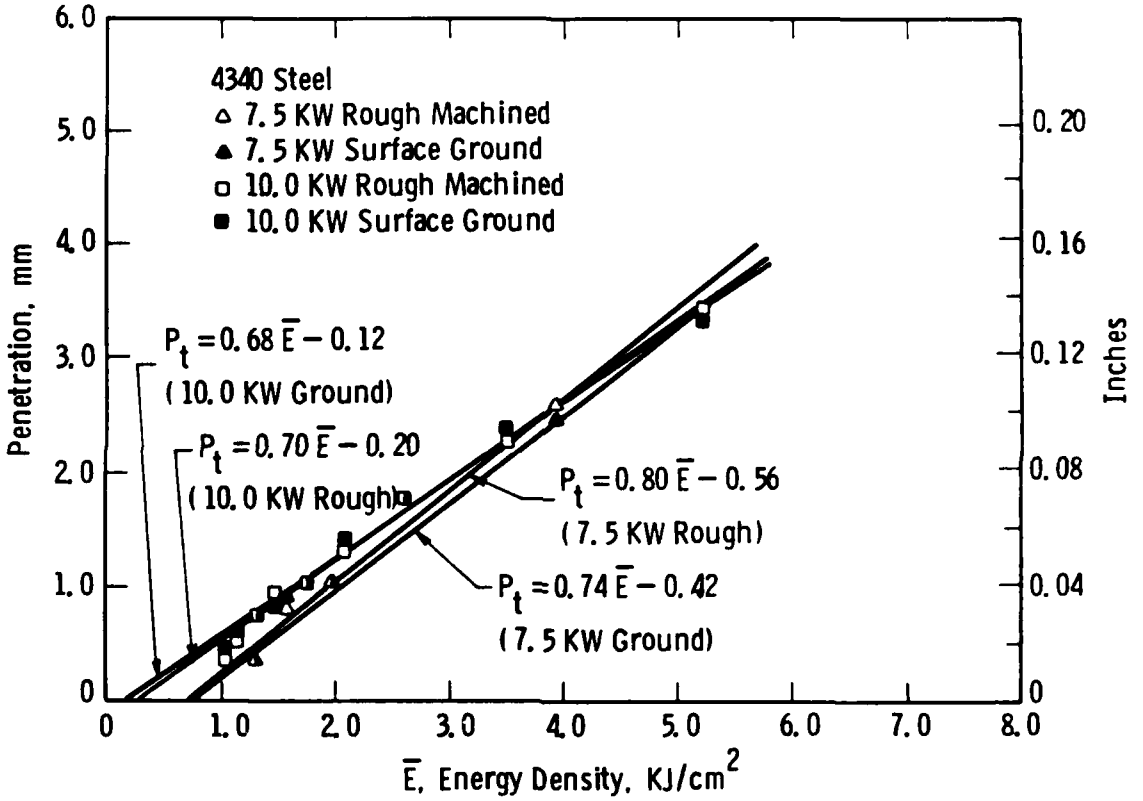

Figure 3--Comparison of Penetration in 4340 Steel with Rough Machined or Surface Ground Specimens.

Curve 741992-A

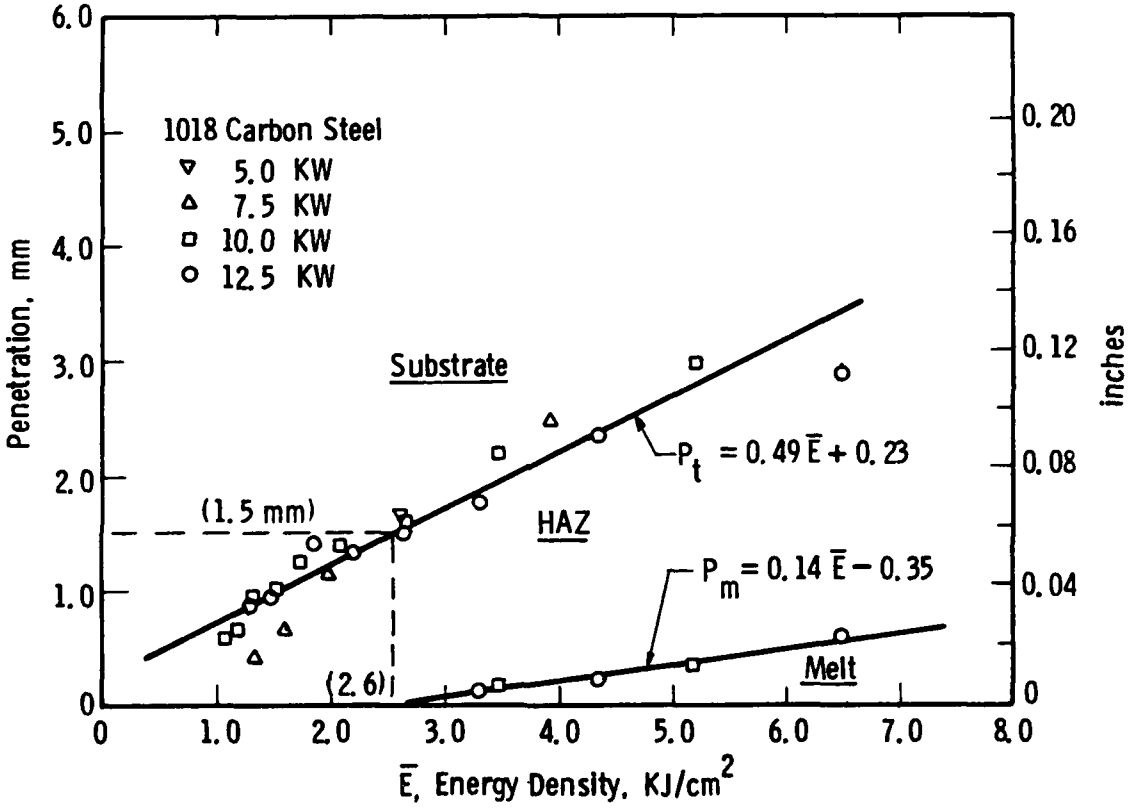

Fig. 4--General Effect of Energy Density on Penetration in 1018 Steel.

Curve 746050-A

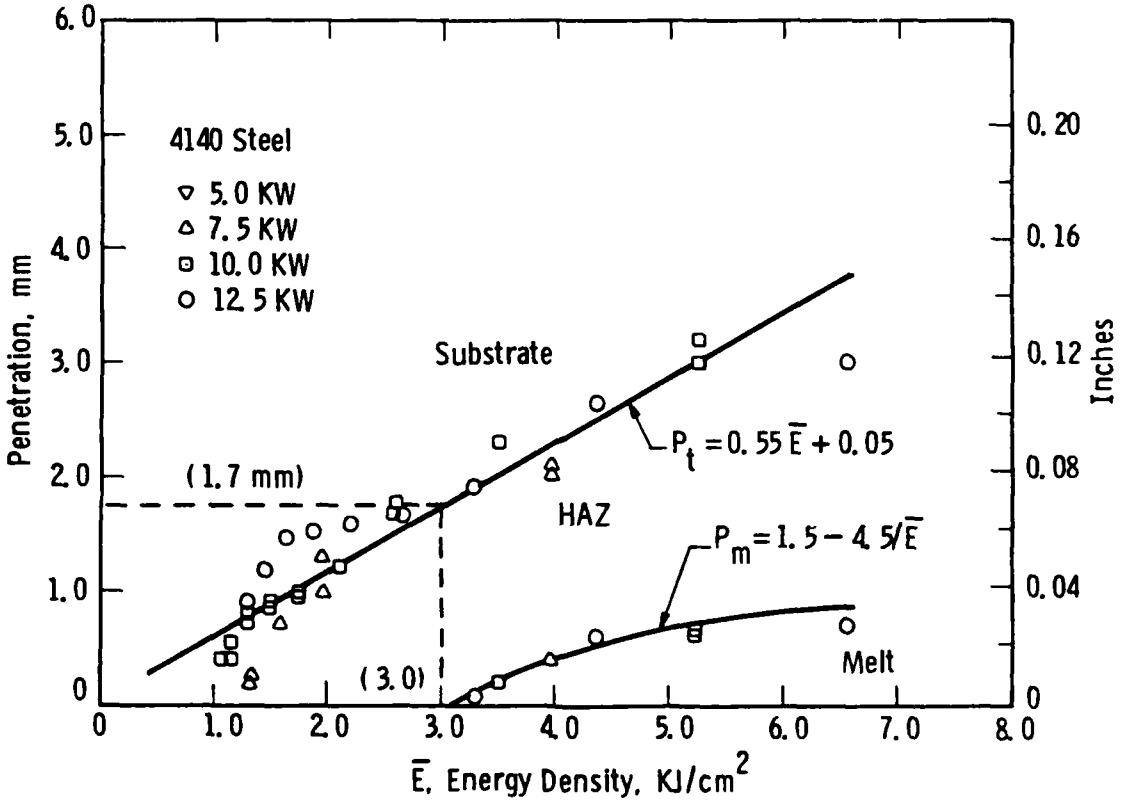

Figure 5--General Effect of Energy Density on Penetration in 4140 Steel.

Curve 746051-A

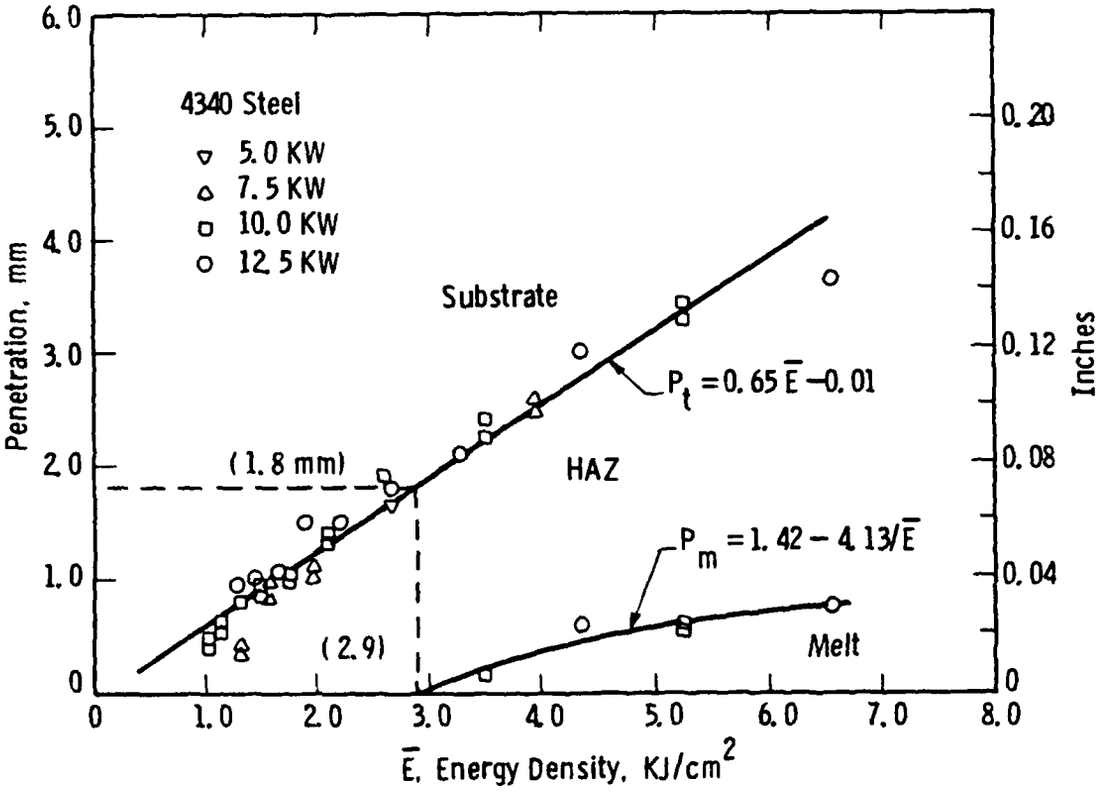

Figure 6--General Effect of Energy Density on Penetration in 4340 Steel.

Curve 727203-A

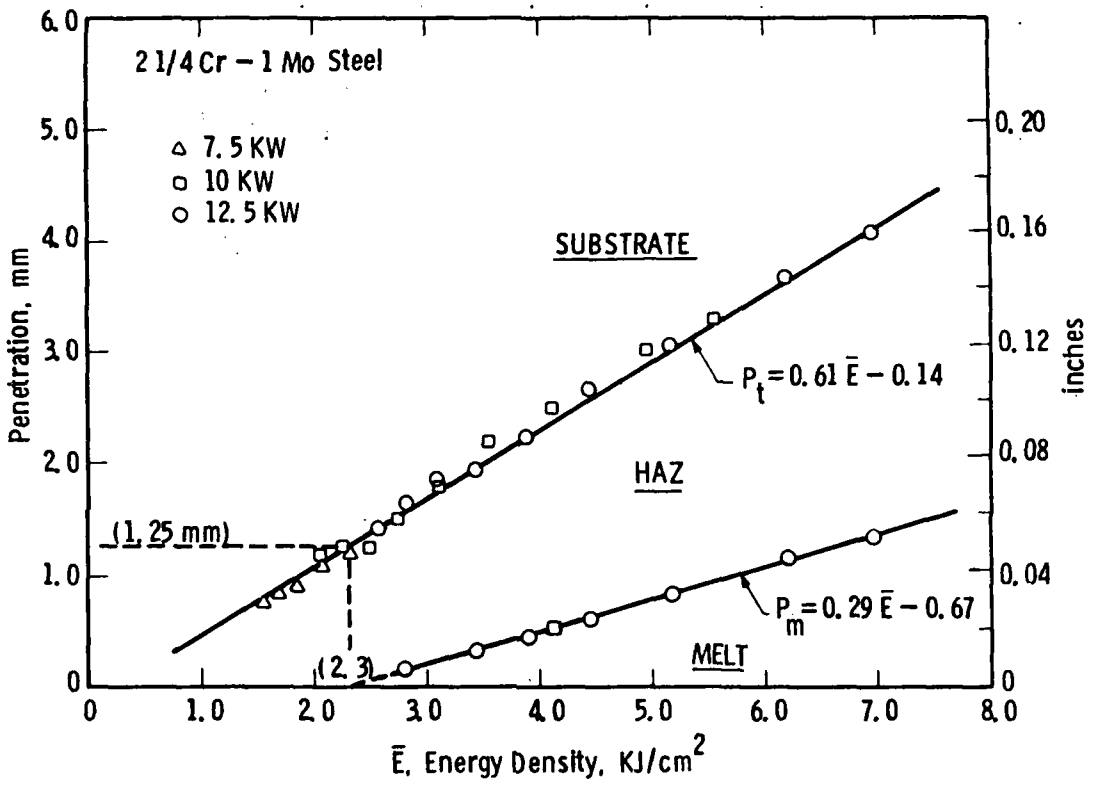

Fig. 7--General Effect of Energy Density on Penetration in 2-1/4 Cr-1 Mo Steel.

Curve 741984-A

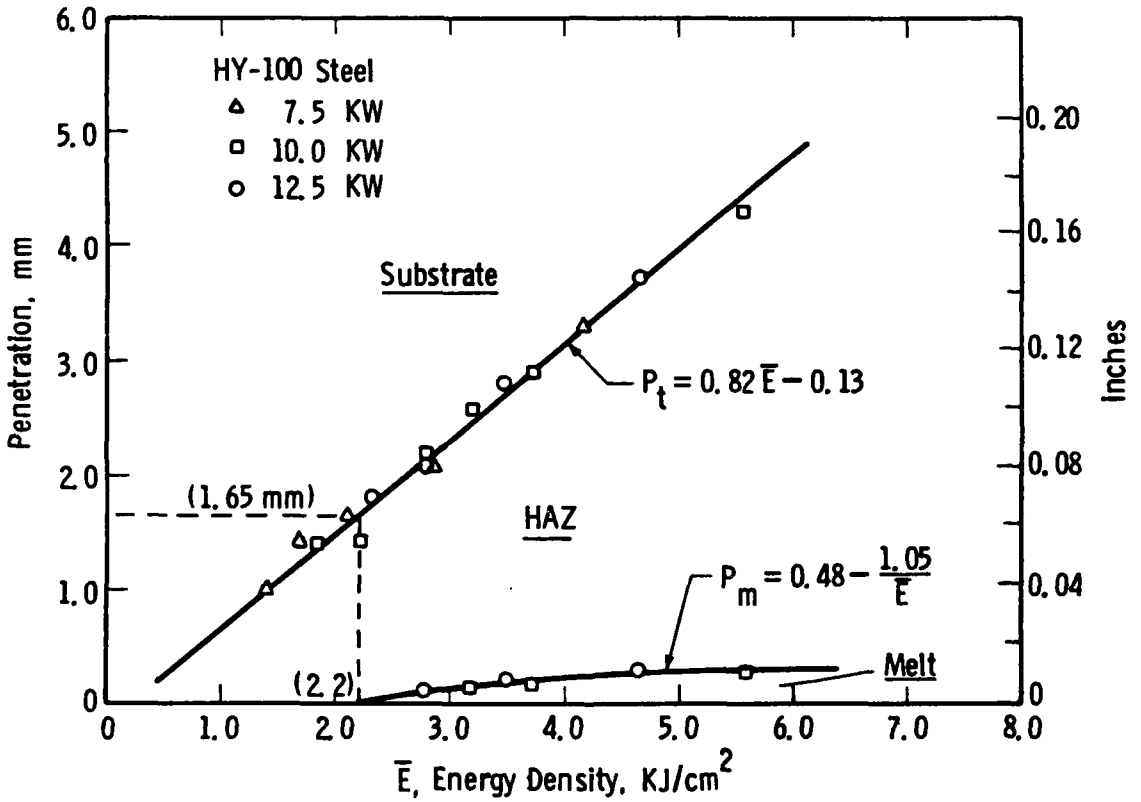

Fig. 8--General Effect of Energy Density on Penetration in HY-100 Steel (Not valid for thick sections).

Curve 741985-A

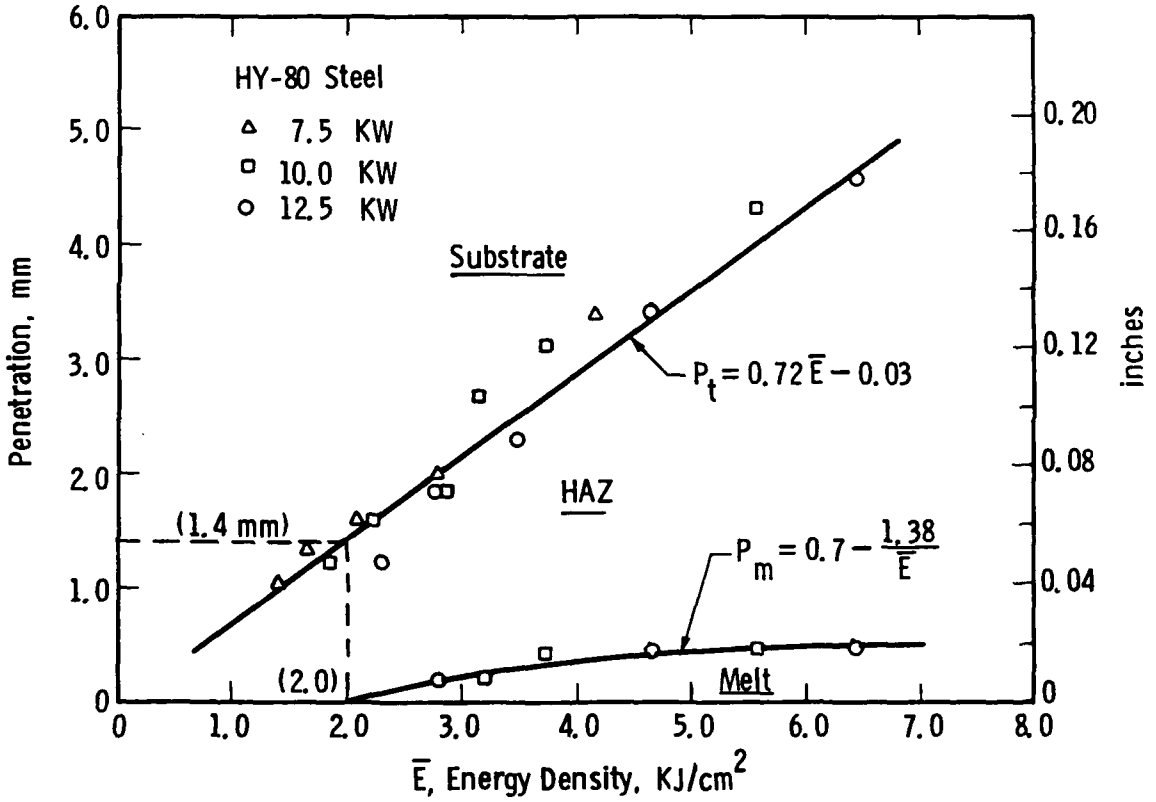

Fig. 9--General Effect of Energy Density on Penetration in HY-80 Steel (Not valid for thick sections).

Curve 741988-A

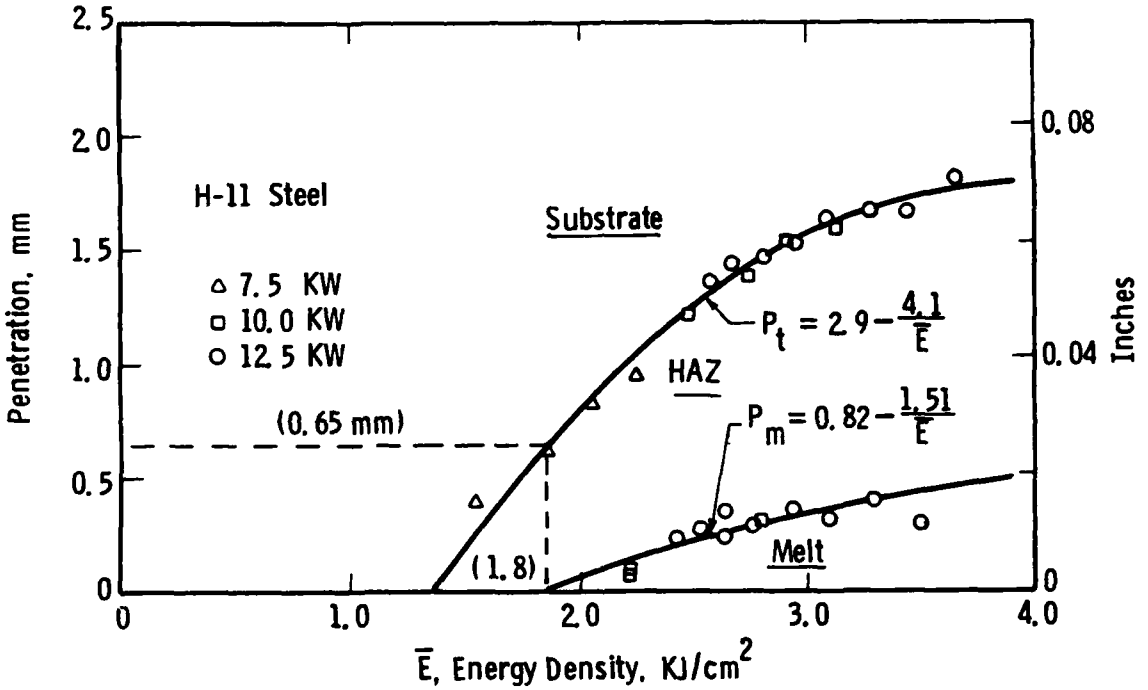

Fig. 10--General Effect of Energy Density on Penetration in H-11 Steel.

Curve 746049-A

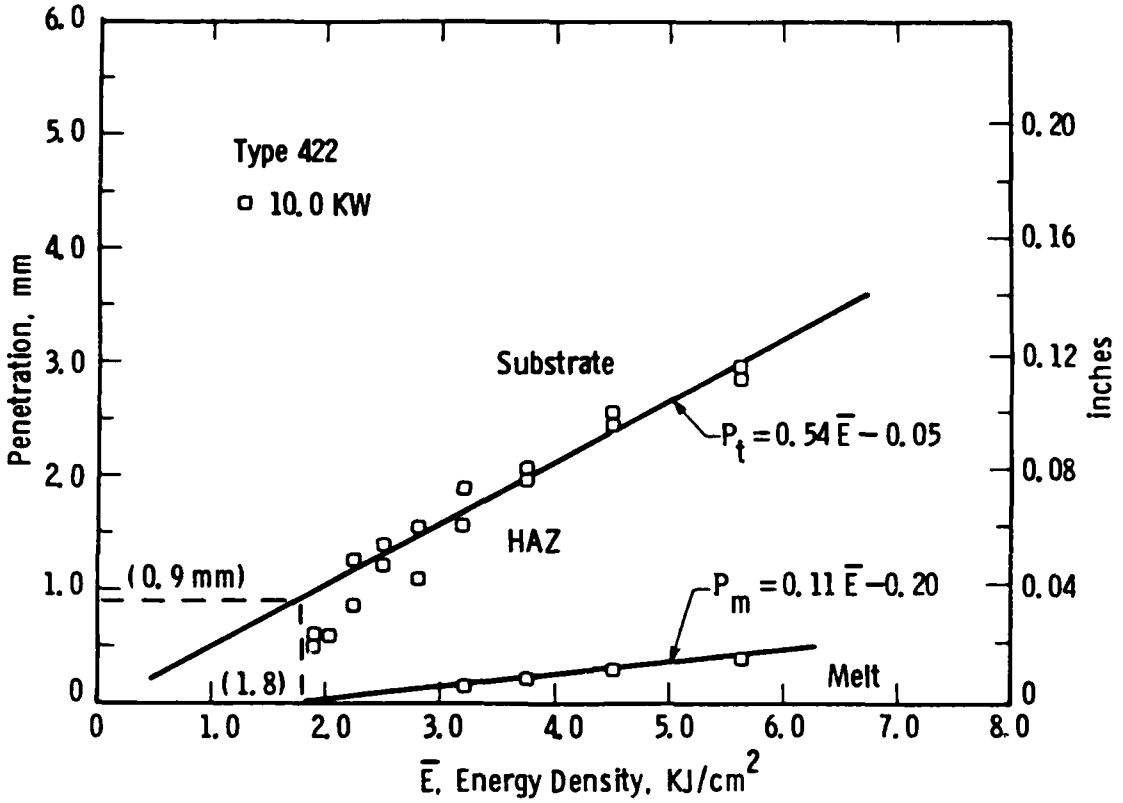

Figure 11--General Effect of Energy Density on Penetration in Type 422 Steel.

Curve 741990-A

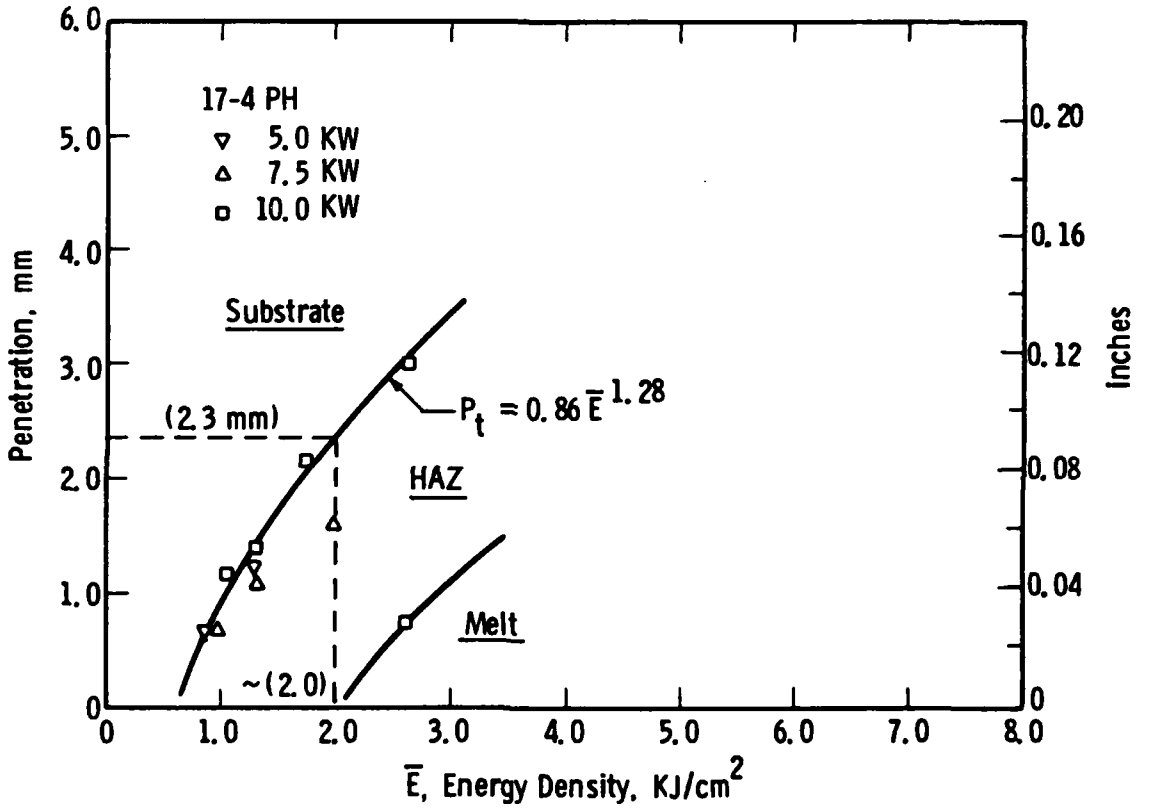

Fig. 12--General Effect of Energy Density on Penetration in 17-4 PH Steel.

Curve 746129-A

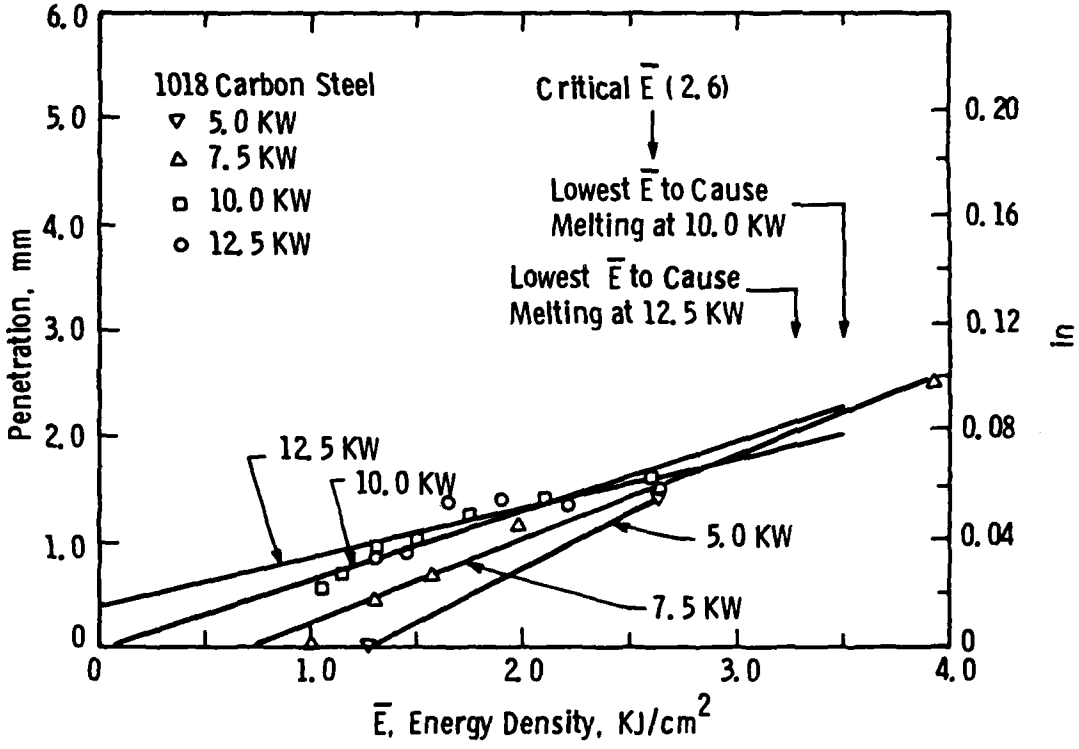

Figure 13--Effect of Energy Density on Penetration in 1018 Steel at Laser Outputs of 5.0, 7.5, 10.0 and 12.5 KW.

Curve 746130-A

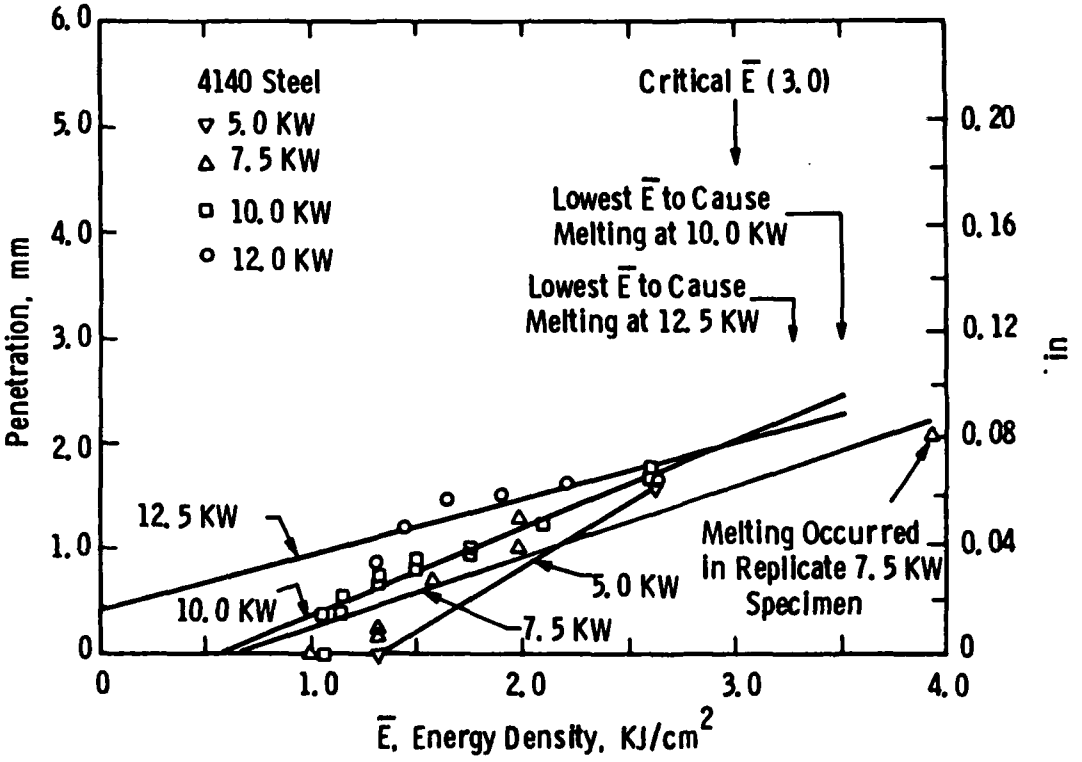

Figure 14--Effect of Energy Density on Penetration in 4140 Steel at Laser Outputs of 5.0, 7.5, 10.0 and 12.5 KW.

Curve 746125-A

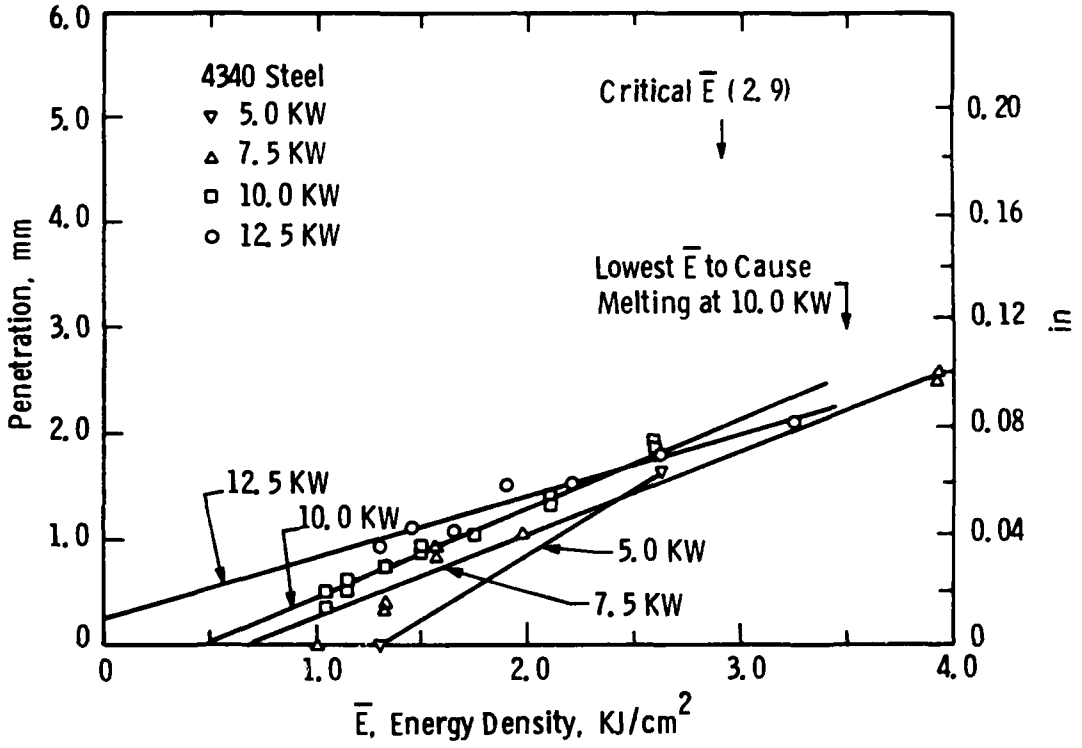

Figure 15--Effect of Energy Density on Penetration in 4340 Steel at Laser Outputs of 5.0, 7.5, 10.0 and 12.5 KW.

Curve 746048-A

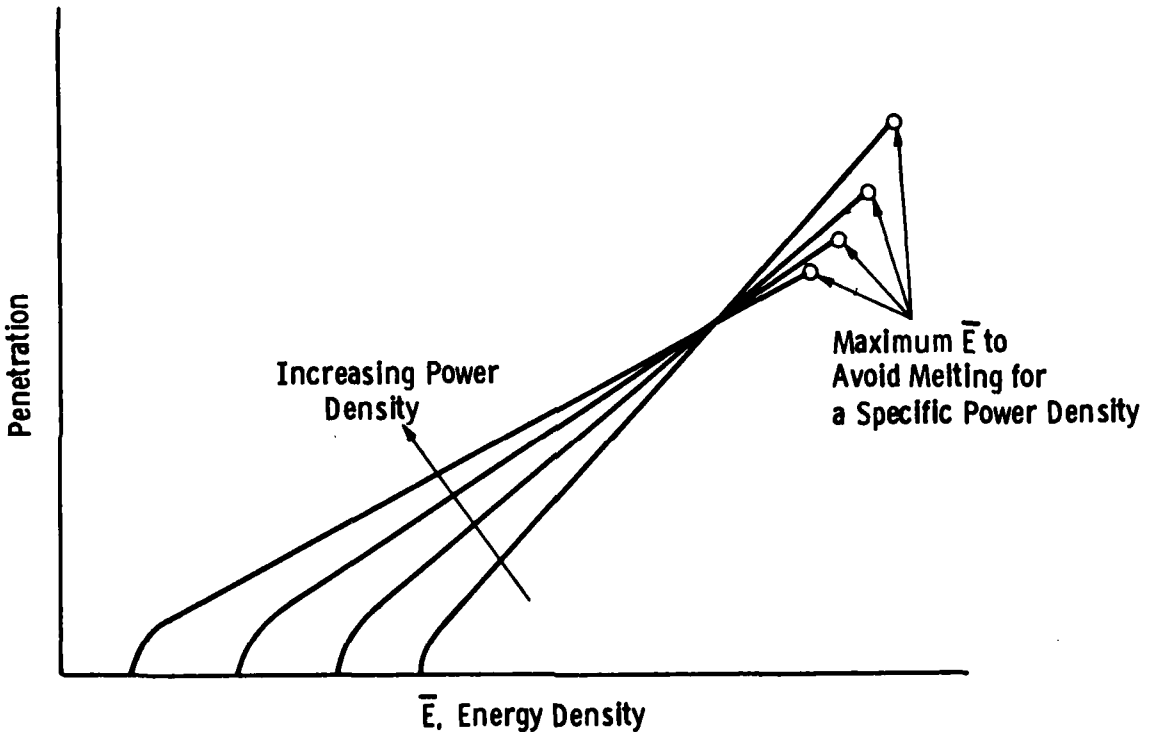

Figure 16--Schematic Illustration of the Penetration/Energy Density Relationship Showing the Influence of Laser Power on the Initiation of Penetration and Surface Melting.

Curve 746127-A

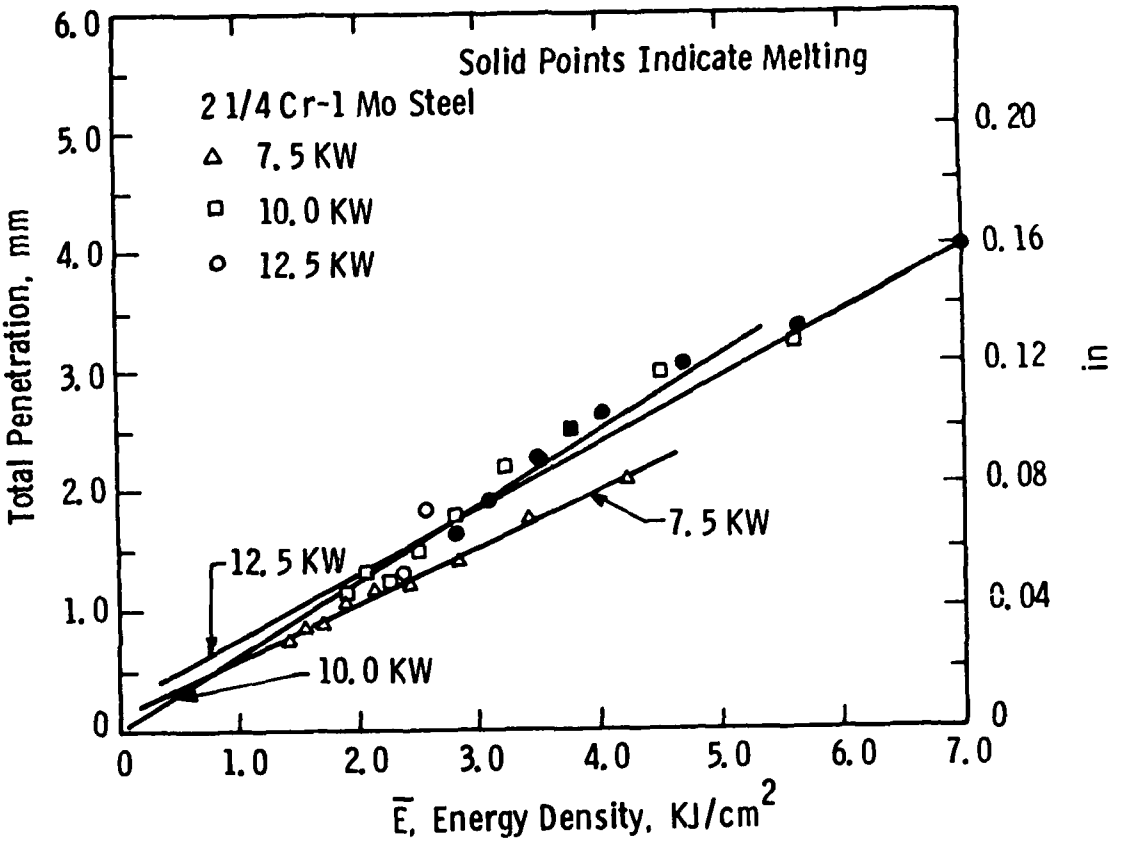

Figure 17--Effect of Energy Density on Penetration in 2-1/4 Cr-1 Mo Steel at Laser Outputs of 7.5, 10.0 and 12.5 KW.

Curve 746126-A

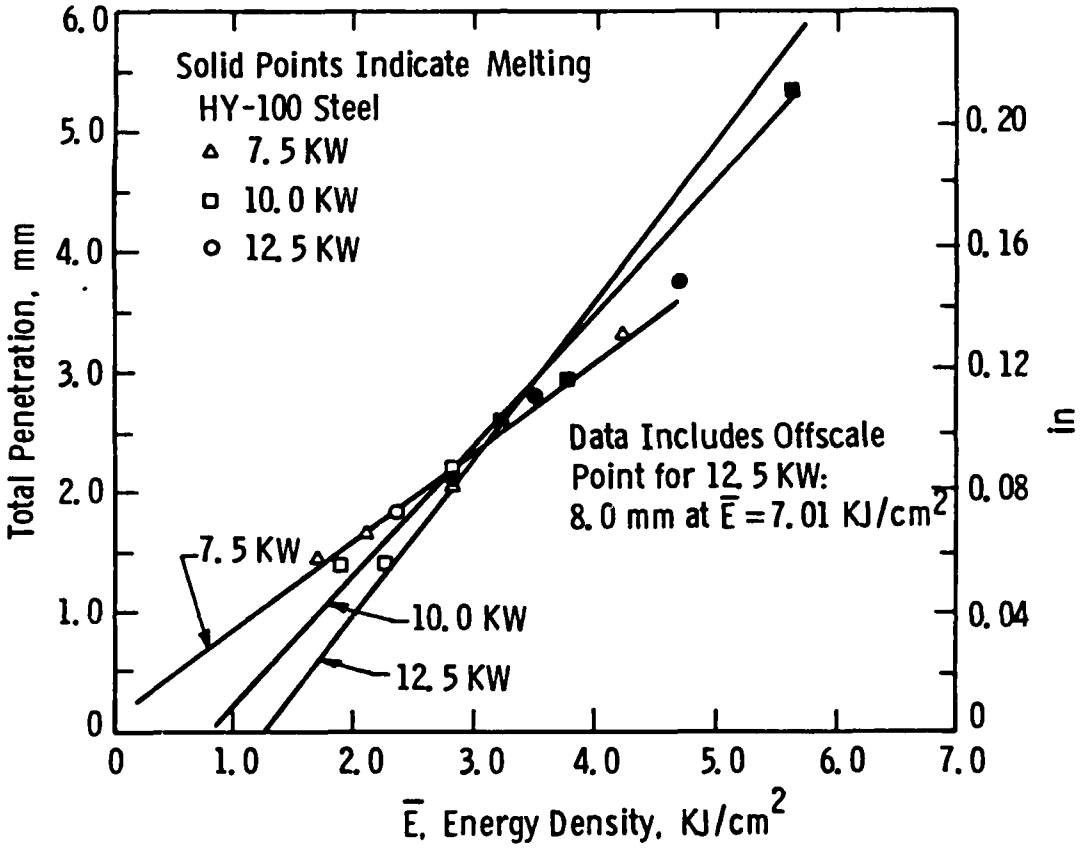

Figure 18--Effect of Energy Density on Penetration in HY-100 Steel at Laser Outputs of 7.5, 10.0 and 12.5 KW (Not valid for thick sections).

Curve 746131-A

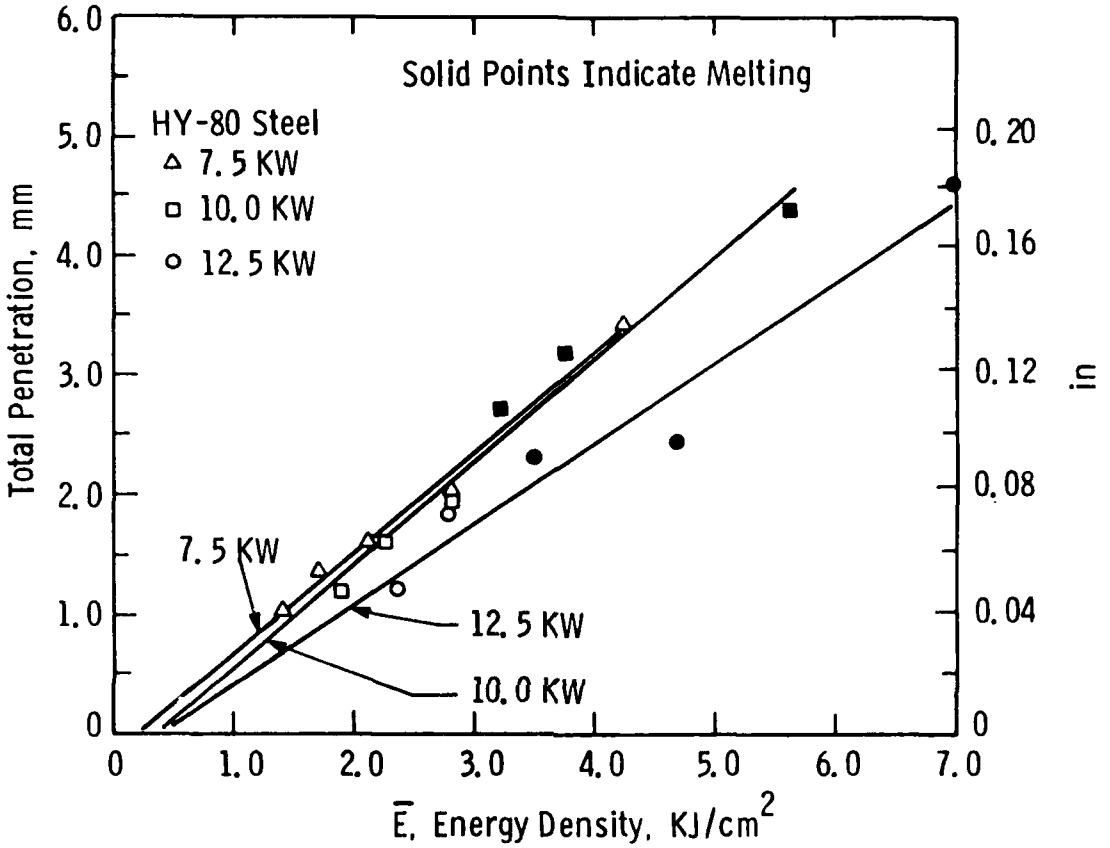

Figure 19--Effect of Energy Density on Penetration in HY-80 Steel at Laser Powers of 7.5, 10.0 and 12.5 KW (Data for 7.5 and 10.0 KW not valid for thick sections).

Curve 746128-A

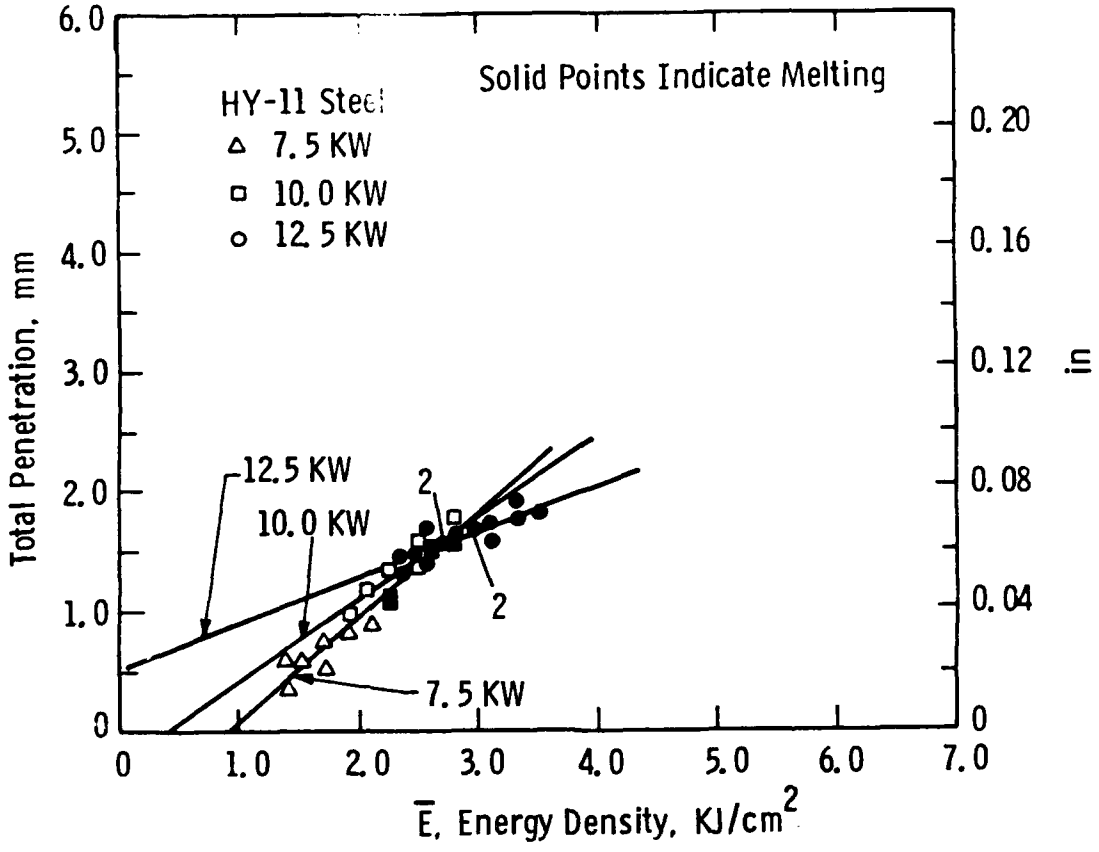

Figure 20--Effect of Energy Density on Penetration in H-11 Steel at Laser Powers of 7.5, 10.0 and 12.5 KW.

Curve 746133-A

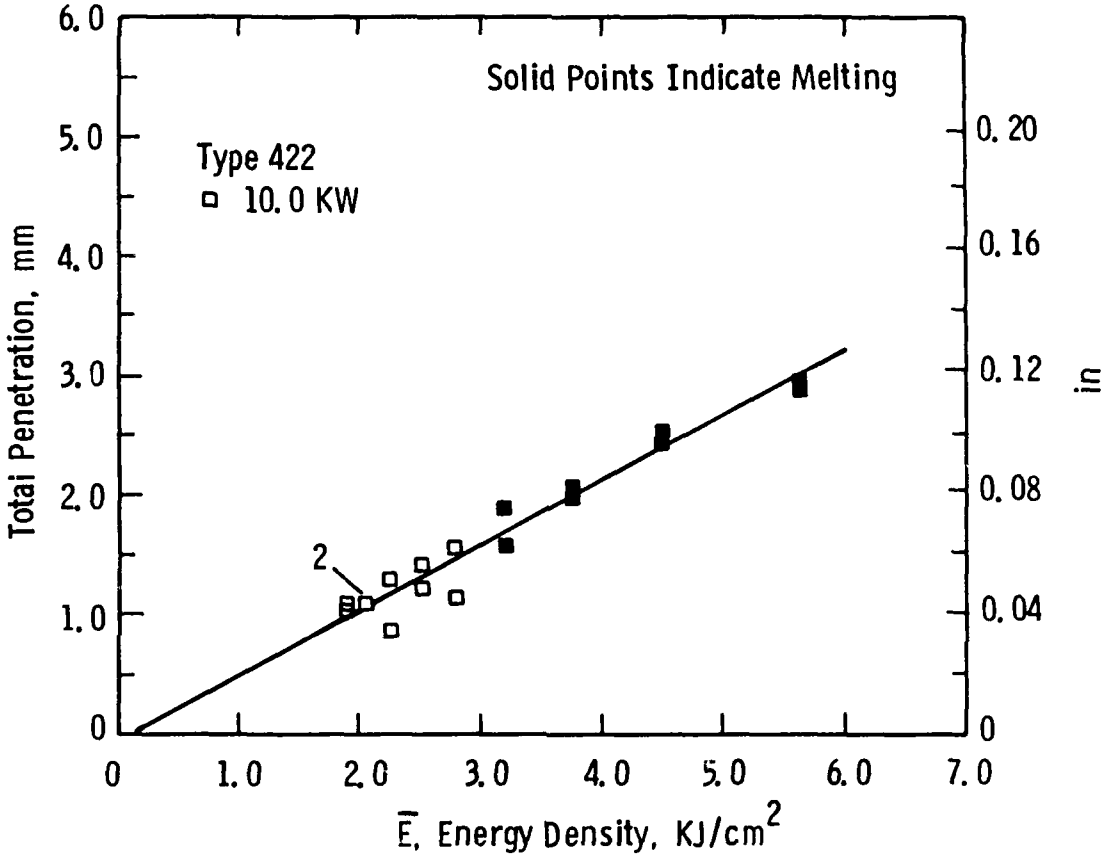

Figure 21--Effect of Energy Density on Penetration in Type 422 Steel at a Laser Power of 10.0 KW.

Curve 746132-A

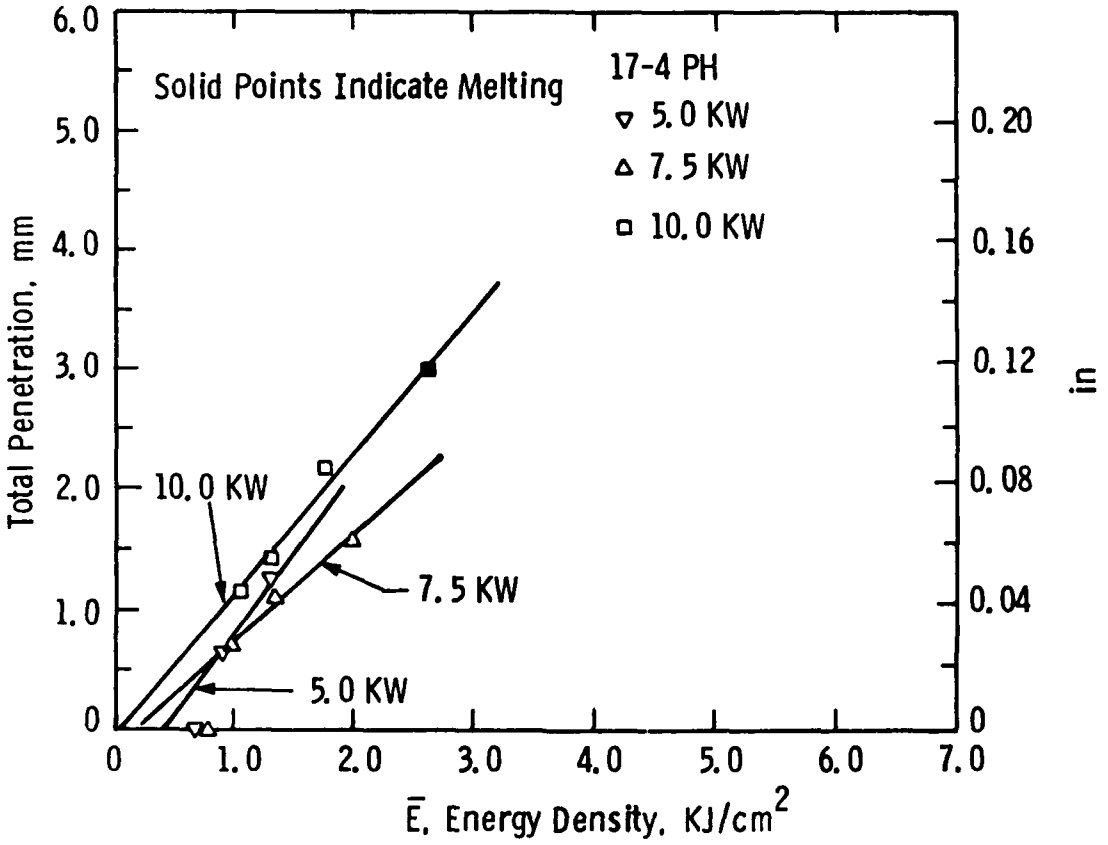

Figure 22--Effect of Energy Density on Penetration in 17-4 PH at Laser Powers of 5.0, 7.5 and 10.0 KW.

Curve 746134-A

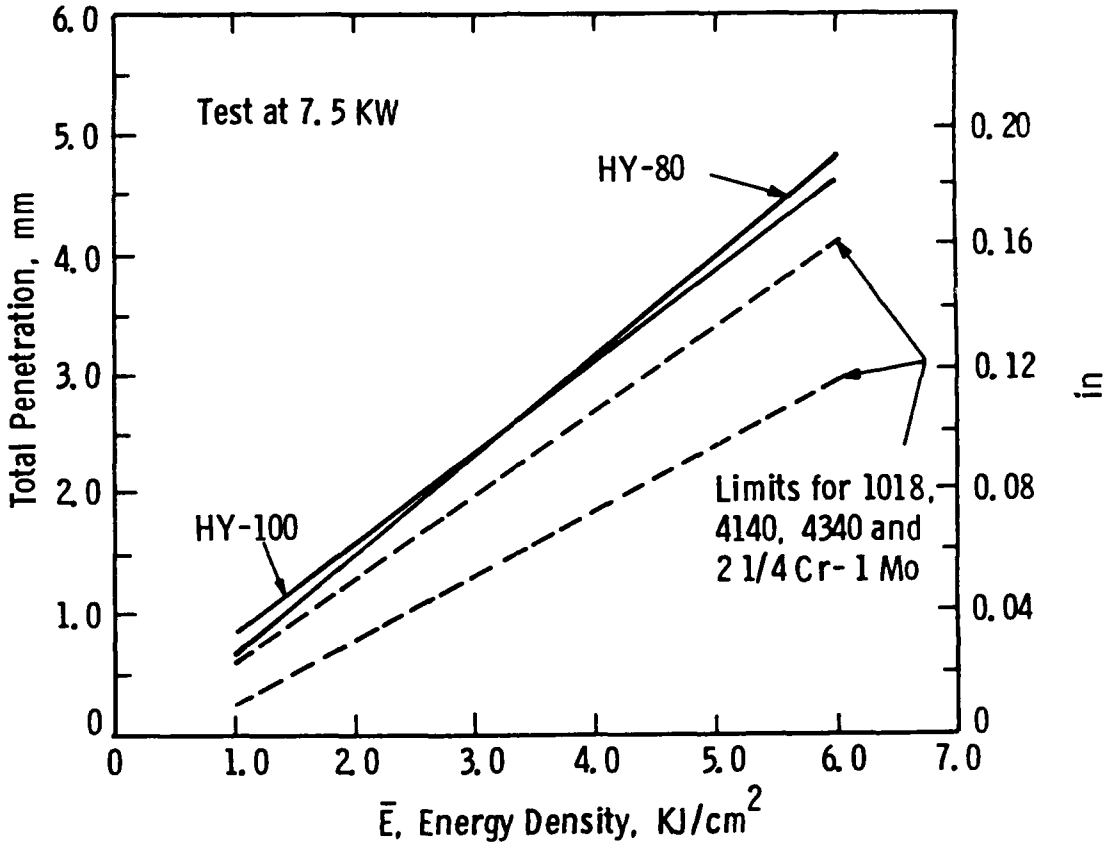

Figure 23--Comparison of Penetration in 5/16-Inch-Thick HY-100 Steel and 1/4-Inch-Thick HY-80 Steel with the Penetration Scatterband for Thick-Section Conventional Steels--Tests at a Laser Power of 7.5 KW.

Curve 746136-A

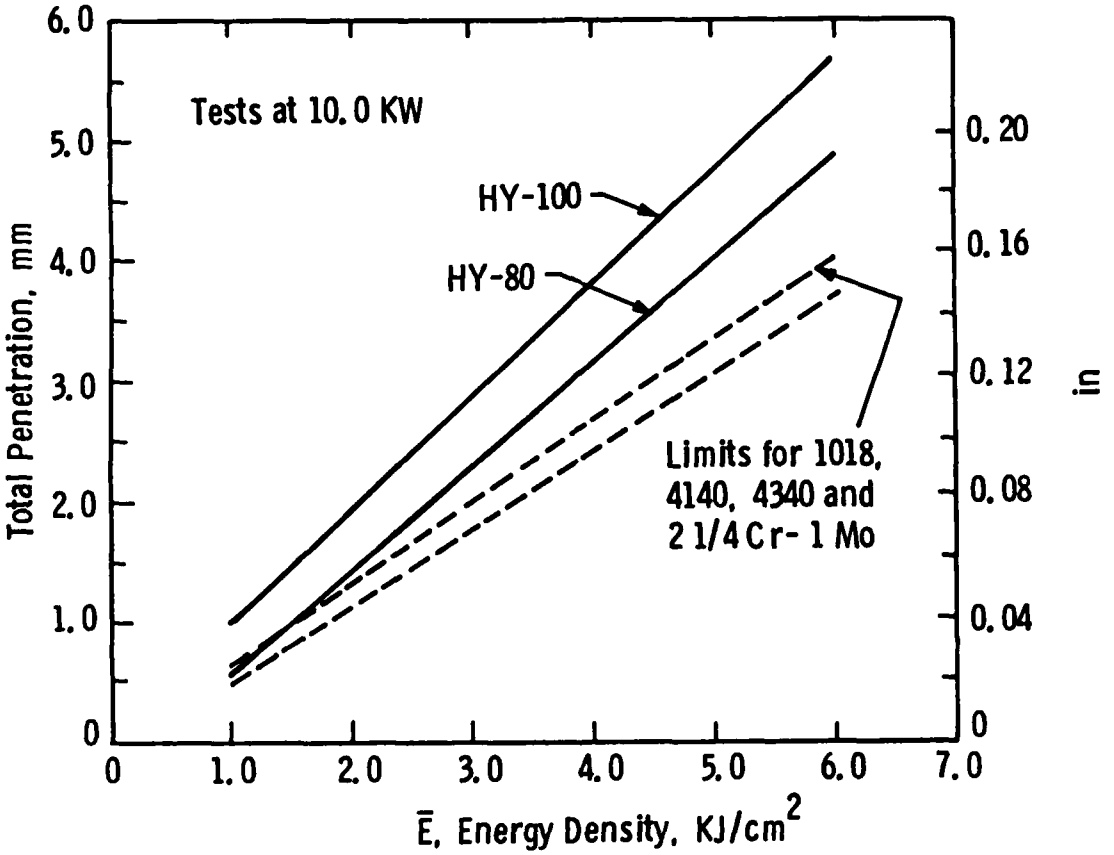

Figure 24--Comparison of Penetration in 5/16-Inch-Thick HY-100 Steel and 1/4-Inch-Thick HY-80 Steel with the Penetration Scatterband for Thick-Section Conventional Steels--Tests at a Laser Power of 10.0 KW.

Curve 746135-A

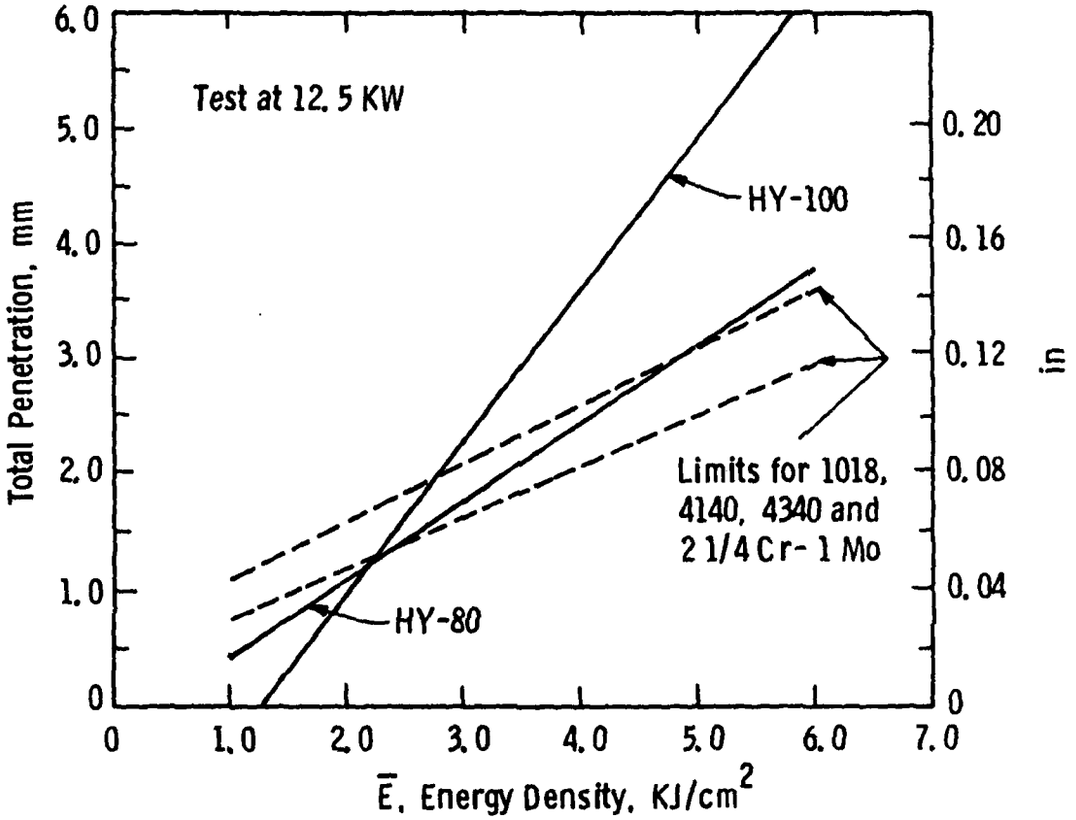

Figure 25--Comparison of Penetration in 5/16-Inch-Thick *HY-100 Steel and 1/4-Inch-Thick HY-80 Steel* with the Penetration Scatterband for Thick-Section Conventional Steels--Tests at a Laser Power of 12.5 KW.

Curve 746080-A

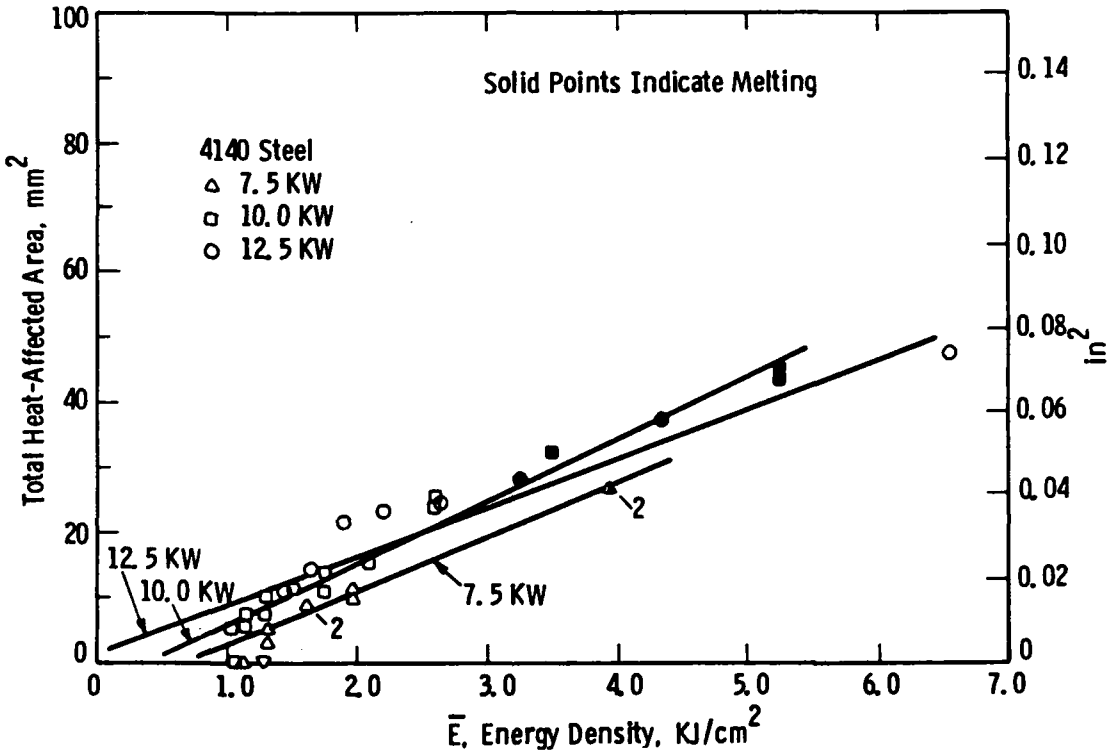

Figure 26--Effect of Energy Density on Total Heat-Affected Area in 4140 Steel at Laser Outputs of 7.5, 10.0 and 12.5 KW.

Curve 746079-A

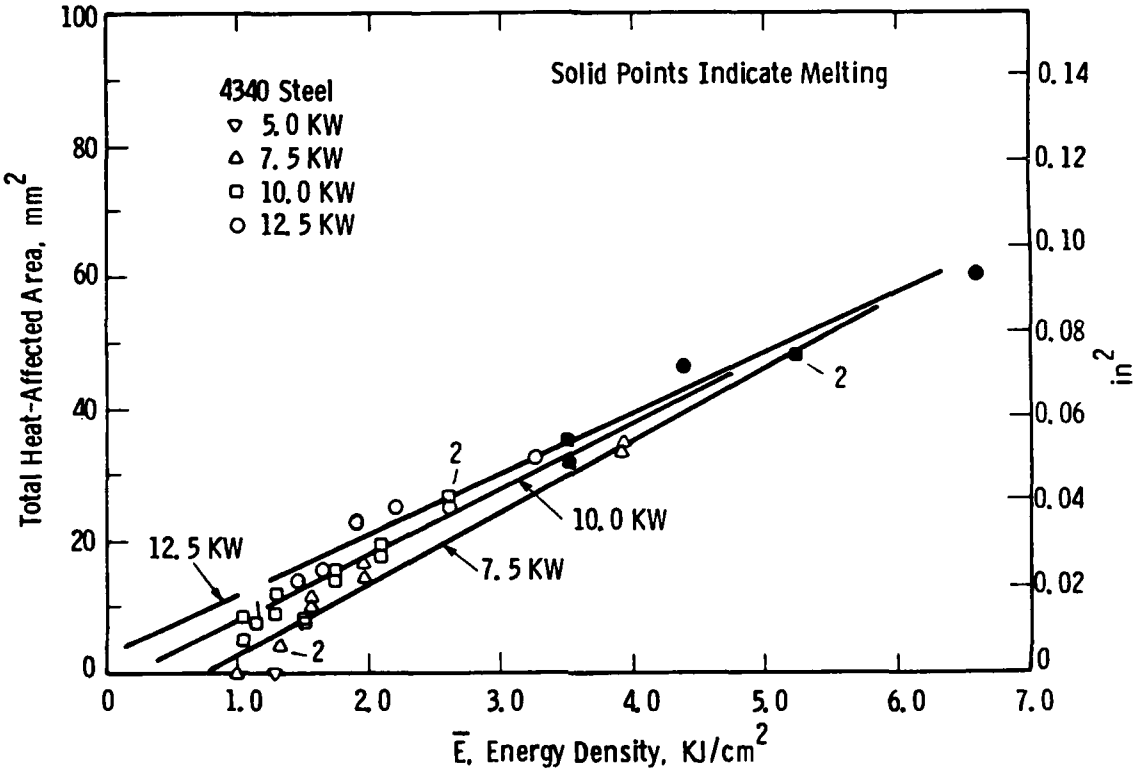

Figure 27--Effect of Energy Density on Total Heat-Affected Area in 4340 Steel at Laser Outputs of 7.5, 10.0 and 12.5 KW.

Curve 746086-A

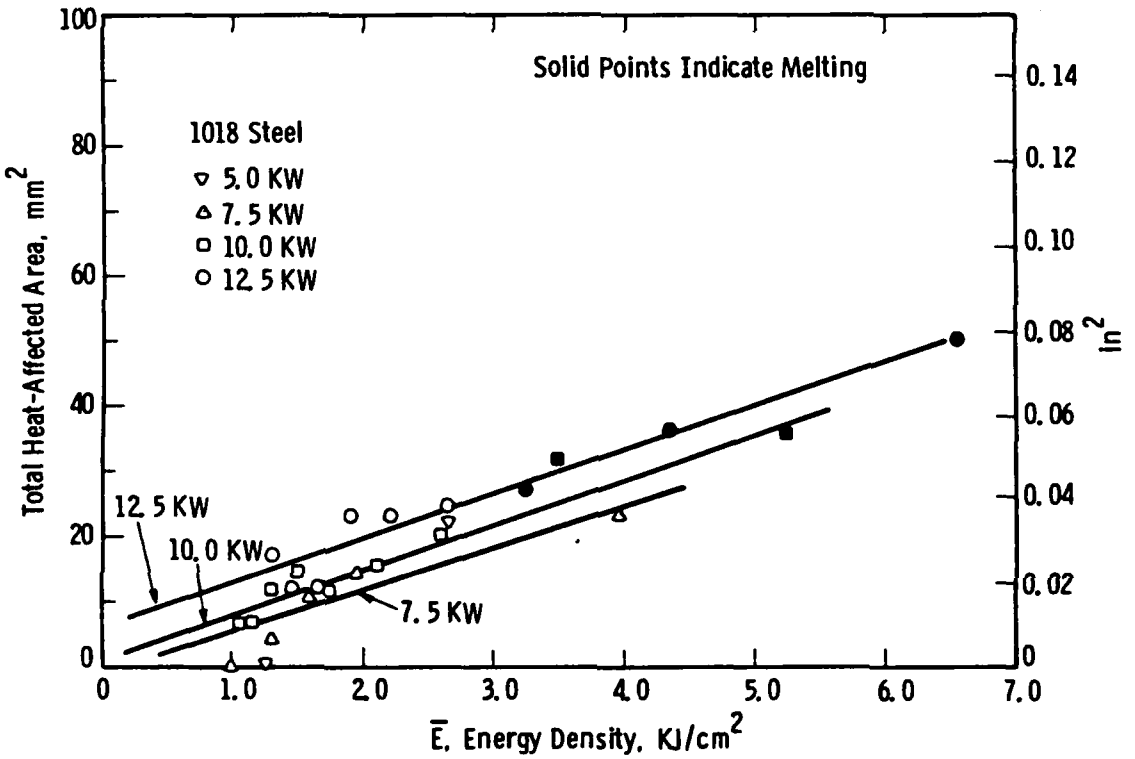

Figure 28--Effect of Energy Density on Total Heat-Affected Area in 1018 Steel at Laser Outputs of 7.5, 10.0 and 12.5 KW.

Curve 746089-A

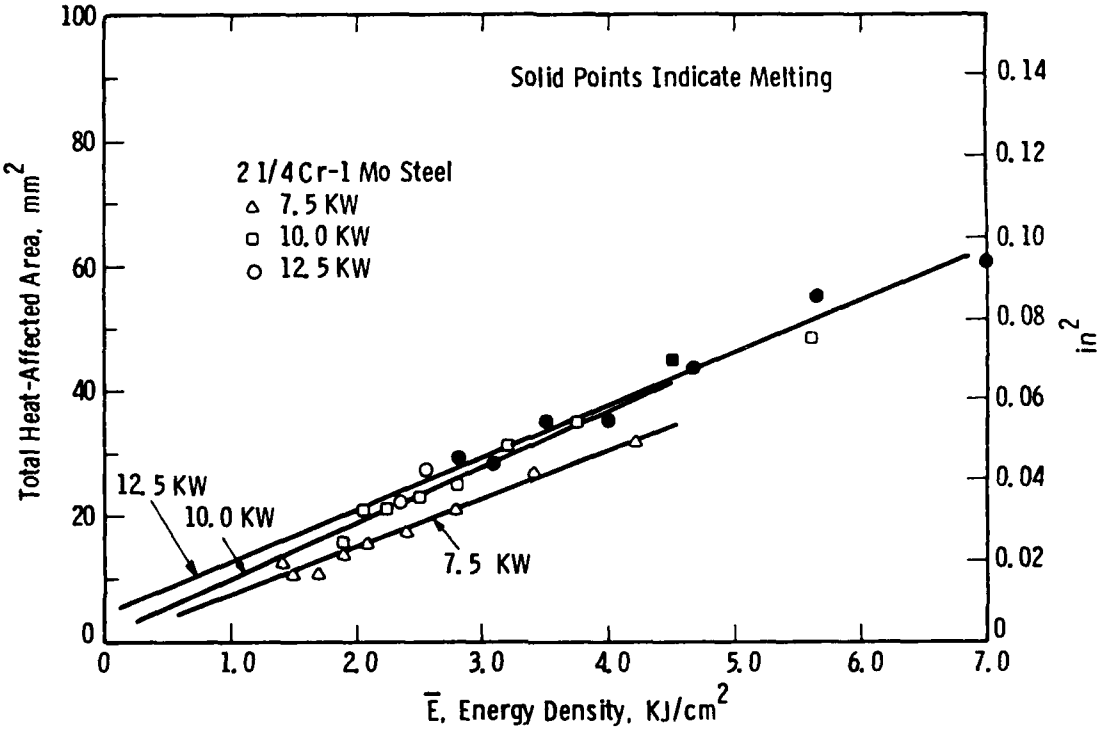

Figure 29--Effect of Energy Density on Total Heat-Affected Area in 2-1/4 Cr-1 Mo Steel at Laser Outputs of 7.5, 10.0, and 12.5 KW.

Curve 746082-A

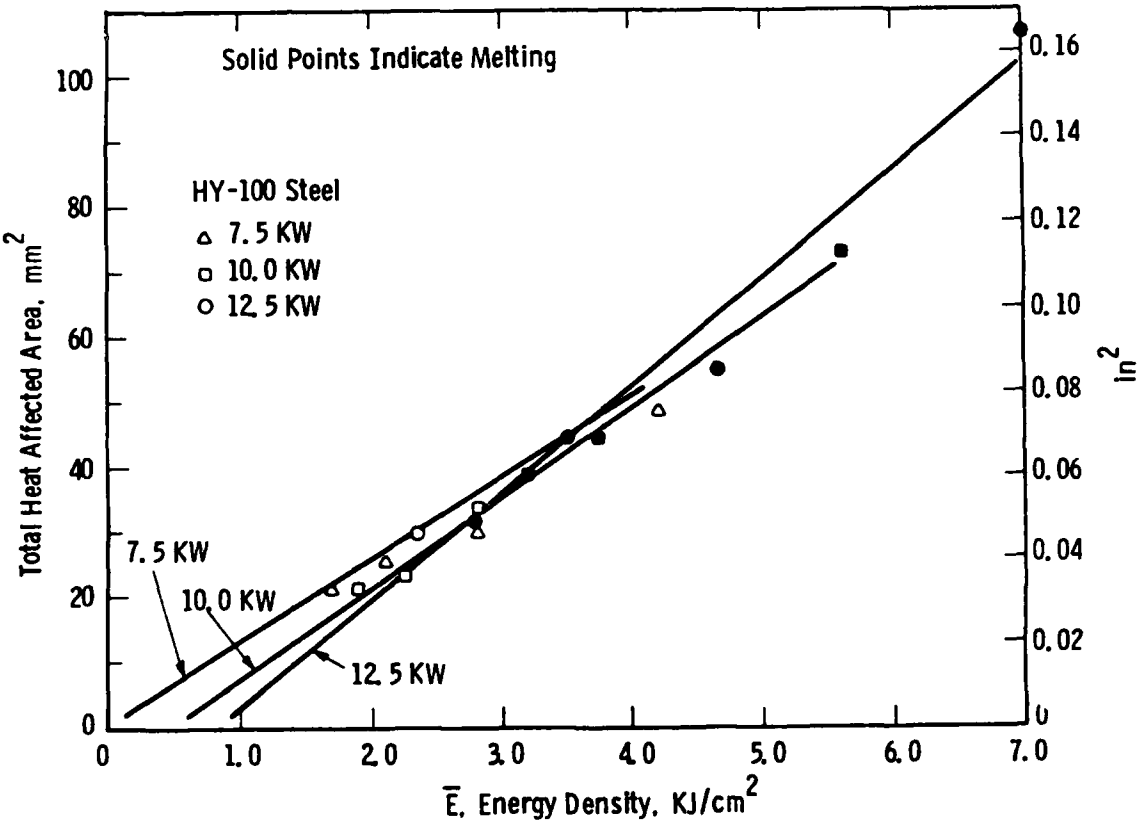

Figure 30--Effect of Energy Density on Total Heat-Affected Area in HY-100 Steel at Laser Outputs of 7.5, 10.0 and 12.5 KW (not valid for thick sections).

Curve 746081-A

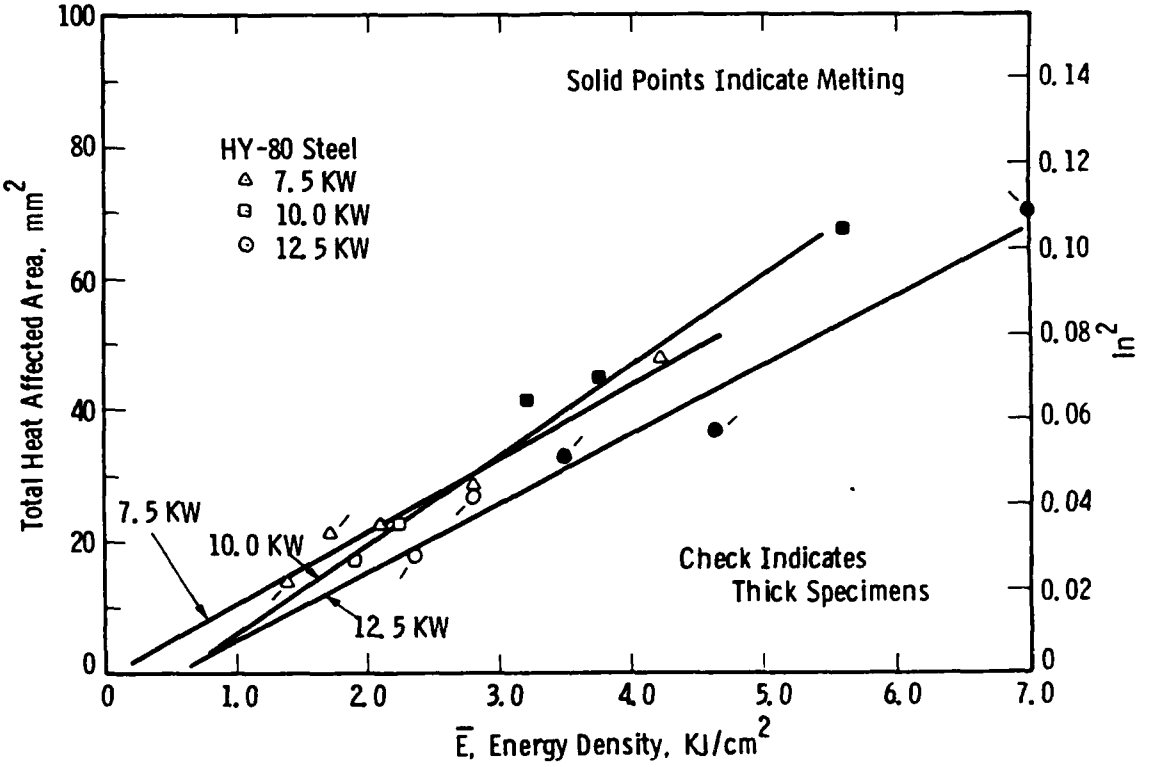

Figure 31--Effect of Energy Density on Total Heat-Affected Area in HY-80 Steel at Laser Outputs of 7.5, 10.0 and 12.5 KW (Data for 7.5 and 10.0 KW not valid for thick sections).

Curve 746083-A

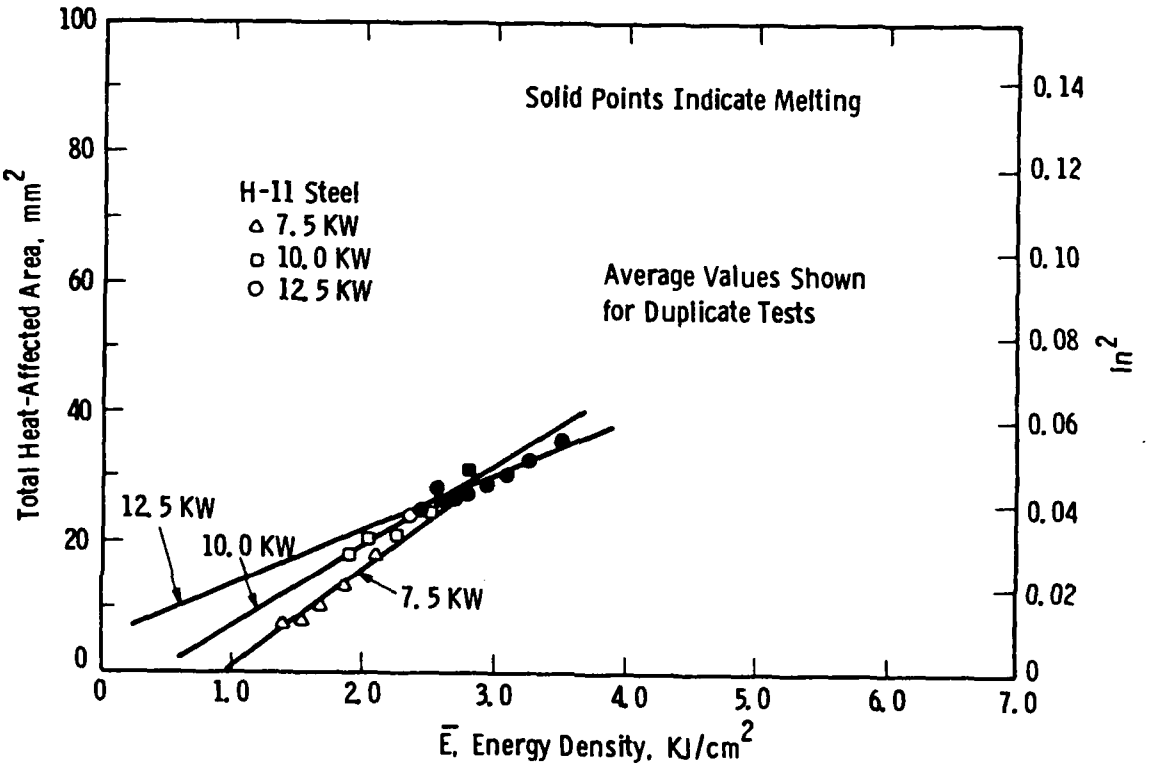

Figure 32--Effect of Energy Density on Total Heat-Affected Area in H-11 Steel at Laser Outputs of 7.5, 10.0 and 12.5 KW.

Curve 746088-A

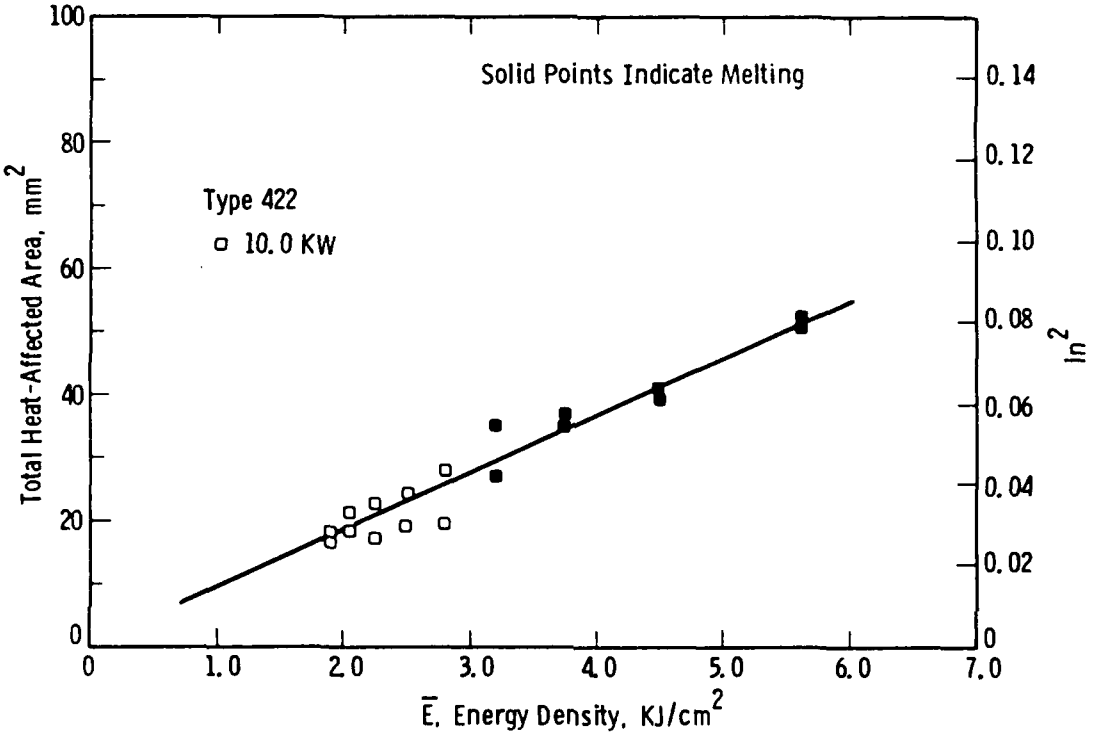

Figure 33--Effect of Energy Density on Total Heat-Affected Area in Type 422 Steel at a Laser Output of 10.0 KW.

Curve 746090-A

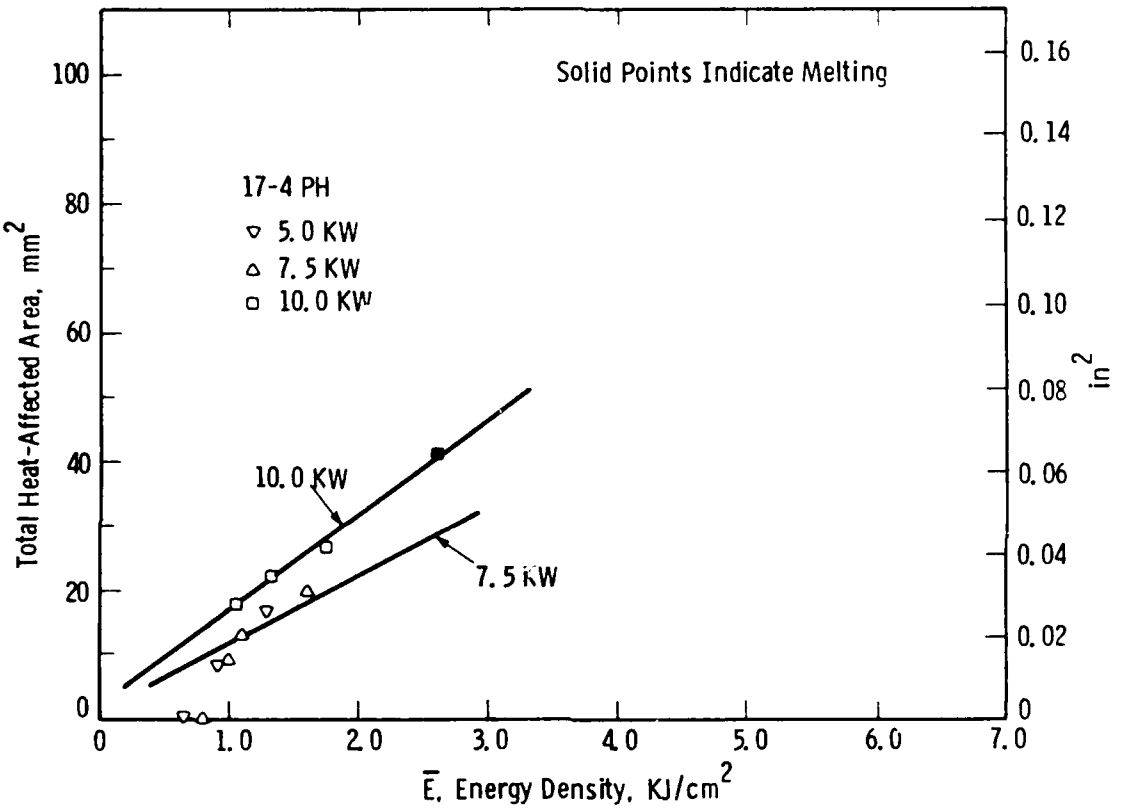

Figure 34--Effect of Energy Density on the Total Heat-Affected Area in 17-4 PH Steel at Laser Outputs of 5.0, 7.5 and 10.0 KW.

AD-A140 160 A PARAMETRIC STUDY OF SURFACE TRANSFORMATION HARDENING WITH HIGH-POWER LA.. (U) WESTINGHOUSE RESEARCH AND DEVELOPMENT CENTER PITTSBURGH PA G E GROTKE ET AL. 2/2

UNCLASSIFIED 02 FEB 84 84-9D4-SURFC-R1 N00014-82-C-2339 F/G 20/5 NL

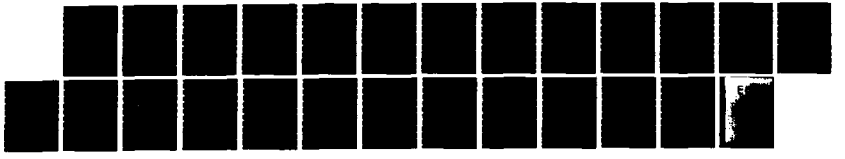

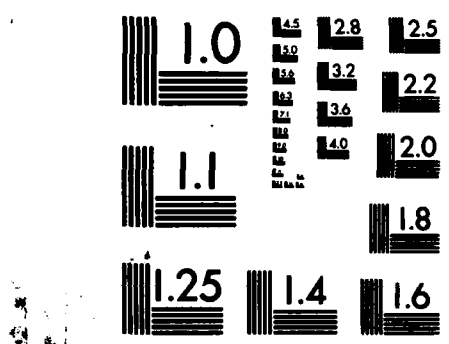

MICROCOPY RESOLUTION TEST CHART
NATIONAL BUREAU OF STANDARDS-1963-A

Curve 746085-A

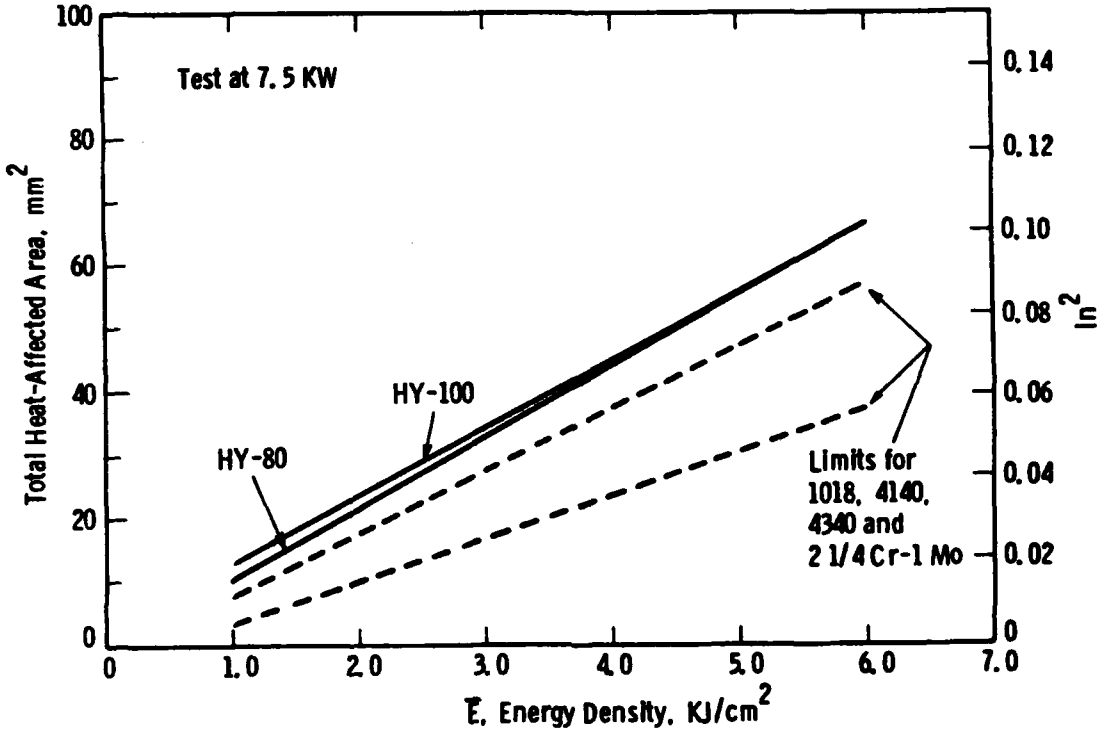

Figure 35--Comparison of Areas for 5/16-Inch-Thick HY-100 Steel and 1/4-Inch-Thick HY-80 Steel with the Area Scatterband for Thick-Section Conventional Steels--Tests at a Laser Power of 7.5 KW.

Curve 746090-A

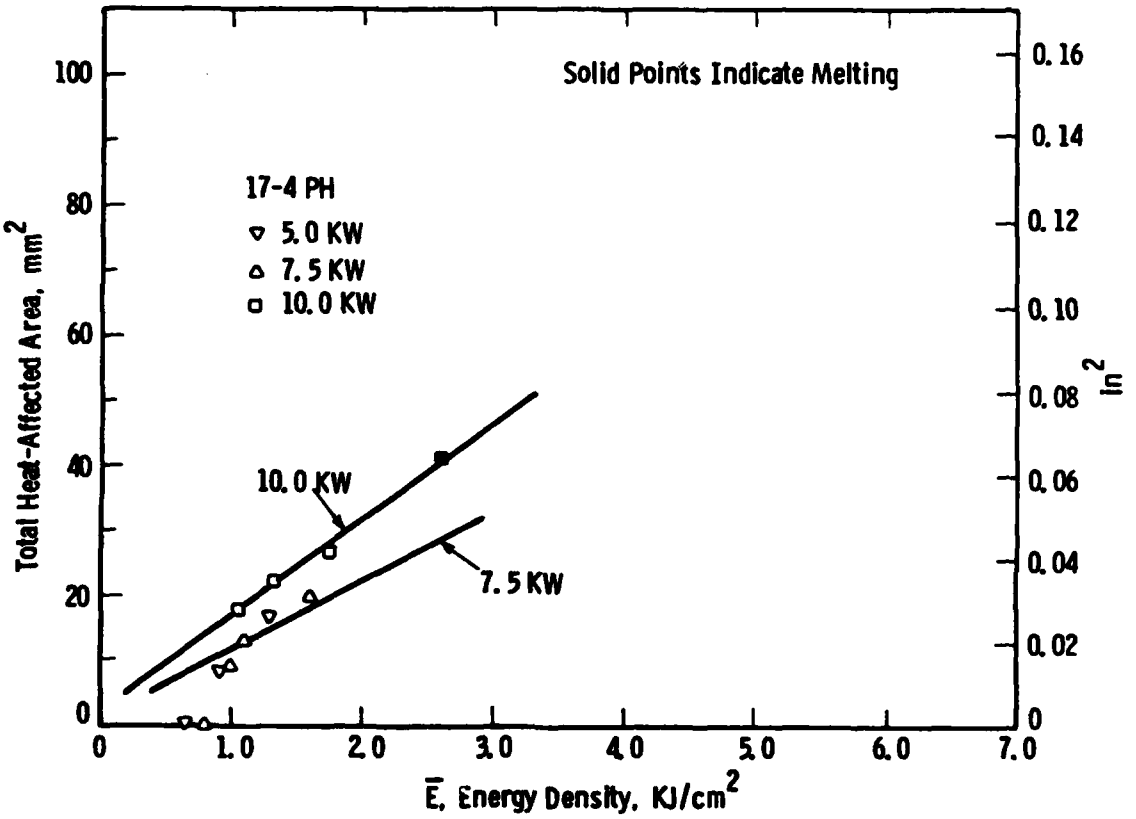

Figure 34--Effect of Energy Density on the Total Heat-Affected Area in 17-4 PH Steel at Laser Outputs of 5.0, 7.5 and 10.0 KW.

Curve 746084-A

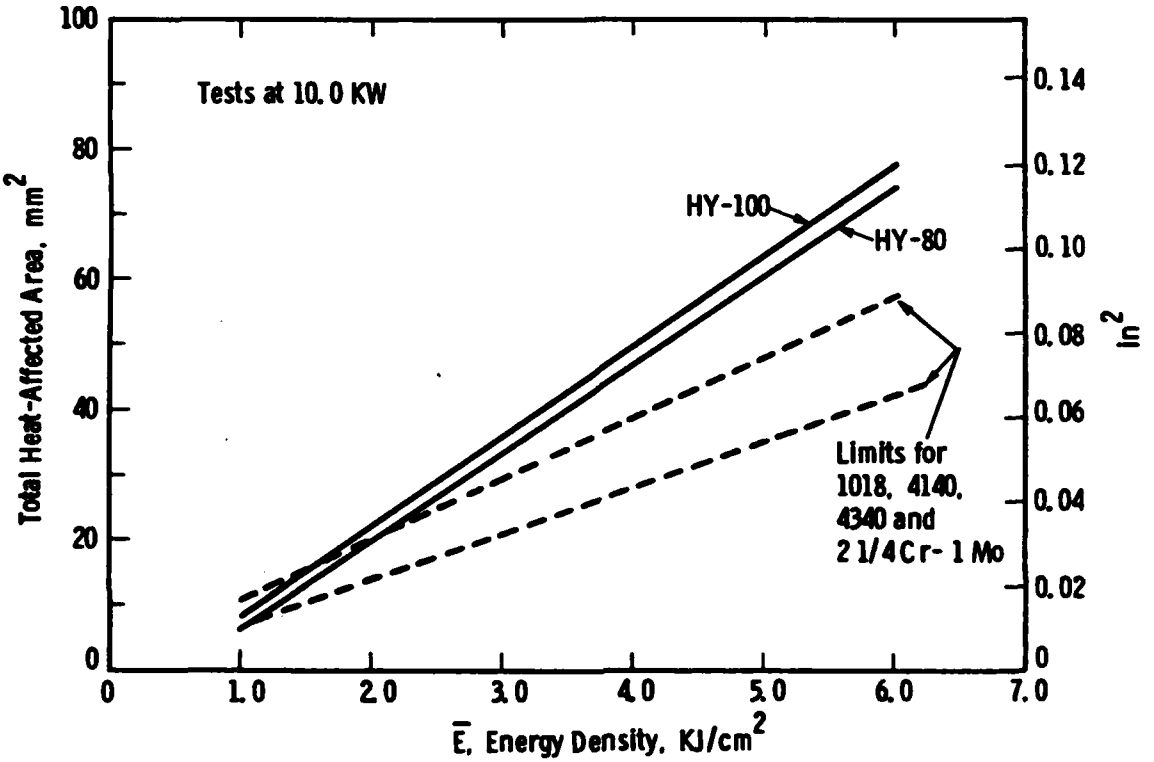

Figure 36--Comparison of Areas for 5/16-Inch-Thick HY-100 Steel and 1/4-Inch-Thick HY-80 Steel with the Area Scatterband for Thick-Section Conventional Steels--Tests at a Laser Power of 10.0 KW.

Curve 746087-A

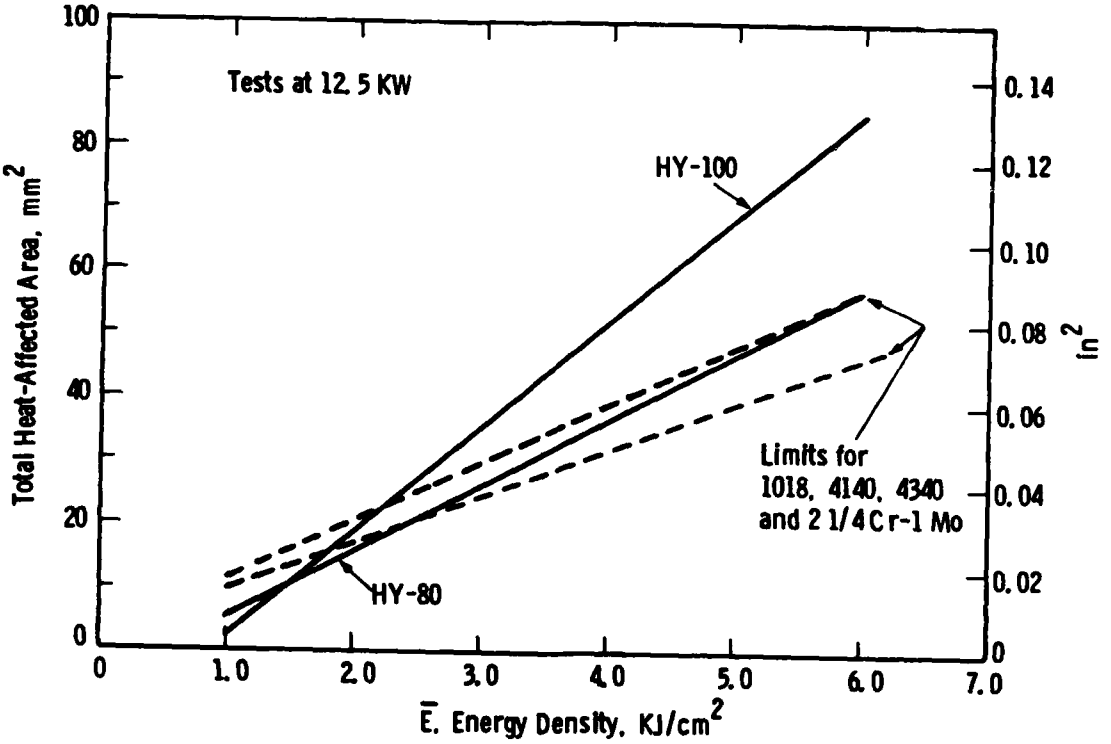

Figure 37--Comparison of Areas for 5/16-Inch-Thick HY-100 Steel and 1/4-Inch-Thick HY-80 Steel with the Area Scatterband for Thick-Section Conventional Steels--Tests at a Laser Power of 12.5 KW.

Curve 745940-A

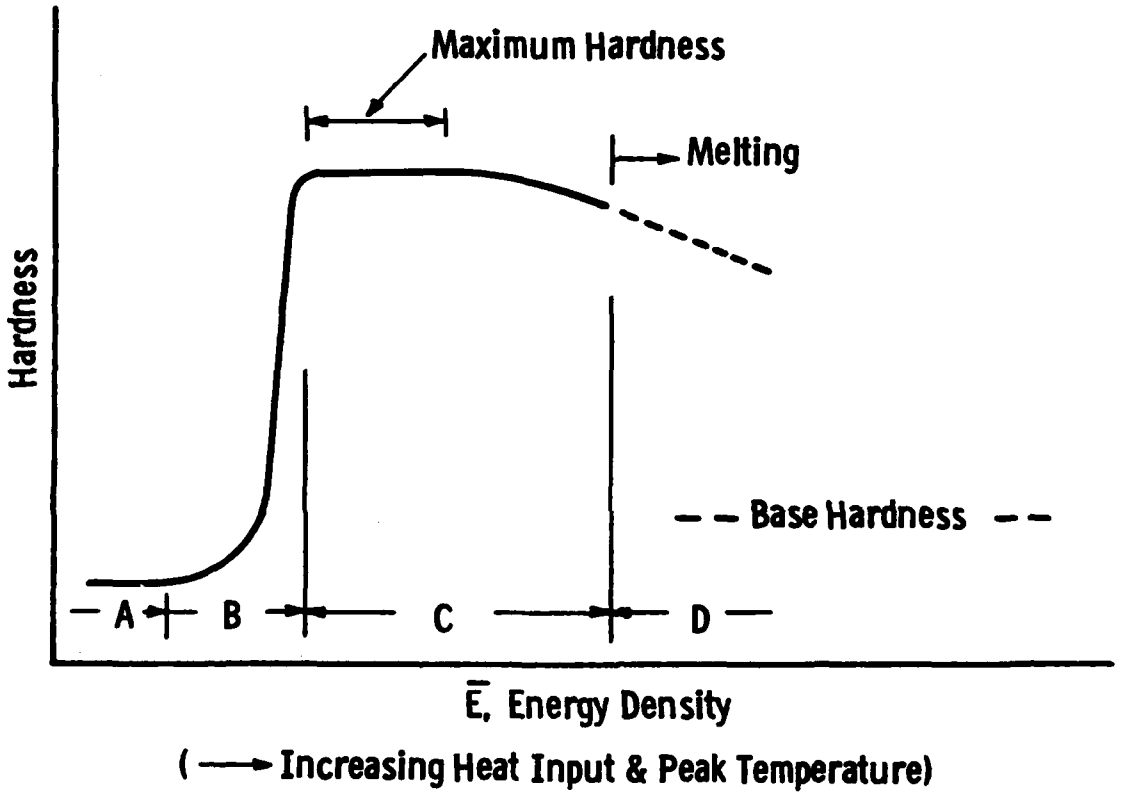

Figure 38--Illustration of the Development of Hardness in a Hardenable Steel with Increasing Energy Density.

Curve 745952-A

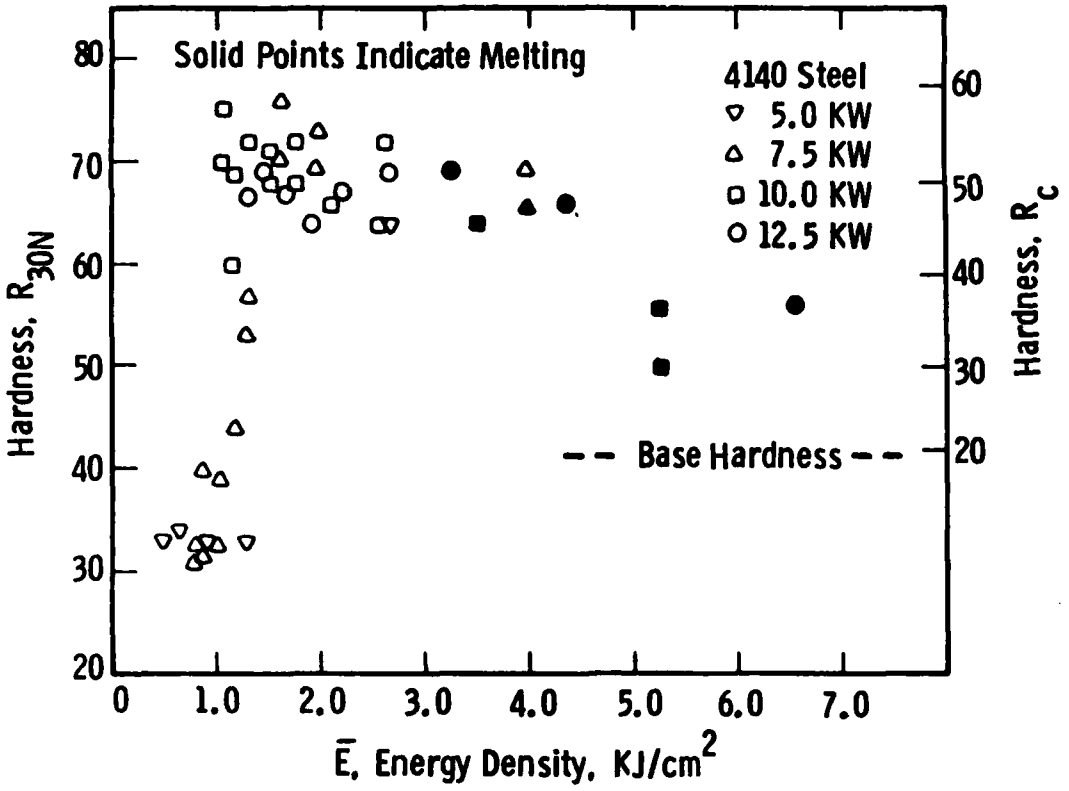

Figure 39--General Effect of Energy Density on the Hardness of 4140 Steel.

Curve 745951-A

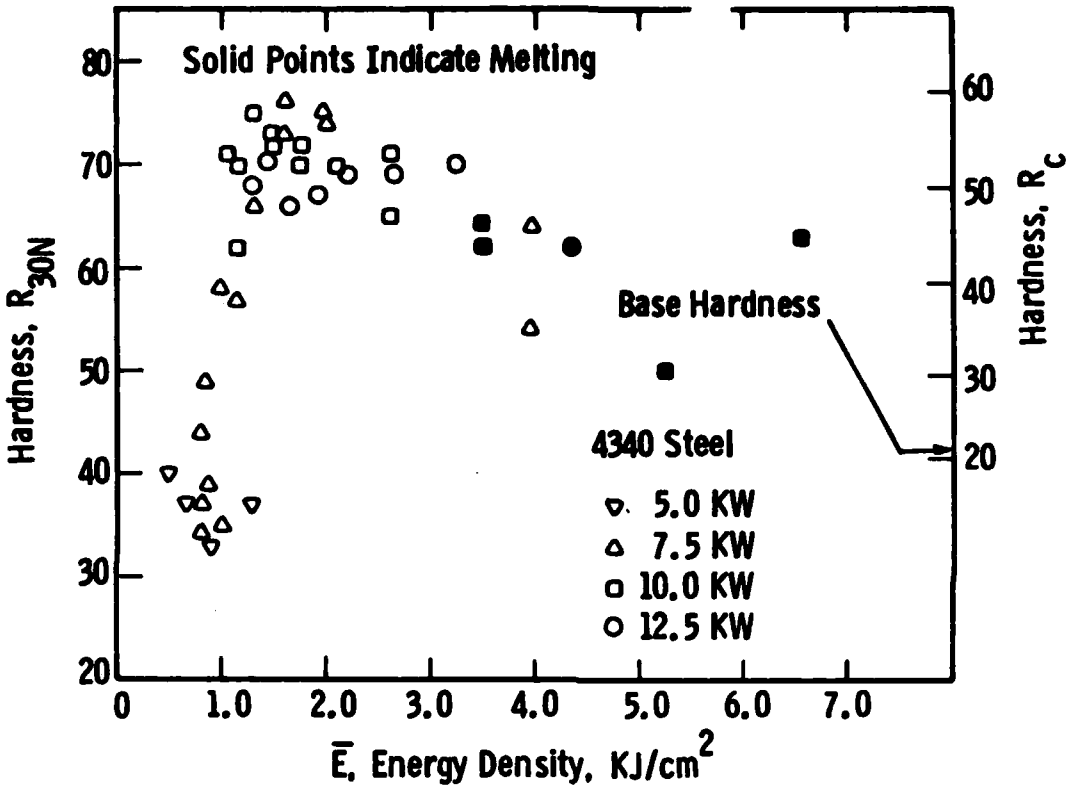

Figure 40--General Effect of Energy Density on the Hardness of 4340 Steel.

Curve 745946-A

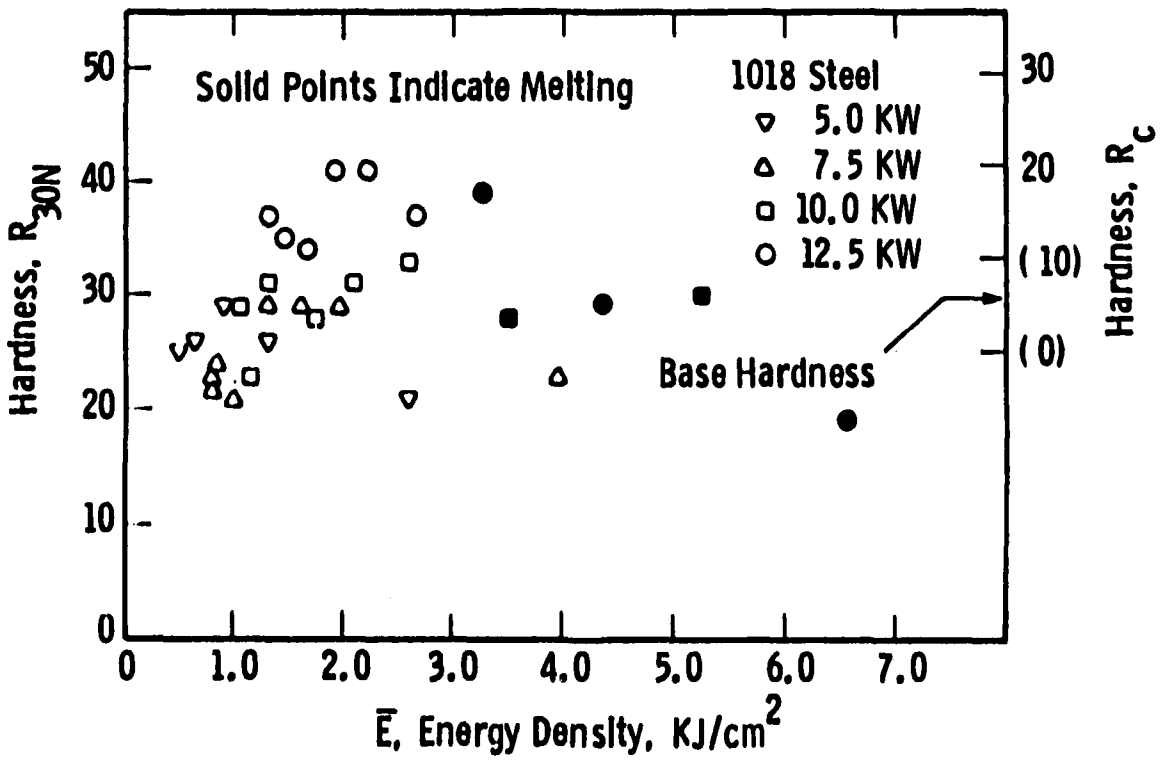

Figure 41--General Effect of Energy Density on the Hardness of 1018 Steel.

Curve 745947-A

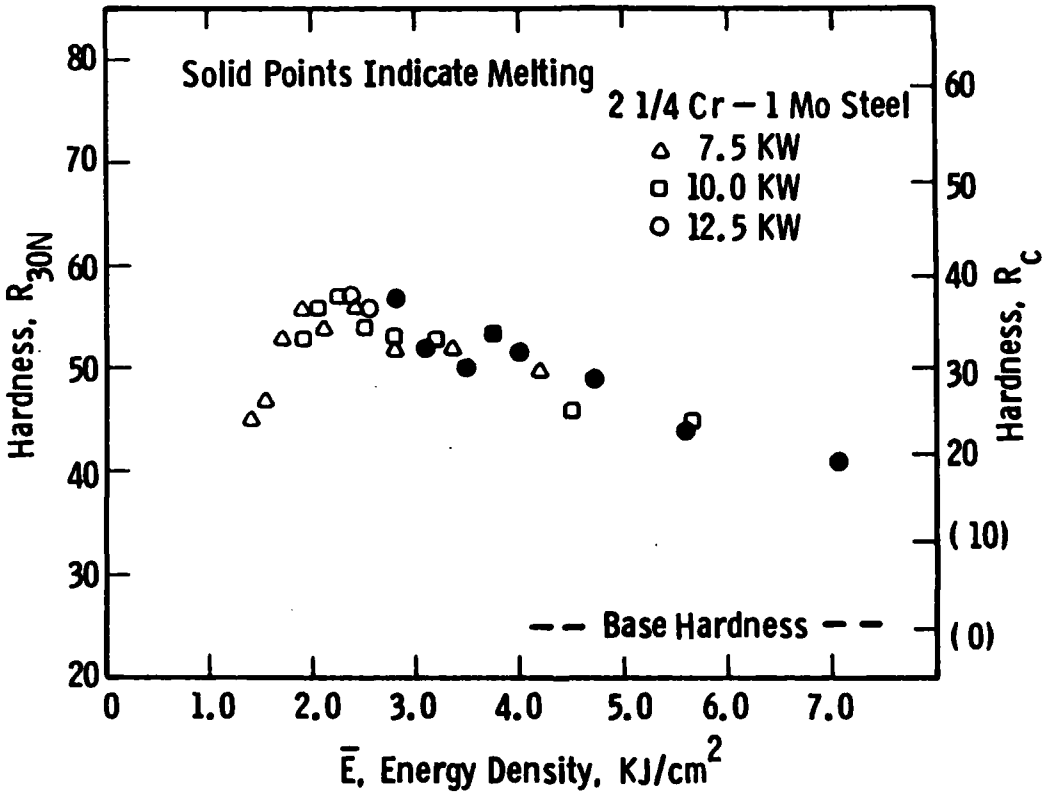

Figure 42--General Effect of Energy Density on the Hardness of 2-1/4 Cr-1 Mo Steel.

Curve 745944-A

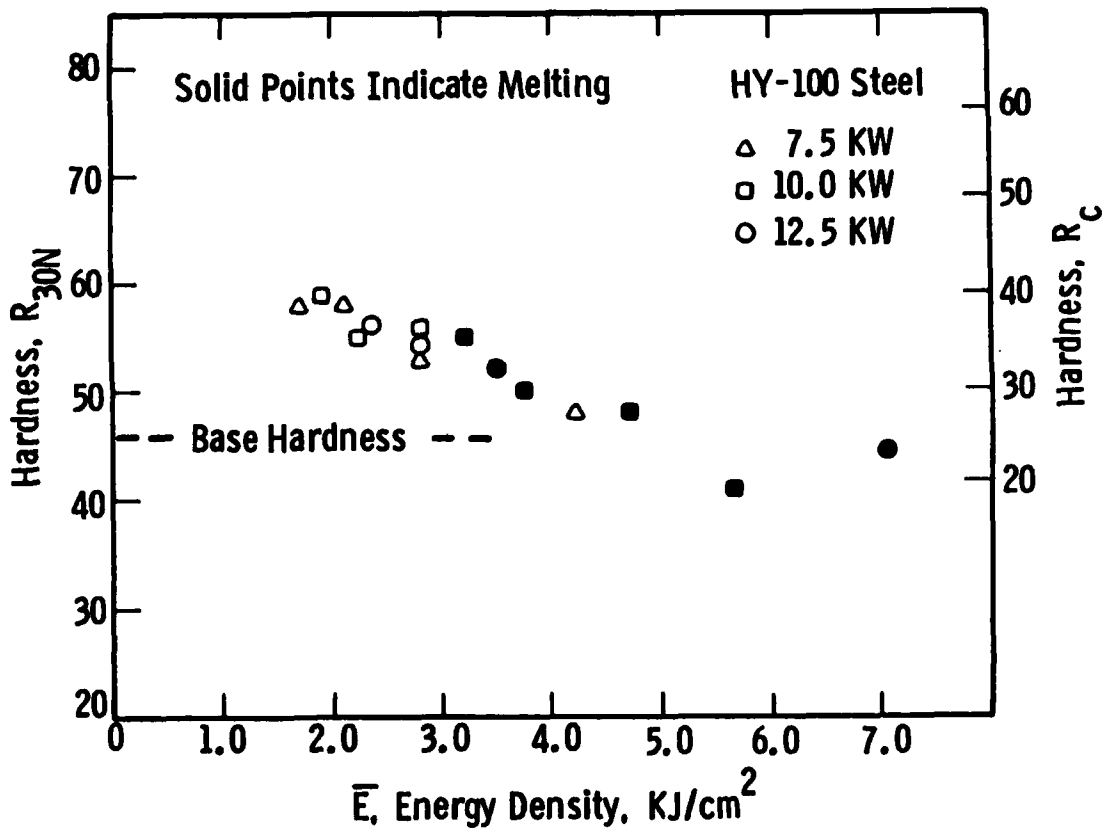

Figure 43--General Effect of Energy Density on the Hardness of HY-100 Steel.

Curve 745945-A

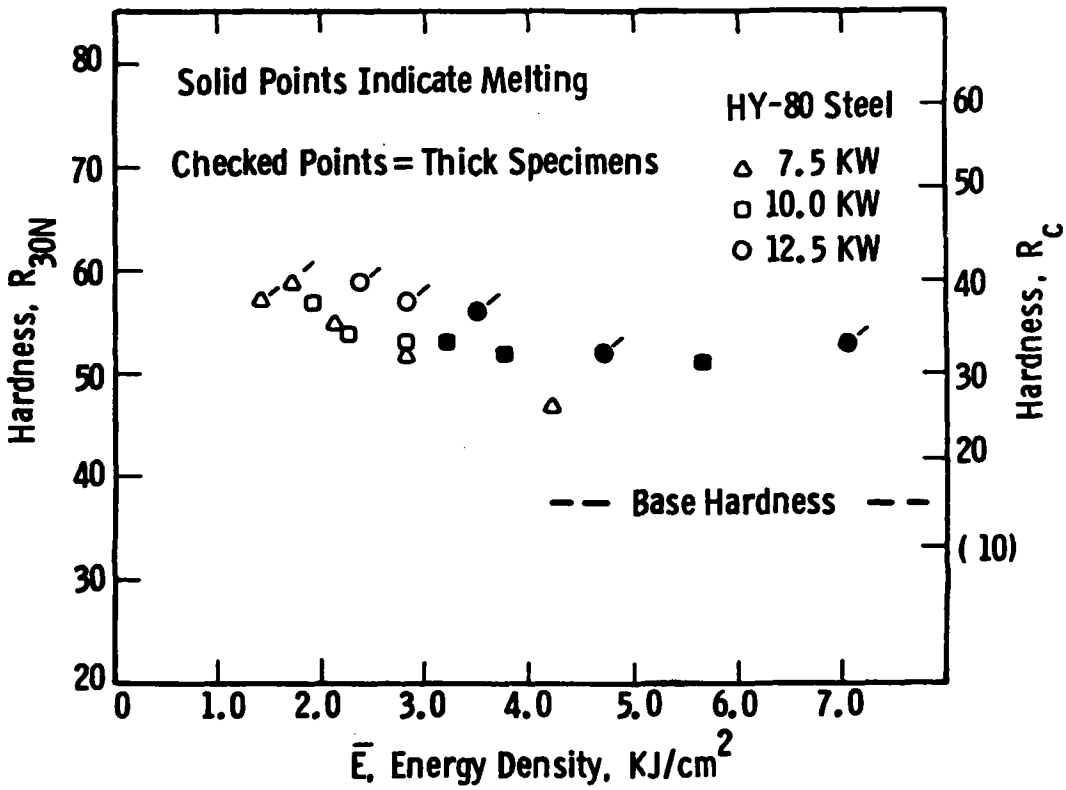

Figure 44--General Effect of Energy Density on the Hardness of HY-80 Steel (data for 7.5 and 10.0 KW not valid for thick sections).

Curve 745943-A

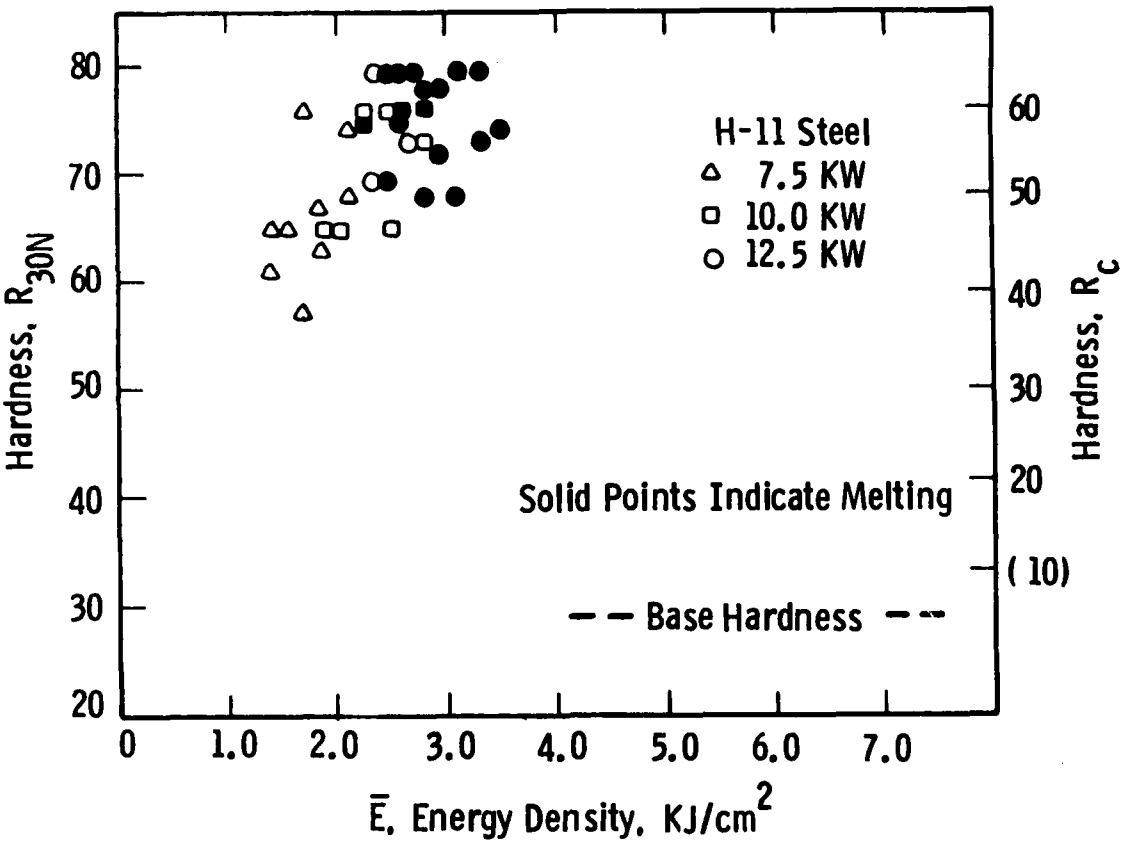

Figure 45--General Effect of Energy Density on the Hardness of H-11 Steel.

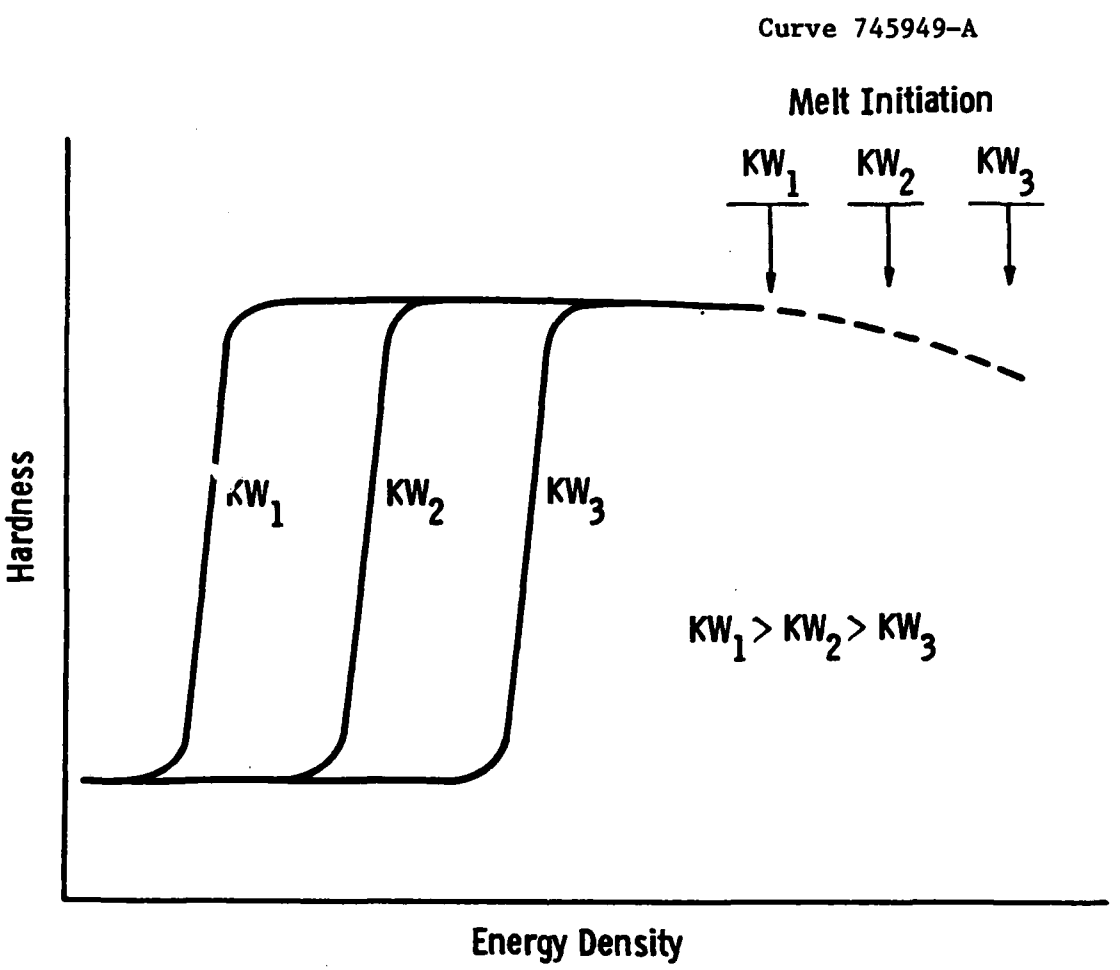

Figure 46--Illustration of the Influence of Laser Power on the Development of Hardness in a Hardenable Steel with Increasing Energy Density.

Curve 745950-A

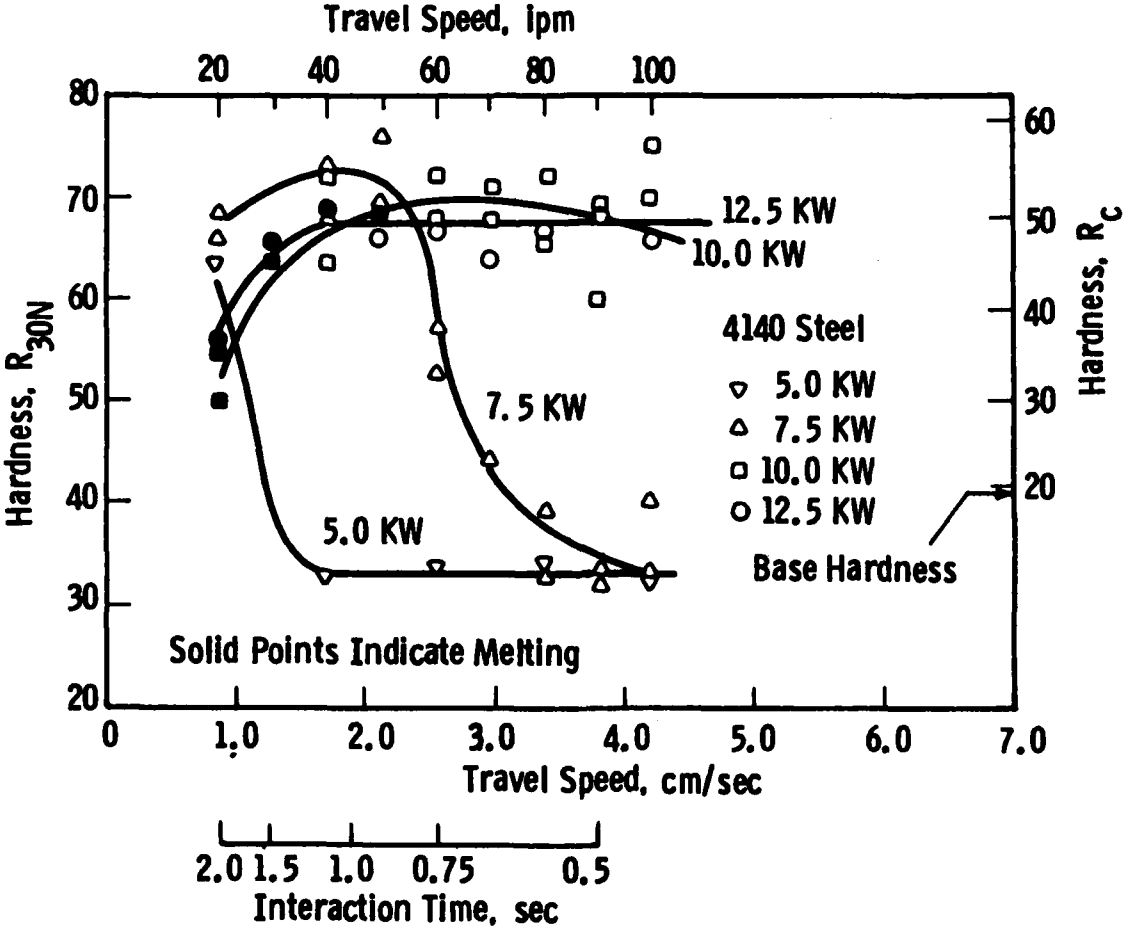

Figure 47--Effect of Travel Speed on the Hardness of 4140 Steel at Laser Powers of 5.0, 7.5, 10.0 and 12.5 KW.

Curve 745948-A

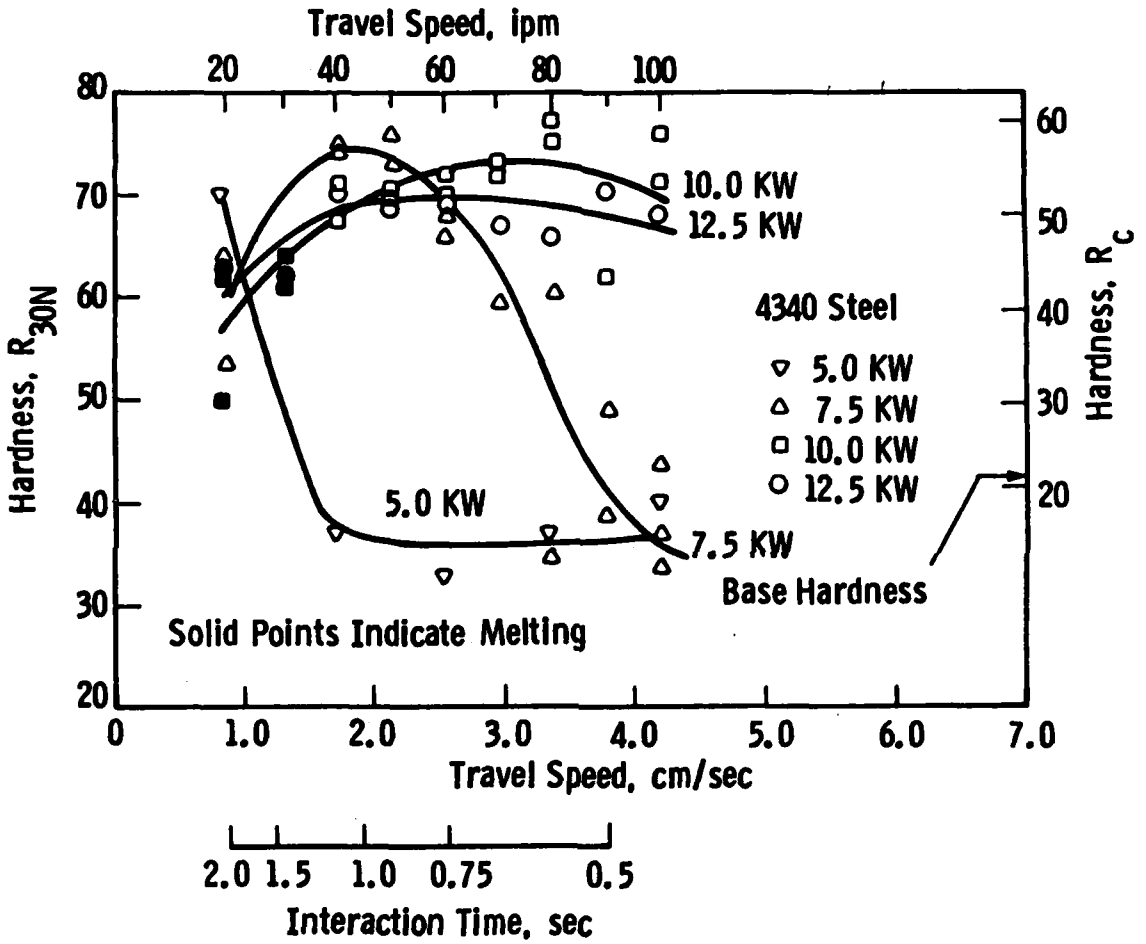

Figure 48--Effect of Travel Speed on the Hardness of 4340 Steel at Laser Powers of 5.0, 7.5, 10.0 and 12.5 KW.

Curve 745410-A

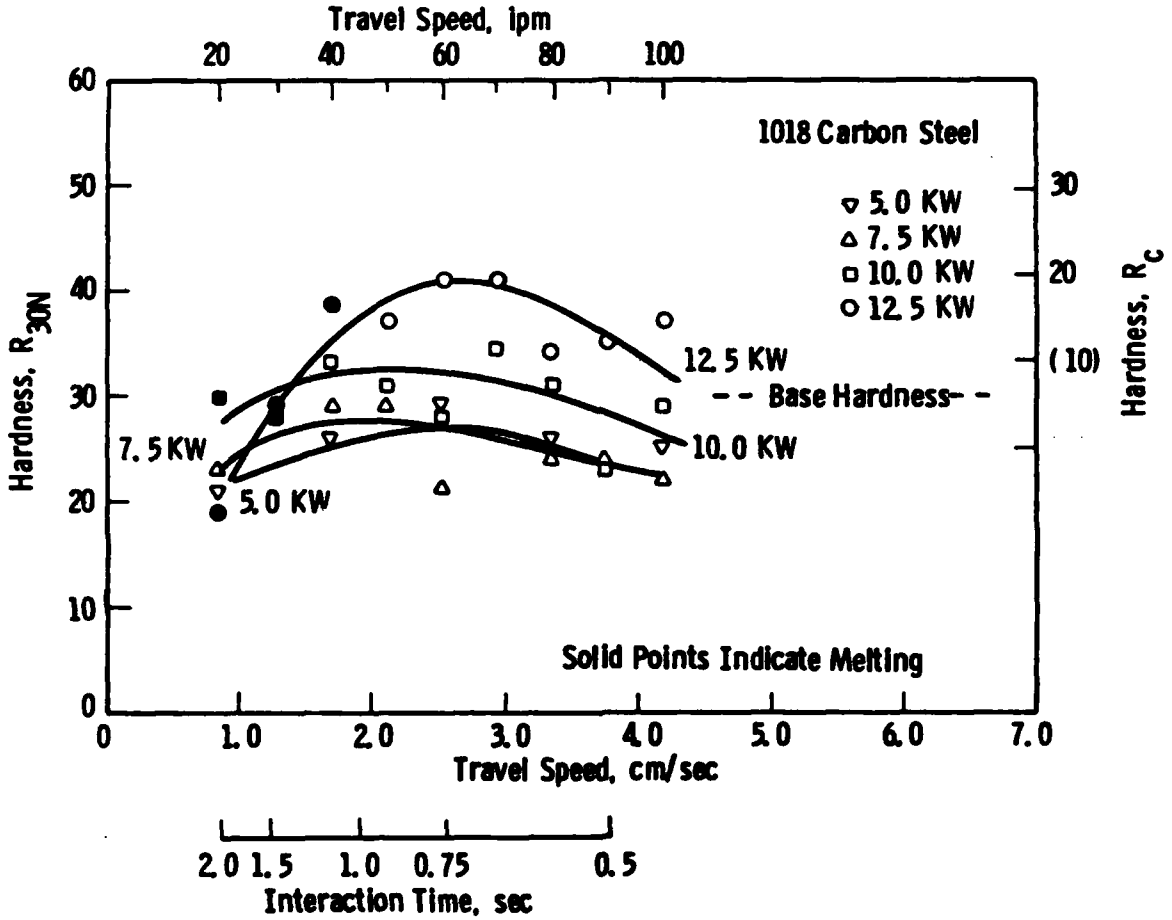

Figure 49--Effect of Travel Speed on the Hardness of 1018 Steel at Laser Powers of 5.0, 7.5, 10.0 and 12.5 KW.

Curve 745418-A

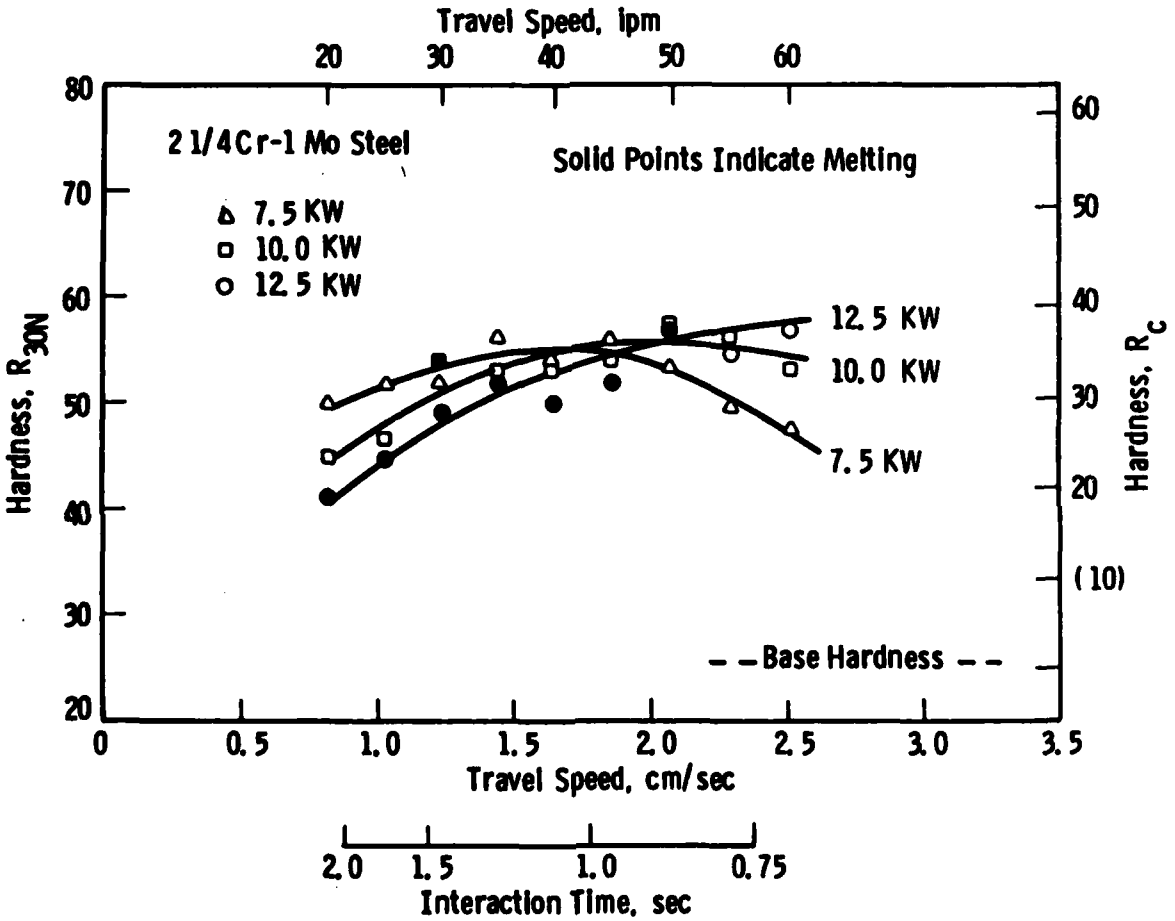

Figure 50--Effect of Travel Speed on the Hardness of 2-1/4 Cr-1 Mo Steel at Laser Powers of 7.5, 10.0 and 12.5 KW.

Curve 745419-A

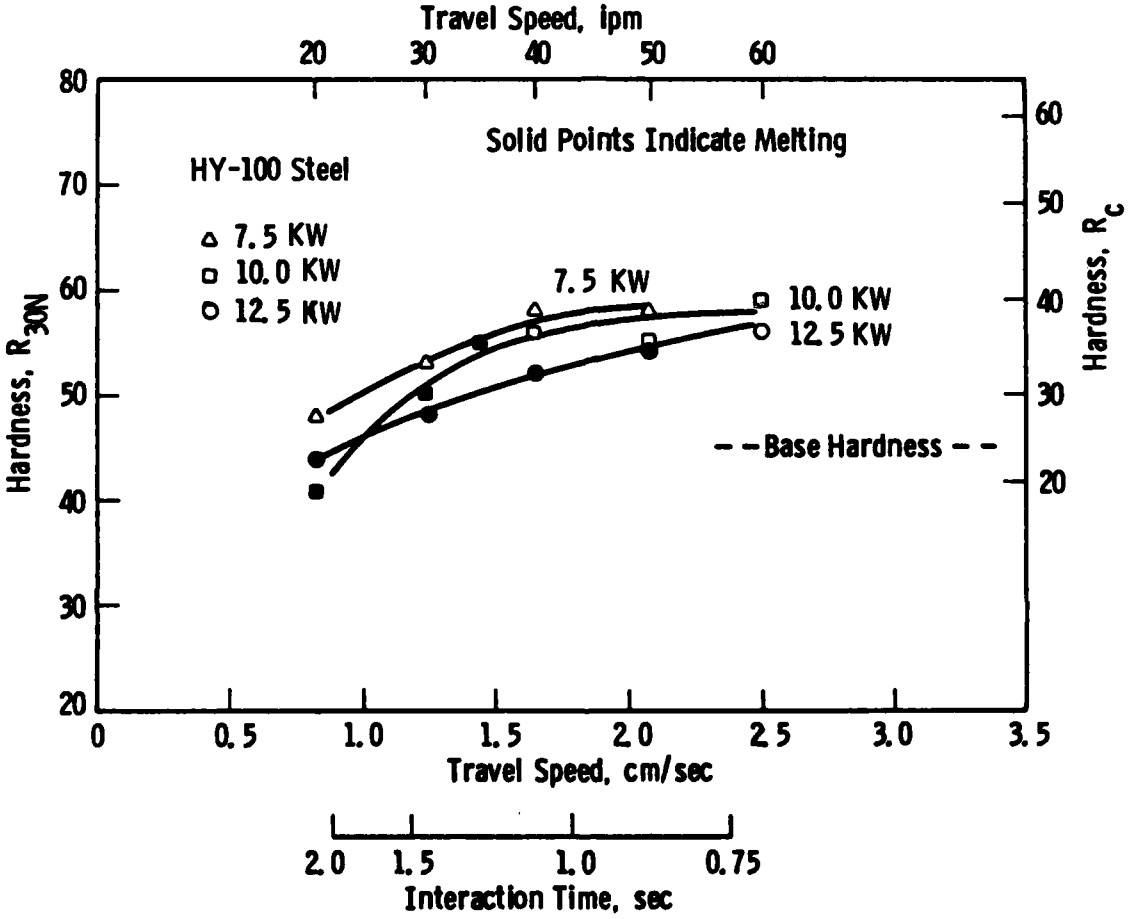

Figure 51--Effect of Travel Speed on the Hardness of HY-100 Steel at Laser Powers of 7.5, 10.0 and 12.5 KW.

Curve 745409-A

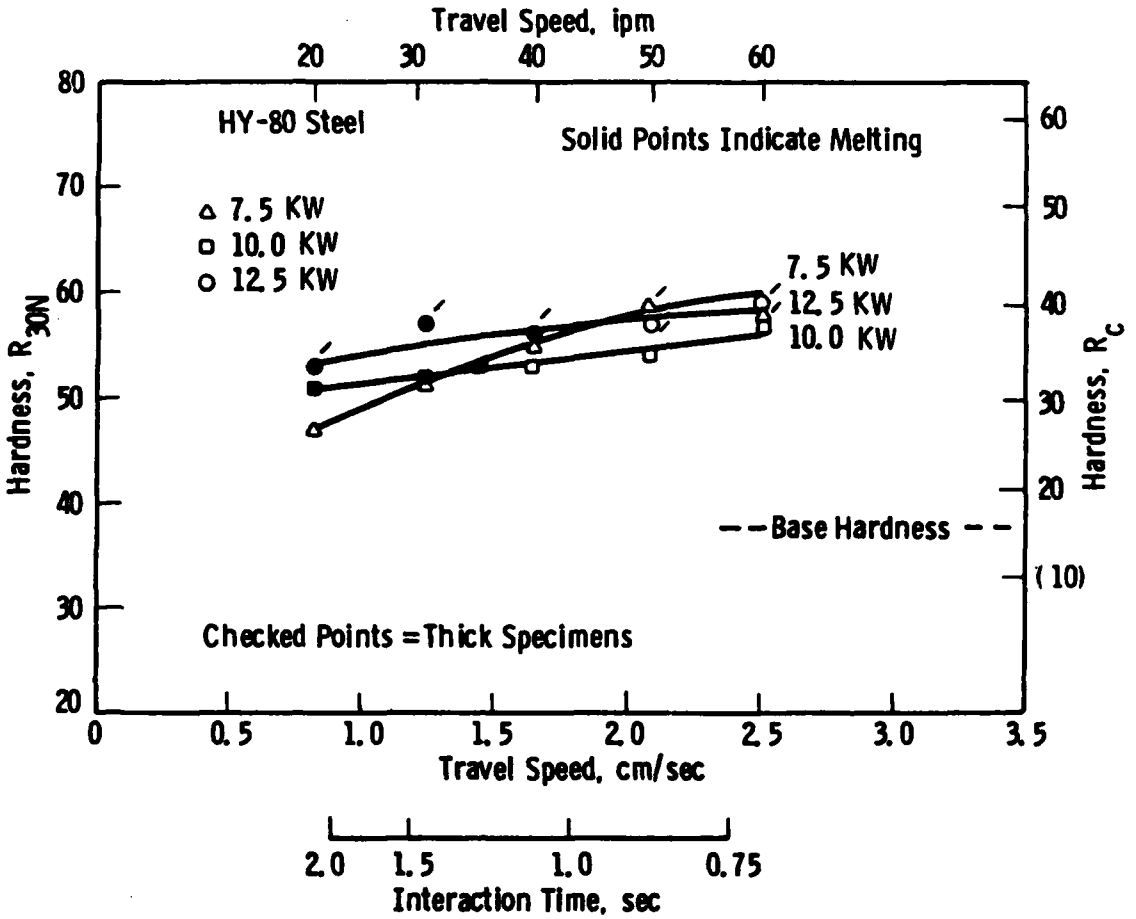

Figure 52--Effect of Travel Speed on the Hardness of HY-80 Steel at Laser Powers of 7.5, 10.0 and 12.5 KW (data for 7.5 and 10.0 KW not valid for thick sections).

Curve 745417-A

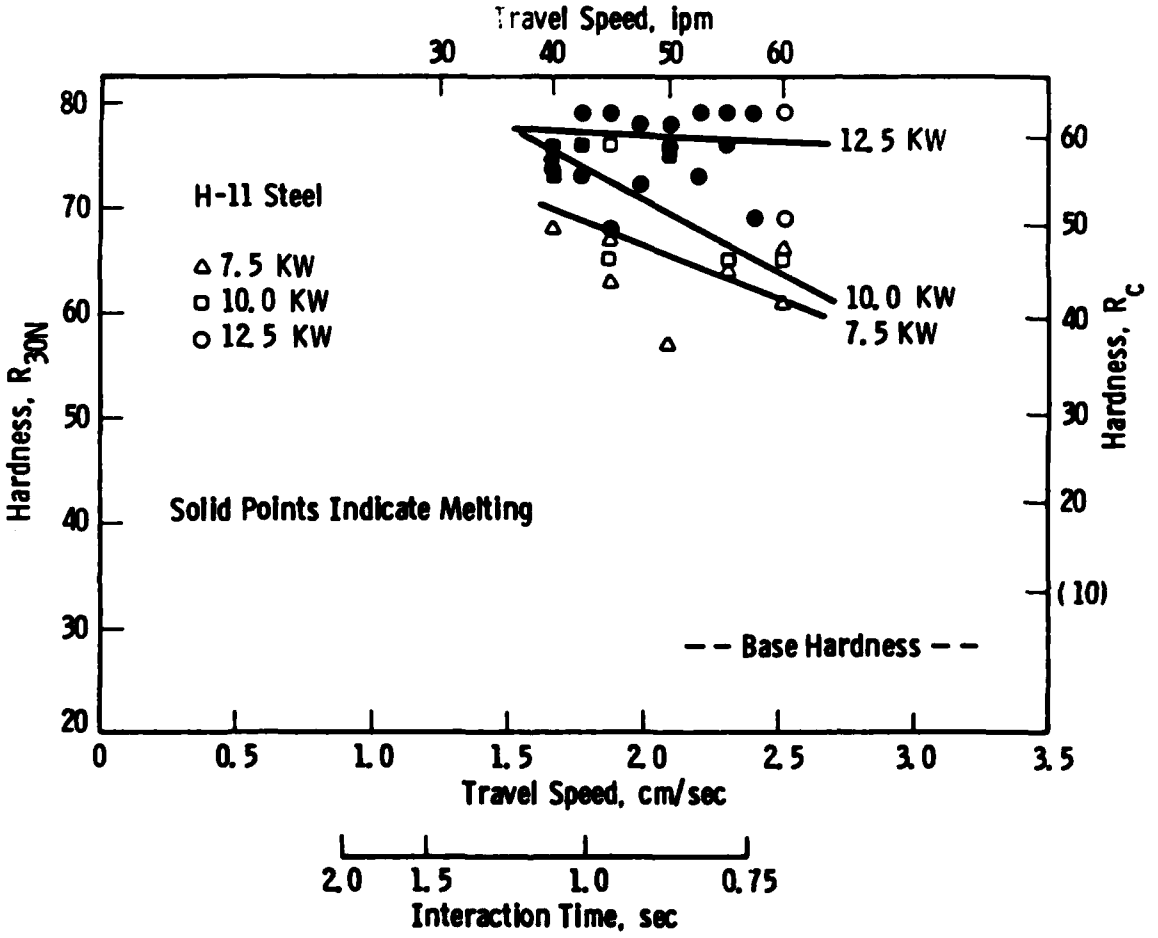

Figure 53--Effect of Travel Speed on the Hardness of H-11 Steel at Laser Powers of 7.5, 10.0 and 12.5 KW.

Curve 745941-A

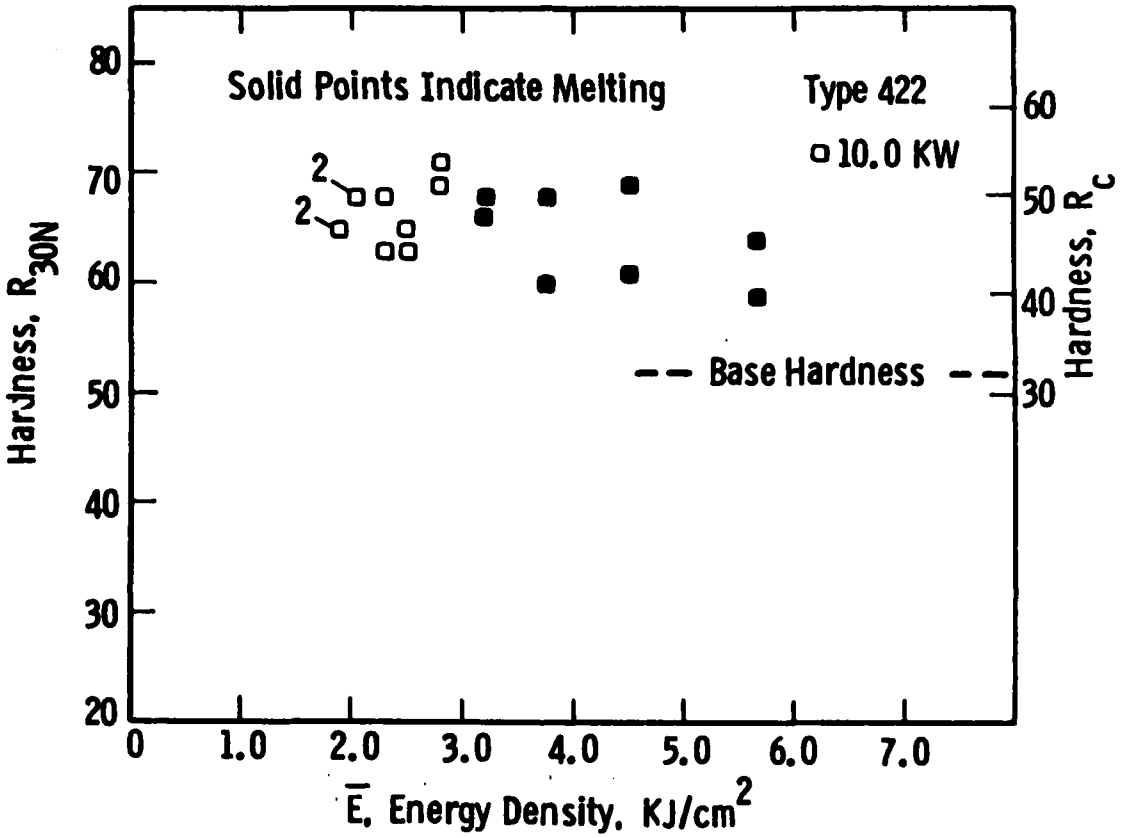

Figure 54--Effect of Energy Density on the Hardness of Type 422 Steel at a Laser Power of 10.0 KW.

Curve 745416-A

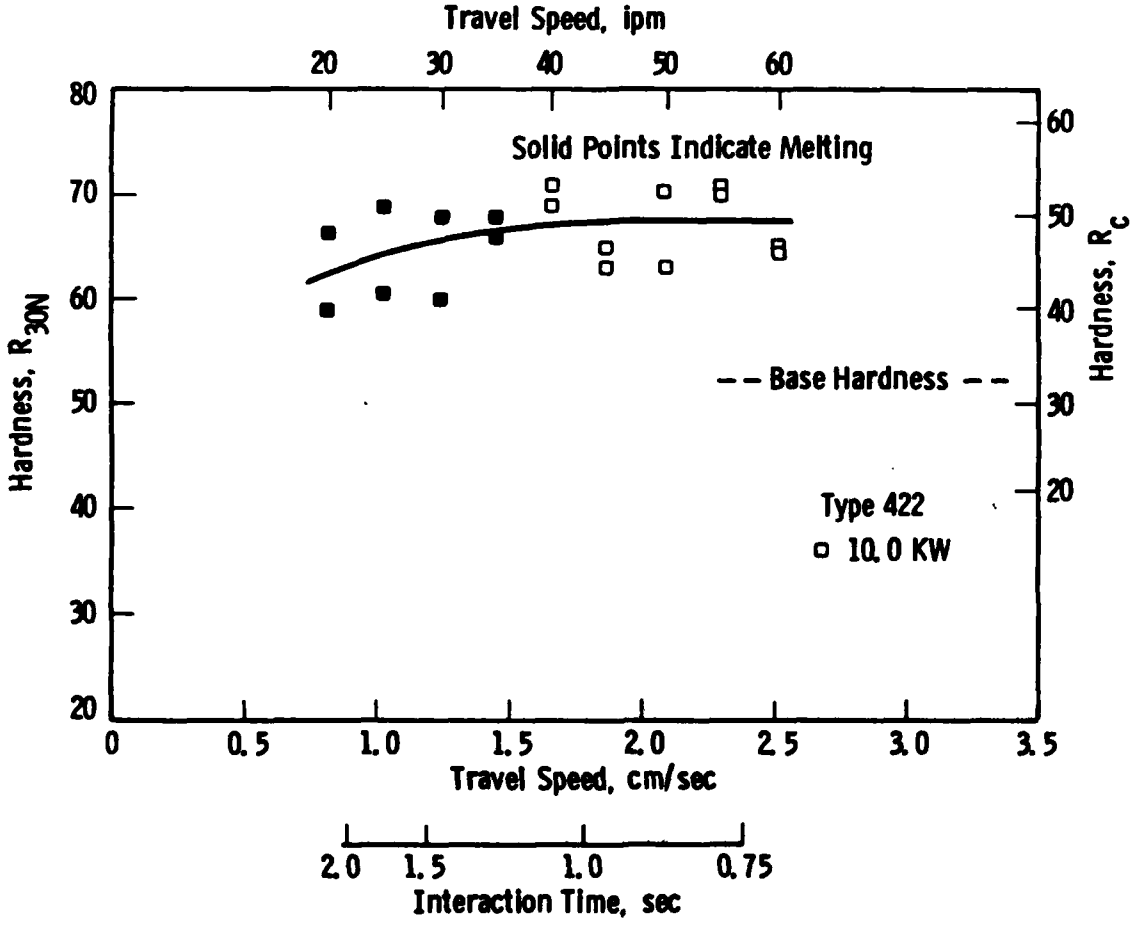

Figure 55--Effect of Travel Speed on the Hardness of Type 422 Steel at a Laser Power of 10.0 KW.

Curve 745942-A

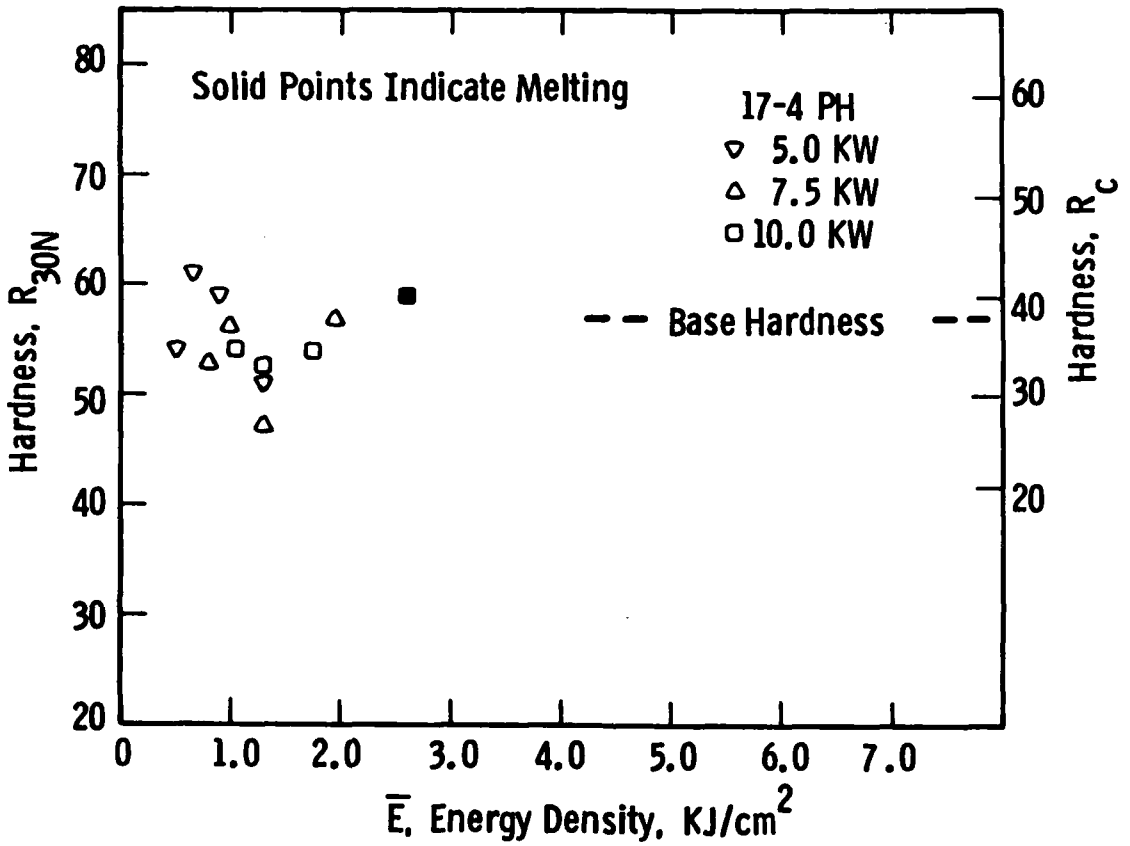

Figure 56--General Effect of Energy Density on the Hardness of 17-4 PH Steel.

Curve 745415-A

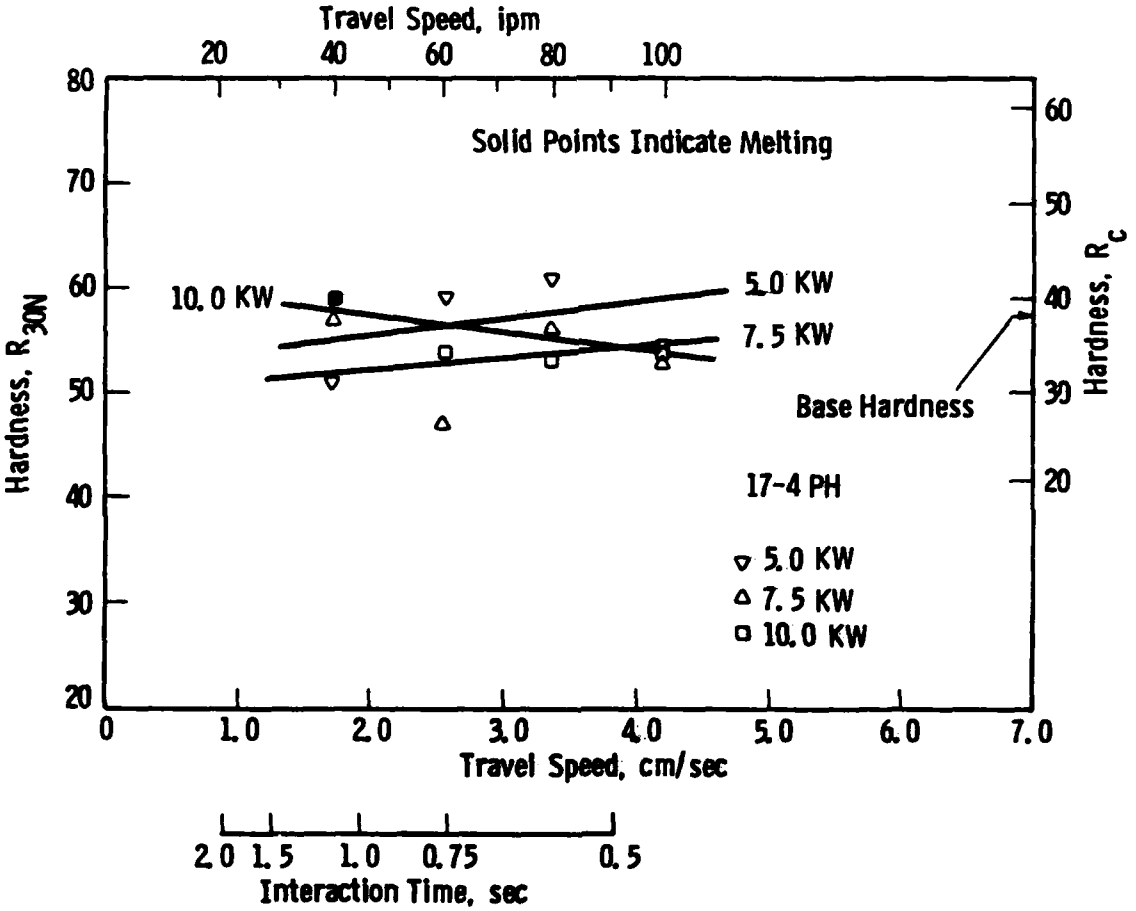

Figure 57--Effect of Travel Speed on the Hardness of 17-4 PH Steel at Laser Powers of 5.0, 7.5 and 10.0 KW.

END

FILMED

5-84

DTIC